ABSTRACT

LYONS, NATHAN JAY. Landslide Inventories and Grain Size Trends in Debris Flow-Dominated Channels. (Under the direction of Dr. Helena Mitasova).

Recent research in the field of geomorphology has approximated the location in mountainous headwater streams where the transition from debris flow to fluvial-dominated channel erosional processes occurs. The dominant channel process controls channels' sediment transport capacity and geomorphology, which affects streambed grain size and hillslope response. The transition has often been observed at a scaling break in a channel's plot of log drainage area versus log slope (DS Plot) that can be created from a digital elevation model (DEM). Little research has investigated channel process transitions or explore the wide-ranging implications and applications of the dominant channel process type throughout geomorphic realms in the southern Appalachians, an area with a long history of debris flow activity, and complex sediment transport and hillslope response dynamics.

The importance of the dominant channel process relative to the ability to inventory landslides and evaluate streambed grain size distribution in the Great Smoky Mountains of the southern Appalachians is investigated here. Researchers continue to improve inventory accuracy with new technology and techniques, though rarely is the dominant channel process incorporated into the inventory process despite the ability to confine debris flow activity to areas upstream from the scaling break. In this investigation of debris flow-dominated channels, we test an inventory technique that limits a land surface segmentation and classification algorithm to areas that are upstream from the scaling break in DS plots of five mountainous streams. 79% of surfaces were correctly classified when the algorithm incorporated the process-based analyses that limited the study area to areas upstream of the DS Plot scaling. 61% was correctly classified when the entire study area was included. This method allows a more focused approach to statistically characterize the land surface which resulted in a more accurate inventory in this study area.

In the second investigation, a streambed grain size model was created with a modified form of the Shields equation in order to determine grain size trends of mountainous streams relative to the DS Plot scaling breaks. Typically, grain size becomes progressively finer downstream despite local factors that disrupt this trend. This observation has mostly been made in alluvial reaches far from headwaters where debris flows occur. *In situ* grain size measurements in debris flow-dominated streams in the Smoky Mountains, however, coarsen downstream. Stream wide grain size trends modeled with DEM inputs parameterized with field data also coarsen downstream where the maximum grain size occurs at approximately the DS plot scaling break. This rarely studied and observed trend may have important effects on geomorphology and stream ecosystems where it arises. A case study to illustrate a potential impact of downstream coarsening, the control of grain size in competitive advantages amongst trout species, is also presented here. Encroachment of exotic trout species are confining brook trout (*Salvelinus fontinalis),* the only salmonid native to the southern Appalachians, to headwater streams. Previous region-specific studies have investigated the impact of hydrologic, biologic, and land use controls on salmonid distributions. Streambed grain size availability may be an additional control on species fecundity since brook trout use a significantly smaller grain size than the invasive salmonids to construct redds, the streambed mounds in which salmonids deposit their eggs.

The type of analyses required to conduct these investigation require datasets that spans multiple scales and methods of data collection. A considerable part of this work required reconciliation of data surveyed in the field and derived from remotely obtained topographic and spectral data. Problems common in geospatial data are addressed. Moderate correlations between field surveyed and modeled channel metrics were observed that provided further insight into the methodology of this study and dominant channel processes.

Landslide Inventories and Grain Size Trends in Debris Flow-Dominated Channels

by
Nathan Jay Lyons

A thesis submitted to the Graduate Faculty of
North Carolina State University
in partial fulfillment of the
requirements for the degree of
Master of Science

Marine, Earth, and Atmospheric Sciences

Raleigh, North Carolina

2011

APPROVED BY:

_____	_____
Dr. Helena Mitasova Committee Chair	Dr. Karl W. Wegmann

_____
Dr. Ilona Peszlen

BIOGRAPHY

Nathan Lyons was born in south Florida, and upon witnessing topographic variation and complexity in North Carolina, pursued a bachelor's degree in geology at Guilford College. A position with the National Park Service during the summer prior to his first semester of graduate studies at North Carolina State University greatly influenced the topic of this thesis.

ACKNOWLEDGMENTS

First and foremost, I wish acknowledge the chair of this thesis's committee and my academic advisor, Dr. Helena Mitasova, for providing continual guidance, expertise, and encouragement. Committee members Drs. Karl W. Wegmann, and Ilona Peszlen who sacrificed their valuable time and resources to help me produce this thesis and improve my understanding of topics contained within its pages.

Numerous members of the Great Smoky Mountains National Park community also provided invaluable council and logistical assistance. This includes members of the National Park Service: Kris Johnson, Matt Kulp, Ben Zank, Tom Remaley, Debbie Gilbreath, Nancy Finley, Paul Super, Dr. Keith Langdon and several others. This also includes others who shared what they learned when they worked in the area: Richard Ketelle presently of Oak Ridge Laboratory, Scott Southworth of the USGS, and Dr. Bill Witherspoon presently of the Fernbank Science Center.

And to family and friends for constant encouragement and expressing interest in my work.

TABLE OF CONTENTS

LIST OF TABLES

CHAPTER 2:

CHAPTER 3:

LIST OF FIGURES

CHAPTER 1:

CHAPTER 2:

CHAPTER 3:

APPENDICES:

CHAPTER 1: INTRODUCTION

1.1. Background

1.1.1. The Role of Debris Flows in Channel Processes

The form of a drainage channel as observed in its longitudinal profile reflects the processes that dominate its formation and function as the primary sediment conduit of a landscape (Crosby and Whipple, 2006; Howard, 1994; Tucker and Slingerland, 1997). In mountainous terrain with steep hillslopes and moderately-sized drainage areas, a highly efficient sediment transport process, debris flow, leaves its signature on the channel's form as it erodes both hillslopes and channel areas (Seidl and Dietrich, 1992). Hillslope failures, following the widely used classification system of Cruden and Varnes (1996), are described by the material that is translated and the method of translation. Debris flows occur when frictional forces of regolith and bedrock are overcome by gravitational forces, dependent on the shear strength of the regolith's composition, resulting in rapid downslope transportation of water, rock, soil, and vegetation (Varnes, 1978). Debris flows, triggered by high precipitation events, initiate in areas with convergent topography, and then leave their signature while transporting sediment and other material down channels.

Recent scientific literature has proposed that debris flows can be the primary agent of mountain denudation resulting in hillslope and fluvial geomorphic alteration that affects the geo- and biospheres across multiple spatial and time scales (Eaton *et al.*, 2003; Hovius *et al.*, 1998; Korup *et al.*, 2010; Stock and Dietrich, 2003). Infrequent, high magnitude events, notably debris flows, are often more efficient in denuding mountainous basins compared to frequent low magnitude events, such as low return interval floods (Korup *et al.*, 2010). Severely dissected valleys, entrenched channels, and decreased steepness in upper hillslopes are the topographic outcomes of debris flows in timespans greater than 100 years (Eaton *et al.*, 2003; Korup *et al.*, 2010). Adjustment of sediment detachment and transport

competence, stream morphology, vegetation in the tracks of debris flows, and debris flow scar incision by flowing water are the topographic outcomes in short time scales (Benda, 1990; Pearce and Watson, 1983). Throughout multiple timescales, debris flows can be the primary agent of stream incision superseding incision efficacy of exclusively fluvial processes in valleys with high slopes and moderately-sized drainage areas (Stock and Dietrich, 2003). Evidence to confine the extent of debris flows, pertinent to questions related to the causes and effects of this prominent geomorphic agent, is contained within the channels' form since the form is in large part dictated by the process that dominants channel incision. Attempts to understand and characterize the transition from debris flow- to fluvial-dominated channels have been conducted, though little work has investigated the implications and applications of the process transition throughout geomorphic realms.

The efficacy of mass wasting to incise bedrock channels and/or remove regolith is noticeably higher than stream power alone, thus locating areas of increased incision along streams can assist in determination of areas susceptible to mass wasting and that drain to debris flow-dominated channels. A scaling break, a break in the linear relationship in log-log plots of drainage area and slope (DS Plots), is often used to determine the transition between debris flow- and fluvial-dominated channels (Figure 1.1). The high efficacy of debris flows to incise channels is apparent above the scaling break where stream power laws typically over predict slope. Additionally, the scaling break often coincides with field observations of stream deposits near the upstream terminus of strath terrace deposits and below the lowest debris flow deposit (Stock and Dietrich, 2003).

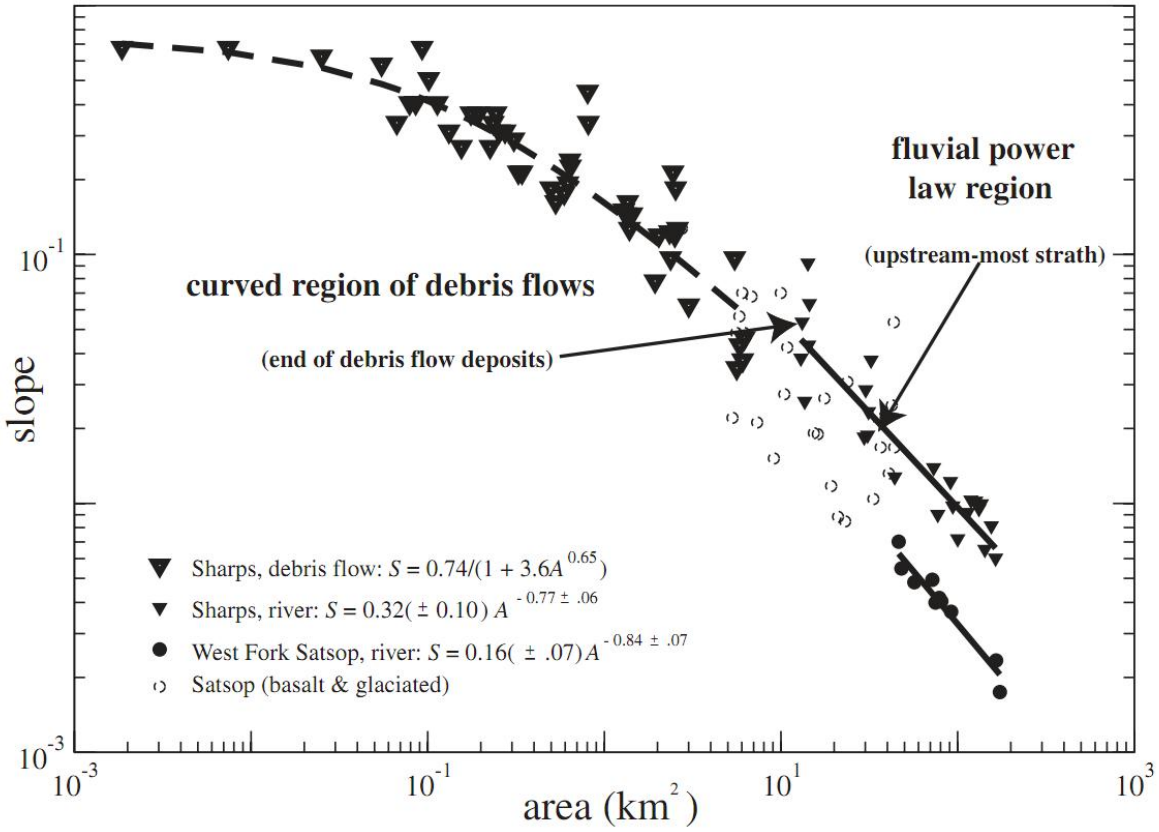

Figure 1.1. The dominant channel process regions in this drainage area vs. slope plot are separated by a scaling break between the curved and power law regions. Data was obtained from the Sharps Creek and West Fork Satsop and Satsop Rivers in the Olympic Mountains with 7.5' contour maps. Figure is from Stock *et al*. (2005).

1.1.2. The Role of Vegetation in Landscape Evolution

The mechanisms that control the relationship between vegetation and geomorphology including the central role the former has in the causes and effects of hillslope failure have long been viewed to act unidirectionally where one is responding to the other that remains static (Marston, 2010). The effect of vegetation is also commonly viewed to affect geomorphology in only small spatial and time scales, though advances in geographic information systems and improved geochronologic techniques has exposed exceptions to this view (Renschler *et al.*, 2007). Further, some researchers have proposed that vegetation and

geomorphology co-evolve, which is supported by investigations of landscape evolution mechanisms particularly at the intersection of vegetation and mass movements, including debris flows (Marston, 2010).

Topographic position, landform, and vegetation community composition co-evolve, discussed here specifically to debris flows in large scales, due to the following mechanisms that operate in smaller scales. Soil moisture, an important factor in debris flow initiation, is modulated by vegetation moisture uptake transferred to the atmosphere through evapotranspiration (Harden, 2006). Roots reinforce hillslopes and retard shallow mass movements, though roots are typically stronger on ridges than in areas with convergent flow (Roering *et al.*, 2003). Treefall from debris flows increases soils susceptibility to erosion from overland flow by decreasing surface shear strength, and bioturbation alters flow paths through changes in soil permeability (Gabet *et al.*, 2003). Further, exposure of tree roots by a debris flow causes stress to surviving trees since water and nutrient uptake ability is reduced (summarized by Stoffel and Bollschweiler, 2008). Mechanisms that rapidly reduce tree health and increase treefall result in higher stream wood and sediment entrainment. An area's climate, geology, and vegetation greatly control the degree that these mechanisms promote hillslope failures and the impact that debris flows have upon landscape evolution. Therefore, the physiology of an area must be considered as factors in the spatial extent of channel processes.

1.2. General Physiology of the Great Smoky Mountains

The study area is five adjacent watersheds totaling 343 km^2 in the Great Smoky Mountains National Park (Figure 1.2). The National Park encompasses 2110 km^2 in the Southern Blue Ridge physiographic province of the Appalachian Mountains. The Southern Blue Ridge province is bounded by the Brevard fault zone to the southeast, the Blue Ridge fault systems to the northwest, and the Roanoke River separates the Northern and Southern Blue Ridge provinces (Fenneman, 1928; Hatcher and Goldberg, 1991). The landscape is characterized by rounded

mountaintops, steep slopes, and highly eroded valleys (Fenneman, 1928). The crest of the range approximately demarcates the state boundary between North Carolina and Tennessee within the Park. Drainage is to the west via the Little Tennessee River on the North Carolina side and the French Broad River on the Tennessee side. These rivers ultimately drain into the Gulf of Mexico via the Tennessee, Ohio, and Mississippi Rivers.

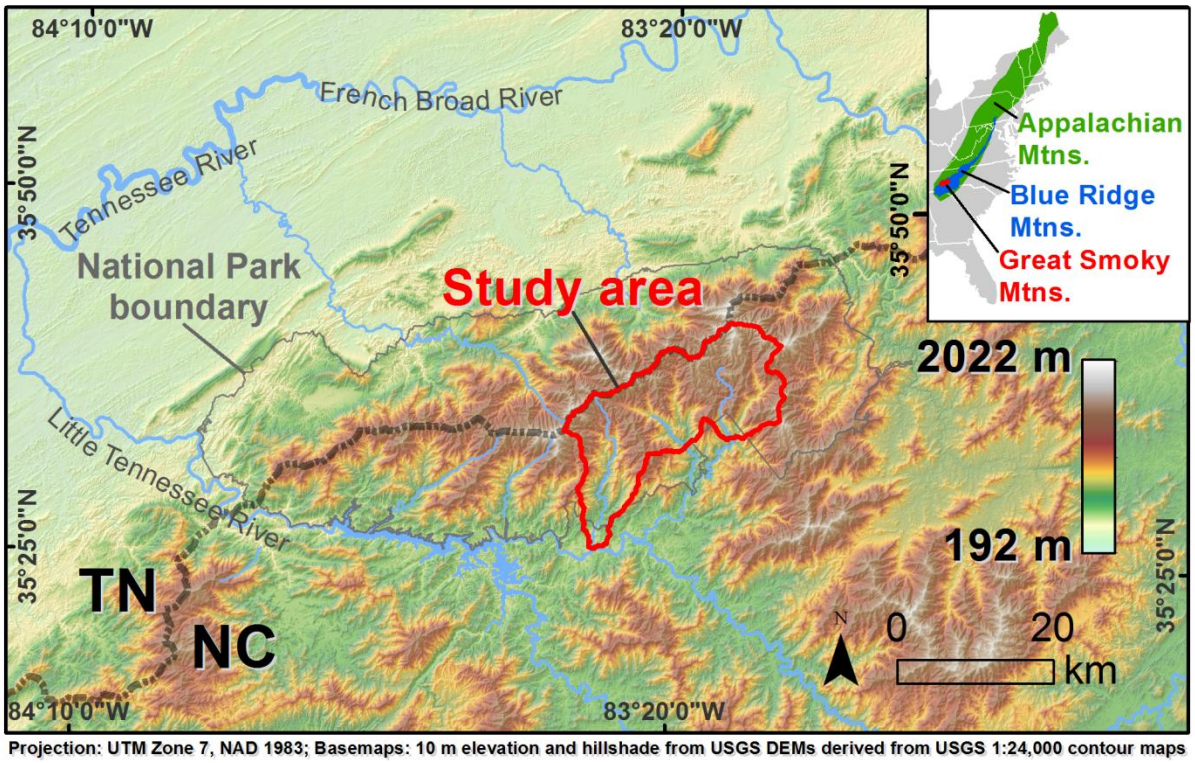

Figure 1.2. The location of the study area is in five watersheds in a southeast high elevation section of the National Park.

This area was selected for this study due to its history of numerous debris flows, well documented geologic history, and data availability. All of the analyses were limited to the North Carolina side of the Smoky Mountains since high resolution elevation data on the Tennessee side were not available at the time of this study. This area largely falls within Swain County, which makes up the majority of the National Park in North Carolina.

1.2.1. Climate

The Smoky Mountains region is classified as a warm-temperate rain forest and it receives among the highest average annual precipitation amounts in the U.S. (Thornthwaite, 1948). Annual precipitation for the years 1930 to 2003 averages 1420 mm with a standard deviation of 208 mm (Busing *et al.*, 2005). Climate variations due to high relief and aspect cause large local variations in temperature and precipitation throughout the range, though correlations with these climate variables and topographic parameters have been observed (Busing *et al.*, 2005; Desta *et al.*, 2004).

Precipitation increases and evapotransporation decreases as elevation increases due to orthographic lifting (Busing *et al.*, 2005). Orthographic lifting and the resulting precipitation is increased on the western side of Blue Ridge Mountains since prevailing wind direction is from the west with exception of tropical storms and hurricanes that most often come from the south and southeast. In comparison with the temperature at the foothills on the Tennessee side of the mountains, the average high temperature at the foothills on the North Carolina side was higher and the average low temperature was lower (Gaffin *et al.*, 2009). This wide diurnal variation indicates that the foothills on the leeward side of the mountains are in a drier air mass than the windward side. Rainfall storm frequency of the southern Appalachians determined from isopluvial national maps for storms with a 5, 10, 25, 50, and 100 year return period have precipitation normals of 114, 127, 152, 165, and 178 $mm \cdot day^{-1}$, respectively (Hershfield, 1961).

The average temperature between 1921 and 2008 for winter, spring, summer, and fall was 40.3, 55.6, 72.4, and 57.6 °C, respectively (SRCC, 2009). Gaffin *et al.* (2009) found that the moist adiabatic lapse rate, which is the rate of temperature change with changing altitude, ranges between 3 and 4 ° F per 1000 ft at sites they compared. Temperature variation between the sites was due to temperature inversions and the rain shadow effect. Additionally, temperature varies on average

from a north aspect by -0.3, 5.3, 4.2 °C for the east, south, west, and southwest aspects, respectively, during a study completed in 2004 (Desta *et al.*, 2004).

1.2.2. Geology

Geologic maps and reports by King *et al.* (1968) and Southworth *et al.* (2005) provided the information for this section except where it is indicated otherwise. Most pertinent to this study, bedrock of the Ocoee Supergroup and recent debris flows are presented here (Figure 1.3).

1.2.2.1. Historical Geology

The present-day topography of the Smoky Mountains was largely formed between 350 and 300 million years ago during orogenic events, though counteracting process such as erosion and isostatic rebound continue to control the region's topography (Matmon *et al.*, 2003a). The highlands of the Range constitute a horst block formed during the Alleghanian Orogeny or younger by the Gatlinburg Fault System and earlier by the Greenbriar fault in the early Paleozoic (Southworth *et al.*, 2005). The Gatlinburg Fault System in the Smoky Mountains is one of the many systems of the Blue Ridge Fault systems. These fault systems fascilitated the movement of Precambrian and Early Paleozoic metamorphosed volcanic and sedimentary rocks over the Paleozoic sedimentary rocks of the Valley and Ridge province (Hatcher and Goldberg, 1991). Most of the faults were initiated during the Taconic and Alleghanian Orogenies when terrains accreted to the proto-North American eastern coast and when much of the regional metamorphism had occurred. The majority of rocks in the range have been metamorphosed during these and other orogenies. Further uplift during the Mesozoic and early Cenozoic is indicated by fission track and cosmogenic nuclide evidence (Matmon *et al.*, 2003b; Southworth *et al.*, 2005).

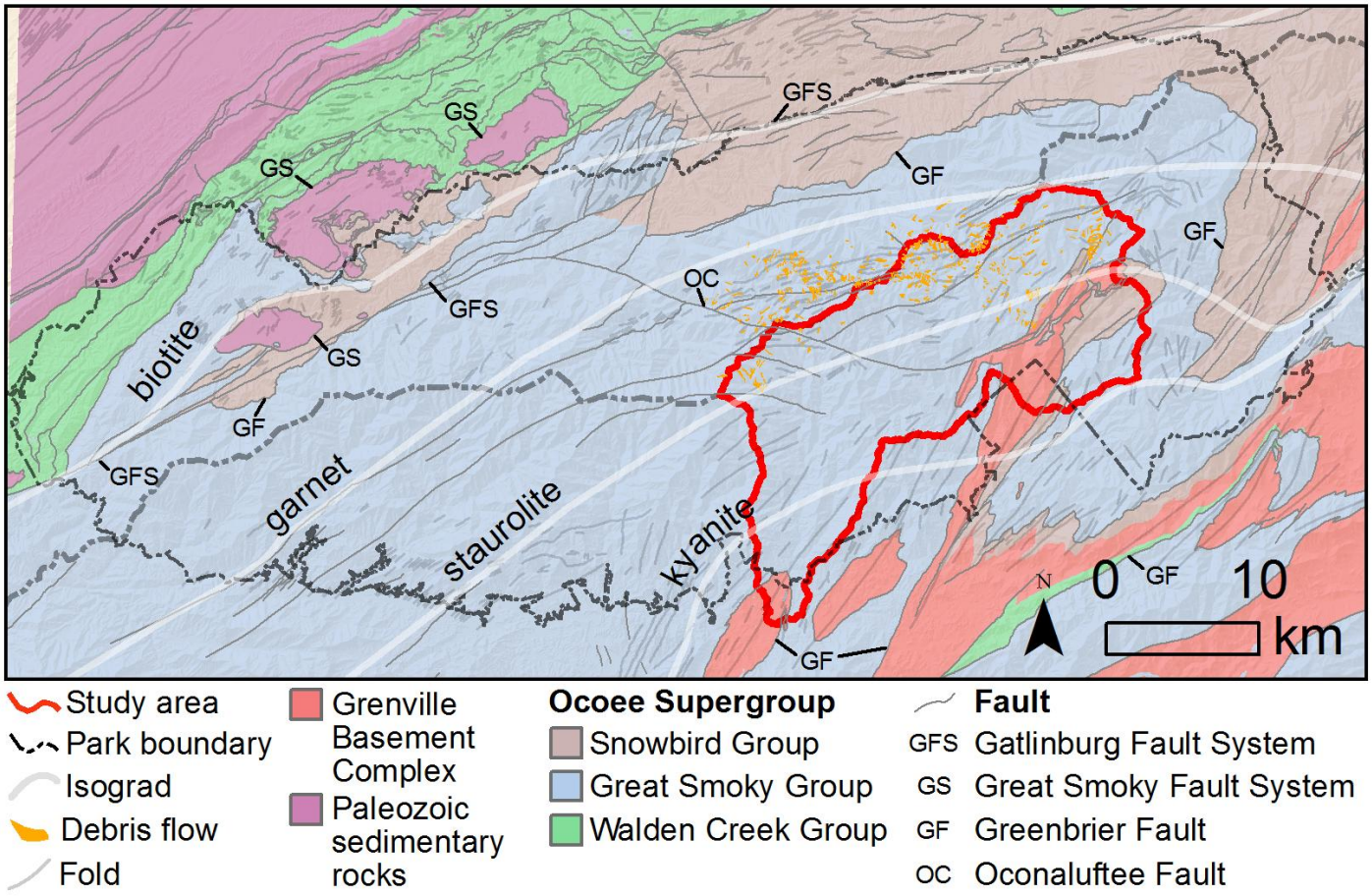

Figure 1.3. Generalized bedrock and debris flow spatial data (Southworth *et al.* 2005) shows that the study area is largely underlain by the Ocoee Supergroup. Generally, metamorphic grade of metasedimentary rocks increases from the northwest to the southeast.

Landform relics of the last glacial maxima occurring approximately 19,000 to 23,000 years before present (ybp) exist within the modern landscape. The maximum southern extent of glacial advances never reached the Smoky Mountains, though a periglacial environment existed here (Pittillo *et al.*, 1998). Southworth *et al. (2005)* summarizes the numerous publications that provide the interpretation of two types of boulder deposits that indicate that a periglacial environment did exist here during the late Pleistocene. Block fields and block streams, sheet-like accumulations of blocks that commonly mantle many of the mid to high elevation hillslopes and channels, extend downslope typically from near the uppermost part of a ravine. These suggest that gravity, solifluction, freeze-thaw, and ice wedging were the modes of transportation for boulders during periglacial conditions. Evidence of an increased frequency of debris flows is provided by the large debris fans in lower elevation valley floors. The most common age range of debris fans in the Smoky Mountains, calculated with ^{14}C by other researchers, is 16,000 to 18,000 ybp (Kochel, 1990).

1.2.2.2. Bedrock and Surficial Deposits

Bedrock is principally derived from early Paleozoic rifted continental margin deposits that formed metasedimentary rocks stratigraphically above now metamorphosed basement rocks. Metasedimentary rocks are contained within the Neoproterozoic Ocoee Supergroup that formed in a basin created by the rifting of Rodinia during the formation of the Iapetus Ocean 800 to 545 million years ago (MYA). The Ocoee Supergroup is divided into the Snowbird, Great Smoky, and Walden Groups. The site of this study is primarily underlain, in stratigraphly decreasing order, by the Copperhill Formation, Anakeesta Formation, and Thunderhead Sandstone of the Great Smoky Group.

The units of the Great Smoky Group consist of interbedded: (1) metasandstone, conglomerate, metagraywacke, and/or slate; and (2) dark-colored graphitic and sulfidic metasiltstone. The rock types of (1) were deposited by turbidity currents, which are underwater avalanche-like events that result from earthquakes,

faulting, and other disturbances. The metasiltstone of (2) was deposited in a sub-basin of the Ocoee basin. The chemical characteristics of the metasiltstone are due to the precipitation of graphitic and sulfidic sediments resulting from the combination of turbidites, which are low velocity water present in deep basins, and oxygen-poor environments. Exposed bedrock in the majority of the North Carolina side of the Smoky Mountains can also be described as containing a geolithology of graphitic and sulfidic siliciclastic rocks. This lithology includes siliciclastic rocks with major and local occurrences of graphitic and sulfidic rocks defined by the presence of iron-sulfide minerals.

1.2.2.3. Debris Flows

In the Smoky Mountains small rock falls, debris slides, and debris flows have resulted in large debris fans and hillslopes blanketed with colluvium. Debris flows, the focus of this study, cause more pronounced geomorphic alteration and wider destruction in the region compared to the other types of hillslope failures due to their size (Wooten *et al.*, 2008).

Debris flows occur when an increase in soil pore water pressure, resulting from heavy precipitation, alters soil porosity to a critical state where the soil no longer can support deformation (Iverson *et al.*, 2000). The hillslope fails on a plane between regolith and bedrock or between heterogeneous layers of soil (Southworth *et al.*, 2005). The mass then flows where hillslope angles, channel length and junction angles permit rapid transportation of soil, rock, and vegetation down slope (Varnes, 1978). In the Smoky Mountains, failure most often occurs on hillslopes with slopes between 35 to 40 degrees, atop the Anakeesta, Copperhead, and Thunderhead bedrock units of the Great Smoky Group, and especially in areas with regolith less than a meter thick (Figure 1.3; Bogucki, 1976; Southworth *et al.*, 2005). Numerous small rockfalls, slides, and slumps have occurred along roads and trails that are likely due to the destabilizing effect of cutting into the hillslope and the adjacent unconsolidated regolith, though the influence of roads and trails upon hillslope failure and specifically debris flows is not fully understood (Bogucki, 1976).

Bogucki (1976) distinguished three sections in debris flows he surveyed in the Smoky Mountains. The uppermost section where the landslide initiated, the scar head, is most often the steepest and fully devoid of vegetation until vegetation reestablishes years after the hillslope failed. The central section, the slide track, has slopes between 15 and 30 degrees, and is much narrower and deeper than the scar head. It is covered with colluvium and alluvium, and may be covered by some vegetation that survived the flow. The lowest section, the depositional area, occurs where the valley slope decreases rapidly. Debris flow material deposition has been observed to occur at other locales often at slopes near 0.03 (Stock and Dietrich, 2003). The lowest section is triangular in shape and often contains a high concentration of logs delivered by the debris flow.

Evidence of debris flow occurence extends to at least the last several thousands of years in the area. The debris fans found in the lower reaches of the mid-elevation valleys are the result of intensified debris flow activity during the Pleistocene (Kochel, 1990; Southworth *et al.*, 2005). These fans are composed of lenses of angular cobbles and gravel that are supported in a silt and fine sand matrix. An increased period of debris flow activity, inferred from a high proportion of sampled debris fan deposits with an age range of 16,000 and 18,000 ybp, is due to retraction of the summer polar front that allowed tropical moisture to return to the southern Appalachians subsequent to the last glacial maxima, which occurred between 19,000 to 23,000 ybp (summarized by Kochel, 1990). Increased sedimentation in the early Holocene was observed by Leigh and Webb (2006) in the lower reaches of Raven Fork that is likely the record of increased debris flow activity due to higher frequency of heavy rainfall during this time. Further, the first terrace entrenchment has been in place for the past 6000 years and easily accommodates a 100-year flood, and possibly a 500-year flood, as determined by hydraulic modeling, which reveals the valley's adaptation to high flows (Leigh and Webb, 2006). At present the fans are being incised by streams primarily through removal of fine sediment.

Recent debris flow activity provides insight into the types of storms that produce debris flows in the Appalachians. Bogucki (1976) documented a cloudburst that occurred in the Smoky Mountains in 1951 that dumped more than 100 mm over approximately one hour that resulted in numerous debris flows. Wooten *et al*. (2008) documented 155 slope movements including at least 33 debris flows from Hurricanes Frances and Ivan that passed through western North Carolina in 2004 causing five deaths. Rainfall during Hurricane Ivan contained short duration rates of 150 to 230 $mm \cdot h^{-1}$. In northwestern Virginia, thousands of debris flows and more than 125 deaths resulted from the remnants of Hurricane Camille in 1969 that dumped 711 mm over a 7 to 8 hour period (Eaton *et al.*, 2003).

Debris flow frequency differs largely throughout spatial and temporal scales and is related to storm return frequency of an area. Precipitation intensities of 125 to 560 $mm \cdot day^{-1}$ have resulted in debris flows in the southern Appalachians (Figure 1.4; Witt, 2005). Comparatively, Wieczorek (2000) determined a debris flow triggering precipitation threshold of 70 $mm \cdot h^{-1}$ for 2 hours in the Blue Ridge Mountains of Virginia by comparing numerous storms throughout the central Appalachians. The return period of a storm that delivers the threshold precipitation amount in the southern Appalachians is 10-year storm (Hershfield, 1961), though Bogucki (1976) indicated that at least a 100-year storm was required to cause debris flows. However, the risk of debris flow is low at the minimum threshold of debris flow initiation, and site factors and antecedent moisture conditions also are factors in hillslope failure.

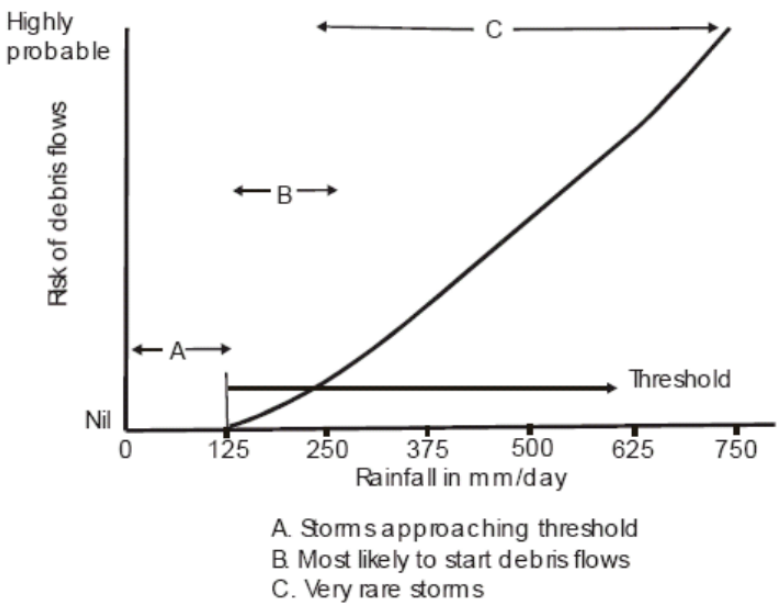

Figure 1.4. The rainfall threshold of debris flow initiation in the southern Appalachians is approximately 125 mm day^{-1} since this is the minimum observed precipitation intensity required to initiate debris flows in the region. Figure is from Witt (2005).

Debris flow recurrence in first-order watersheds of the Smoky Mountains is estimated to be every 400 to 1600 years in first-order basins (Kochel, 1990). The recurrence interval in Northern Virginia is less frequent: 2000 to 4000 years in first-order watersheds though regional watersheds have been subject to debris flows within 10 to 15 year intervals (Eaton *et al.*, 2003). Southworth *et al.* (2005) summarizes the known years of rainfall events that have resulted in debris flows that occurred in the Smoky Mountains: 1938, 1940, 1942, 1943, 1951, 1956, 1967, 1971, 1975, 1984, and 1993. The seemingly contradiction in the southern Appalachians of a 100 year-storm required to initiate debris flows though much longer debris flow recurrence interval is primarily due to the nature of the recurrence interval calculation in the Smoky Mountains. Kochel *et al.* (1990) determined this value for first-order watersheds, thus higher order watersheds and entire areas, such as the entirety of the Smoky Mountains, will have a shorter recurrence interval.

1.2.3. Vegetation

Vegetation within the Smoky Mountains is extraordinary for its old growth stands, species diversity, and high degree of endemism. Old growth forest tracts in area are the largest in the eastern United States (Keller *et al.*, 2004). The rich diversity of plant species is largely explained by past glaciations, wide elevation variation, habitat longevity, and limited human impact (Whittaker, 1956). Cataloging the 100,000 species of living organisms estimated to live in the Park, including flora and fauna, is the primary goal of the All Taxa Biodiversity Inventory – a project of the National Park and Discover Life in America, a non-profit organization that coordinates this project (White and Moore, 2000).

In the Smoky Mountains, old growth forests, mature soil horizons, and bedrocks foliation and dip planes create opportunity for mass failure and a complex grain size distribution. Thick vegetation helps to stabilize slopes and soil, saprolite, and residuum up to 10 m deep cover these slopes (Southworth *et al.*, 2005). However, shallow depth of regolith atop steeply sloping beds encourages failure when soil cohesion and the tensile strength of vegetation needed to support the slope is surpassed by increases in soil pore pressure and/or shear stress inflicted from a translating debris flow. Hales *et al*. (2009) noted the lower tensile strengths of tree roots in hollows compared with roots of trees on ridges and noses in an area about 80 km south of the Smoky Mountains that contains similar topography, bedrock, and hardwood tree species. A shrub species that is rapidly expanding in the region due to fire suppression, Rhododendron (*Rhododendron maximum),* has a notably low tensile strength and shallow root system, increasing the potential of hillslopes dominated by this vegetation type to fail.

A summary of the region's vegetation history by Pittillo *et al.* (1998) follows. The wetter, warmer climate 245 to 120 MYA in North America likely produced an environment ideal for the distribution and evolution of ferns, seed ferns, cycads, and gymnosperms. Angiosperms appeared 130 to 120 MYA, though species similar to the flora present in the Smoky Mountains today did not arise until around 65 MYA.

Changes in climate during the glacial periods of the past two million years are widely believed to be responsible for much of the current vegetation, notably the remarkably high diversity. Montane environments exhibit unique conditions for vegetation distribution through glacial cycles since low-temperature tolerant species migrate horizontally during cooler periods, but then migrate to higher elevations when temperatures become warmer (Whittaker, 1956). The alpine and boreal species of the Smoky Mountains were able to relocate to what was a tropical environment during glacial periods and then retreat to higher elevations during warmer times.

The high relief of the Smoky Mountains permits microclimates and numerous types of overstory forest types. Regionally unique to this Range are the fir and spruce communities along the ridges and montane cove forests that dominate much of the lower to mid elevations of the North Carolina side. The higher elevations of this forest type are largely old growth forests containing species such as sugar maple, beech, yellow birch, red oak, eastern hemlock, and tulip poplar. Present vegetation in the Smoky Mountains is placed into twelve generalized classes. Northern hardwood forests are the most prevalent and cover the highest elevations second only to the Spruce-fir forest class (Figure 1.5). Elevation, moisture, slope, and aspect strongly control what vegetation type grows in a given area. Currently, cove, oak-hickory, pine and hemlock forest dominate low and middle elevations (Whittaker, 1956). Spruce-fir and northern hardwood forests dominate elevations above 1400 m. Vegetation that prefers acidic soils is dominant in the Southern Blue Ridge Mountains as a result of the chemical weathering of bedrock by the moist, temperature climate (Pittillo *et al.*, 1998).

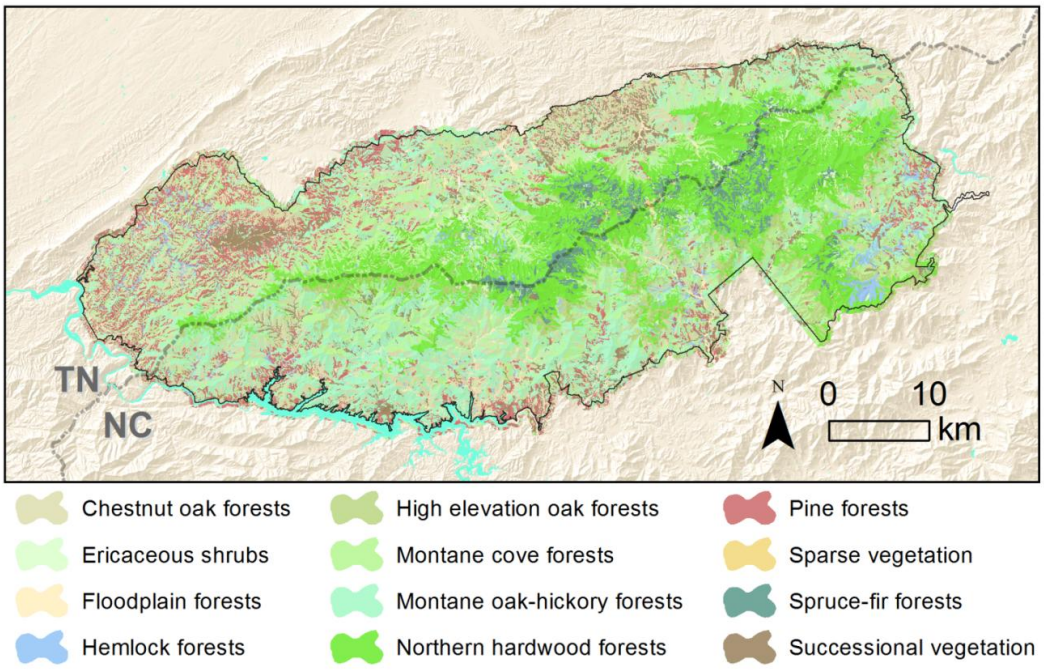

Figure 1.5. Overstory vegetation geospatial data was created by Madden *et al.* (2004) from 1:12,000 scale aerial photographs and field traverses.

Human resource extraction and habitation has impacted the area, though anthropogenic impacts upon the environment have been reduced here since the National Park establishment. Past and present invasive species have negatively impacted the survival of native flora. The chestnut blight in the mid 1900's dramatically changed the Park's canopy (Woods and Shanks, 1959). Presently, the hemlock whoolly adelgid, an aphid native to east Asia, threatens the approximately 4,000 acres of hemlock extent in the Park (Johnson *et al.* 2000). Logging between 1790 and 1900 was selective, only trees that were the desired type and size were cut (Bratton and White 1981). Harvesting was limited to lower and easy accessible elevations. Large-scale mechanized logging began around 1900 that made use of railroads and skidders allowing more rapid and complete logging. Harvesting drastically disturbed soils and reached the scale of entire watersheds and entire watersheds could be deforested in 10 to 15 years (Pyle, 1988). 51% of North Carolina side of GRSM was logged. Trees remnants and sparks from logging

equipment increased fire risk. Logging operations ceased prior to the official park dedication in 1940 (Pyle, 1988). Fires between 1910 and 1930 were largely due to logging operations exacerbated by dry weather conditions and were much more intense than fires begun by settlers (Harmon, 1983; Pyle, 1988). The National Park was exposed to less human-caused fires after its establishment in 1934, which dramatically affected community composition and age structure. Limited anthropogenic land disturbance has occurred in the area due to the difficult terrain and land use restrictions applied by National Park status (Pyle, 1988).

1.3. Research Objectives

The scope of debris flows acting through the geomorphic realms: sediment transport, vegetation, and fluvial ecology; motivates this study. This study investigates two facets of debris flow-dominated channels in the Great Smoky Mountains of the southern Appalachians. The first topic, development of debris flow inventorying techniques with remotely obtained data, is a persistently present topic in scientific literature (Carrara and Pike, 2008; Martha *et al.*, 2010; Moine *et al.*, 2009). Commonly used techniques often rely upon the statistical differences of land spectral and topographic properties to classify the land surface into two populations: debris flow and non-debris flow areas.

Secondly, progressive downstream bedload grain size fining is a widely understood trend, though evidence exists of the opposite trend in debris flow-dominated channels (Brummer and Montgomery, 2003). The impacts of this opposite trend upon channel geomorphology and ecosystems has been rarely studied, thus in addition to determining if downstream coarsening is occurring in the study area, grain size trends relative to salmonid distribution will be explored. Investigations of salmonid spawning grains have been conducted since the 1950's in numerous regions including the southern Appalachians (summarized by Kondolf and Wolman, 1993), though recent efforts to model grain size distribution has been

focused upon salmonids in the northwestern and northeastern regions of North America.

This study aims to advance our ability to map debris flows and understand grain size trends in mountainous streams in the Smoky Mountains. The spatial extent of debris flow-dominated channels must be determined in order to achieve these objectives, thus the first objective of Chapter 2 is to locate these channels in the study area. Also in this chapter, an attempt to improve landslide inventory technique by conducting land classification only upon areas that drain to debris flow-dominated channels is presented. This attempt tests the hypothesis that inventory efficacy increases when the extent of unstable hillslopes are limited, thus improving the statistical classification of land surfaces. Further, this study examines potential linkages between debris flows, grain size distribution, and salmonid habitat. Grain size distribution and its control upon salmonid is the subject of Chapter 3. In summary, the objectives of this thesis are:

(1) locate the extent of debris flow-dominated channels in the Great Smoky Mountains,
(2) compare debris flow inventories created of the entirety of the study area and, experimentally, only of the drainage areas of debris flow-dominated channels, and
(3) determine grain size trends throughout the trunk channels of the study watersheds and consider whether trout habitat potential, based upon grain size trends, differs by the dominant channel type.

CHAPTER 2: IMPROVING LANDSLIDE INVENTORIES BY LIMITING LAND CLASSIFICATION TO DEBRIS FLOW-DOMINATED CHANNELS

2.1. Background

Determination of the spatial and temporal occurrence of debris flows provided by landslide inventories is an important component of hazard modeling (Brardinoni *et al.*, 2003; Carrara and Pike, 2008; Malamud *et al.*, 2004). Slope instability models, such as the widely used SHALSTAB (Shallow Landsliding Stability Model) and SINMAP (Stability Index Mapping), use landslide inventories to evaluate model results or to calibrate parameters of the models (Wooten *et al.*, 2006). The model products are used to guide landuse planning in order to prevent disastrous outcomes from landslides (Dietrich *et al.*, 1998). Unlike the models, the goal of an inventory is to delineate and/or characterize the landslide in a given area and is not intended to forecast future landslides. Landslide inventories have also been used in analyses of landscape evolution processes (Korup *et al.*, 2010; Stock and Dietrich, 2003), though knowledge of a landscape's evolution is rarely utilized when performing inventories. Controls upon mountain elevation, carried out in part by mass wasting, remove regolith systematically across landscapes (Hovius *et al.*, 1998), which limits the extent of hillslope failures to areas that may be predicted with landscape topographic and evolution analyses.

Many published landslide inventory methods follow a similar approach that can be generalized into the following steps: (1) a region with a history of landslides activity is selected, (2) the landslide identification and delineation technique is applied to the region, (3) known false positives, such as roads, are removed, and (4) evaluation is conducted to determine the efficacy of the technique. Classification of land areas in Step 2, into landslide and non- landslide populations, is accomplished by locating areas with the hypothesized properties of the two populations. The properties of the populations are based upon a statistical characterization of

homogenous clusters calculated with topographic, spectral, and/or contextual datasets.

This chapter investigates the efficacy of a landslide inventorying technique to improve landslide inventories that may also result in decreases in time and cost commitments of routine inventories. This technique segments and classifies only areas that are susceptible to the current phase of mass wasting by removing these subareas prior to Step 2 described above. Areas susceptible to mass wasting will be those areas that drain to debris flow-dominated channels. Conducting land surface characterization in these areas is hypothesized here to result in a more accurate classification of debris flow and non-debris flow sites since removal of areas not prone to debris flows that can introduce error is reduced. Limiting areas where inventories need to be conducted that are facilitated with remotely-based techniques may provide a highly efficient method to conduct routine inventories.

Debris flows are the largest and most recurrent mass failure in the study area, motivating the decision to focus only upon this landslide type in this study. Additionally, smaller debris slides and rock falls are difficult to distinguish in aerial photography and other types of landslides vary in morphology, thus must be classified by different parameters (Barlow *et al.*, 2006; Malamud *et al.*, 2004). The debris flow head, track, and toe are considered as one unit since it is difficult and often erroneous to attempt to distinguish these areas (Malamud *et al.*, 2004). The intended output of classification in this study is a map of debris flow areas that primarily includes the head and track of historical debris flows.

The objectives of this chapter are to locate the extent of debris flow-dominated channels and to compare inventories created from classification of the entire study area and areas that just drain to debris flow-dominated channels. Classification will be conducted with an aerial photograph and topographic parameters derived from a digital elevation model (DEM). The inventory will be evaluated by comparing the classification output with debris flows mapped by the USGS. Analyses of watershed parameters will be used to postulate aspects of this

study area's landscape evolution, providing further credence to the quantitatively determined transition from fluvial- to debris flow-dominated channels. A comprehensive understanding of knickpoint formation and propagation in the Smoky Mountains is unknown and is pertinent to the extent of debris flow-dominated channels. Therefore, the distribution of knickpoints in the study area related to bedrock and topographic features will be used to propose facets of the landscape's evolution in the study area.

2.1.1. Landscape Evolution and Dominant Channel Types

Debris flows can be the primary agent of denudation superseding the influence of fluvial incision in valleys with high slopes and moderately-sized drainage areas, thus can be important in a landscape's evolution (Stock and Dietrich, 2003). Rock uplift and associated increases in rock mass and crustal shortening is achieved in convergent tectonic zones. Concomitantly, agents of denudation act to redistribute mass across the landscape that approaches and sometimes counteracts the uplifted mass in what is referred to as steady state topography (Hack, 1960). Local relief in newly active orogens may be modest, though as drainages develop and sediment yields increase, so does the magnitude of the processes of channel incision, namely abrasion, plucking, and saltation. The magnitude of processes depends upon sediment availability and entrainment from hillslopes to the channel, thus water discharge along with slope strongly control stream incision (Howard, 1994). Once channels are entrenched and slopes reach a critical threshold that is site specific, mass wasting begins and is the dominant process by which watersheds expand and the planform geometry of the landscape is roughly fixed (Hovius *et al.*, 1998; Howard, 1994). As uplift continues, slows, or ceases, variations in removal of mass due to variations in bedrock type and climate may cause spatial variability in a landscape's evolution between erosion carried out by fluvial and mass wasting processes (Crosby and Whipple, 2006).

A non-uniform rate of stream incision throughout a fluvial network may be expressed in a channel's longitudinal profile. Incision rates can rapidly change in a stream where upstream reaches have yet to respond to a base level fall, a decrease in elevation to which the channel erodes, or due to stream incision rate contrasts at tributary junctions (Crosby and Whipple, 2006). Adaption of channels' longitudinal profiles do not occur concomitantly throughout a fluvial network, but rather are transmitted upstream time-transgressively as downstream stream incision drives steepening and increased erosion of the adjacent hillslopes. Knickpoints, defined as a local change in channel slope or a highly convex reach in a channel's longitudinal profile, develop at points or zones along the profile. Crosby and Whipple (2006) propose two end-member models of knickpoint propagation: transitory and stationary knickpoints. (1) Knickpoints develop as transient features in response to base level fall and may transgress to a stable feature at a point upstream. (2) Stationary knickpoints can develop at a threshold where sediment supply outpaces sediment transport, due to local variation of rock mass strength, or as the end product of a transitory knickpoint. Transitory knickpoints may develop into stationary knickpoints once stream power from upstream drainage areas decreases below a threshold sufficient to downgrade the knickpoint, effectively halting further upstream propagation.

The transition from debris flow to fluvial incised valleys is often observed to occur in channels where reach average slope decreases below 0.03 to 0.10, which typically coincides with drainage areas between 0.1 to 1 km^2, dependent upon climate, basin geology, and the degree of geomorphic relaxation to a disturbance (Seidl and Dietrich, 1992; Stock and Dietrich, 2003). Increased channel incision upstream from the scaling break is believed to be caused by bedrock scour resulting from debris flows and may be intensified by increased weathering in higher reaches (Seidl and Dietrich, 1992). Systematic removal of regolith, correlated with drainage area and slope, is largely driven by upstream propagation of knickpoints that critically steepens channels followed by hillslope response (Gallen *et al.*, 2011;

Stock and Dietrich, 2003). Determining the extent of hillslopes that are responding by mass failure to critically lowered channels may improve existing landslide inventorying techniques.

2.1.2. Existing Techniques to Create Debris Flow Inventories

At the scale of landscapes, the signature of debris flows in the resolution of single mass failures may be difficult to determine given their small size and overprinting processes. This is the case in the southern Appalachians despite millions of years of debris flows activity (Kochel, 1990). In time scales smaller than debris flow reoccurrence interval and spatial scales equivalent to mass failures, the effects of debris flows upon geomorphology and vegetation are detectable in the field and in aerial photography for a period of years after the debris flow occurred (Figure 2.1). Revegetation is most rapid in the depositional zone, and revegetation rate after the mass failure decreases up the debris flow scar (Bogucki, 1976). May and Gresswell (2004) determined that vegetation may take approximately 3 to 7 years to reestablish upon debris flows in a study in the Oregon Coast Range. However, field observations in the Smoky Mountains during this study indicate that revegetation rate appears to be highly variable. This creates the potential for incomplete landslide inventories if vegetation is a highly weighted criterion of remotely-based methods of landslide classification.

Aerial photography interpretation (API) was the ubiquitous method to create inventories up to the early 21st century. Recently, researchers have developed alternative, automated methods motivated by API's subjectivity in interpretation and inefficiency (Carrara and Pike, 2008; Malamud *et al.*, 2004). Additionally, increases in availability of DEMs have incited efforts to develop new methods. Present-day automated methods conducted with geographical information systems (GIS) and photo processing software share similarities in inputs, methods, and results (Table 2.1). A review of remote sensing publications in relation to landslides by Metternicht *et al*. (2005) shows that aerial photography has typically been used for manual

delineation, characterization, and evaluation. Currently, satellite imagery is the most frequently used imagery type in automated and semi-automated debris flow classification techniques due to recent increases in resolution from 30 m to less than 5 m. Satellite imagery also permits large areas to be inventoried at a more frequent interval than aerial photographs are obtained. The satellite, *Systeme Probatoire d'Obsérvation de la Terre* (SPOT), is often used since it captures multispectral imagery with 10 m resolution and panchromatic imagery up to 2.5 m resolution. Multispectral imagery is commonly used since a normalized difference vegetation index (NDVI) map, which is used to identify green leaf area, can be produced from the infrared band (Barlow *et al.*, 2006; Martha *et al.*, 2010). Panchromatic imagery is beneficial since this imagery is highly sensitive to wavelengths in visible light spectrum and records a high resolution, thus features can be more accurately identified.

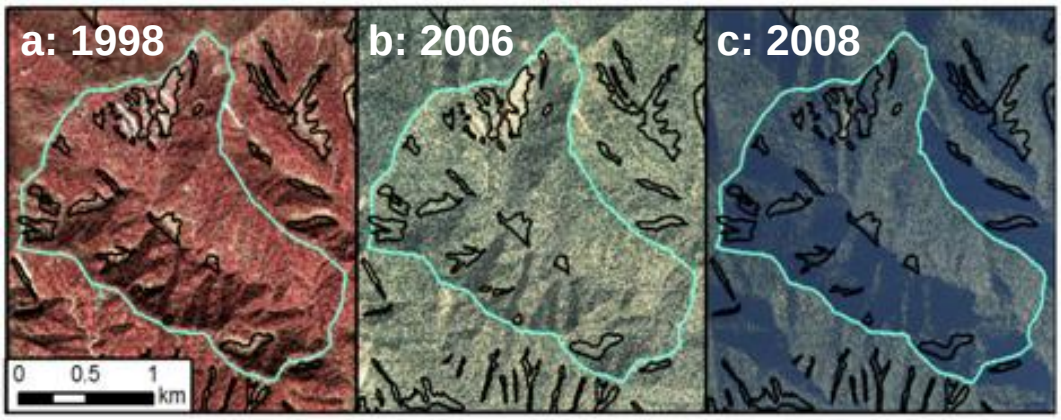

Figure 2.1. Orthophotograph time series: (a) A 1 m color composite infrared Digital Ortho Quarter Quad photo, (b) a 1 m National Agriculture Imagery Program true color photo, and (c) a 1 m true color National Agriculture Imagery Program photo of the watershed (light blue boundary) of Frowning Rock Prong, a tributary of Bradley Fork.

Automated landslide delineation techniques also differ by the use of supervised or unsupervised classification algorithms and by the segmentation method that is used to delineate homogenous objects. Classification algorithms are

Table 2.1. A summary of landslide classification publications.

Reference	Methods and Evaluation Results
Nichol and Wong, 2005	Medium resolution SPOT (resolution = 20 m) used for landslide change detection. **Evaluation:** 70% of landslides in an aerial photo (res = 0.35 m) inventory identified.
Barlow *et al.*, 2006	Supervised classification using image object as classifiers. Multispectral (res. = 10 m) SPOT-5 imagery and a DEM (res. = 25 m) derived from 1:50000 topographic maps were used to create the following inputs for image segmentation: NDVI, slope, and plan curvature. Multiscale segmentation conducted with Definiens software. **Evaluation:** 60% of debris flows in 1:15000 scale aerial photographs stereoscopic image interpretation inventory identified.
Borghuis *et al.*, 2007	[1]Unsupervised and [2]supervised classification with inputs, SPOT-5 multispectral imagery and a mask removing slopes less than 28°, **Evaluation:** 63% of landslides identified from unsupervised classification and 39% identified from supervised classification compared with an aerial photo inventory (res. = 0.35 m) inventory.
Van Den Eeckhaut *et al.*, 2007	Manual delineation by 7 “experts” from lidar derived relief shade, slope, and contour maps. **Evaluation:** Experts identified 55-73% of landslides, when compared with field inventories, in lidar derivative maps.
Moine *et al.*, 2009	Inputs were qualitative indicators from aerial ortho-photo interpretation of multi-temporal infrared and natural color photos. Unspecified image segmentation conducted with Definiens software. **Evaluation:** 26% of landslides identified with panchromatic band of SPOT-5 (res. = 2.5 m) inventory.
Martha *et al.*, 2010	Resourcesat-1 multispectral imagery (res. = 5.8 m) was used to create the following input for image segmentation: spectral characteristics, NDVI, flow direction, curvature, stream network, and shaded relief map. Photogrammetrically derived DEM (res. = 10 m). Chessboard segmentation conducted with Definiens software. **Evaluation:** 69% classification accuracy of land correctly evaluated with stereoscopic image interpretation.

designed to determine discrete land classes that approximate landslide boundaries. Supervised algorithms use training maps, areas where the landslide area is known. Unsupervised algorithms rely upon the statistical differences in data to distinguish classes. Methods of segmentation and classification have transgressed sequentially through the following: pixel-based, object-oriented and contextual object-oriented analyses.

Image segmentation by the spectral values of individual pixels has been shown to be ineffectual when not coupled with additional parameters given the importance of geomorphic context that exists in areas larger than cell size (Barlow *et al.*, 2006). While some efforts are dominantly heuristic, relying solely upon imagery (Moine *et al.*, 2009), other studies incorporate additional datasets that provide theoretical justification for initiation of landslides (Martha *et al.*, 2010). Object-oriented image segmentation has proved to be a powerful tool since it incorporates not just individual pixel values but properties of data in adjacent areas (Martha *et al.*, 2010). Image objects are still in part delineated by homogeneity of adjacent pixel spectral values, but contextual information, such as the objects' shape, texture, and size, also determine the final segmentation. Object-oriented analysis (OOA) incorporates morphometrics of objects pertinent to debris flows, such as their length to width ratio (Barlow *et al.*, 2006) and stream order (Martha *et al.*, 2010), and improves the subsequent classification of debris candidates by limiting false positives.

Several recent efforts have used the proprietary software, Definiens bio-medical image analysis program (Definiens, 2007) to conduct OOA due to the numerous segmentation and image analysis routines as well as modifiable parameters that are included in this software (Moine *et al.*, 2009). Standard segmentation techniques built into routines in this program include (1) chessboard, the image is divided into a grid with a cell's values determined by the dominant values of pixels within the cell; (2) quadtree, the maximum possible size of adjacent cells that share homogeneity criteria are grouped in squares of a variable size; and

(3) multiresolution, an optimization procedure determines the minimum heterogeneity of image objects for inputted resolutions (Definiens, 2007). This program also includes tools that produce texture maps of imagery inputs, and can measure shape and size of segments. Researchers that use this program have reported that it is sensitive to the criteria used to classify the segmentation primitives, imagery units resulting from the segmentation algorithm. Moine *et al*. (2009) created a rule-based classification scheme, where the rules were based upon "qualitative indicators" determined through API. Martha *et al*. (2010) also created rulesets for classification of false positives and landslides, but did so subsequent to segmentation, thus allowing them to determine the rulesets based upon the image primitives.

Some studies have incorporated lidar data to compare inventory techniques and to create inventories. Brardinoni *et al*. (2003) determined that up to 85% of failures in their study area, British Columbia, was obscured by forest canopy by comparing API and field survey inventories. Van Den Eeckhaut *et al*. (2007) compared the results of seven geomorphologists who manually delineated landslides with lidar-derived hillshade, slope, and contour basemaps. 73% of the landslides that were field surveyed were delineated by the geomorphologists. These examples provide motivation for this study to use lidar data in land surface classification to take advantage of the following benefits of this data type: the high resolution of the data, the ability to model the topography of the bare earth, and its ability to capture landslide features.

2.2. Methods

The extent of the drainage areas of debris flow-dominated channels were determined with analyses of trunk channels' drainage area and slope, and parameters of the study watersheds. Debris flow inventories of the entire study area and drainage areas of debris flow-dominated channels were created with supervised classification. Classification was performed using the inputs, topographic derivatives

and a NDVI map. Results were evaluated with georeferenced geologic data. Preparation of analyses inputs, training and evaluation maps, and classification was conducted with GRASS GIS, ArcGIS, and MATLAB.

2.2.1. Study Watersheds

The five study watersheds totaling 343 km^2 (SM in Figure 2.2) are underlain with metamorphosed rocks of the Ocoee Supergroup and Grenville Basement Complex (Ygb). The Grenville Basement Complex is dominantly biotite gneiss that outcrops mostly in SM-4 and 5, and minor amounts in SM-1 and 3. Southworth *et al.* (2005) suggests that the Copperhill Formation (Zch) and Thunderhead Sandstone (Zt) are likely the same unit that are both characterized by massive and graded beds of course-grained metasandstone interbedded with metasiltstone. However, the Copperhill Formation is distinguished by the presence of interbedded slaty rocks. The Anakeesta Formation (Za) is principally composed of sulfidic slate, metasiltstone, and phyllite. This formation is highly resistant to weathering and is exposed atop many of the higher points in the Smoky Mountains. Where the Anakeesta Formation and other formations containing sulfidic rocks are exposed, they often weather to a red color due to the oxidation of iron-sulfide minerals of the rock. Minor amounts of the Roaring Fork Sandstone (Zrf), Longarm Quartzite (Zl), and Wading Branch Formation (Zwb) outcrop adjacent to the Grenville Basement Complex. Many mid to high elevation hillslope areas are blanketed with block fields (Qc) of periglacial origins that is contained within the same map unit as recent talus. Large debris fans (Qd), expansive deposits of bouldery diamicton in lower elevation valley floors, are believed to be the result of increased debris flow activity in the late Pleistocene and early Holocene. A historical debris flow (Qdf) map unit includes the initiation zone, track, and often the deposit location of the bouldery diamiaction and vegetation transported by the debris flow.

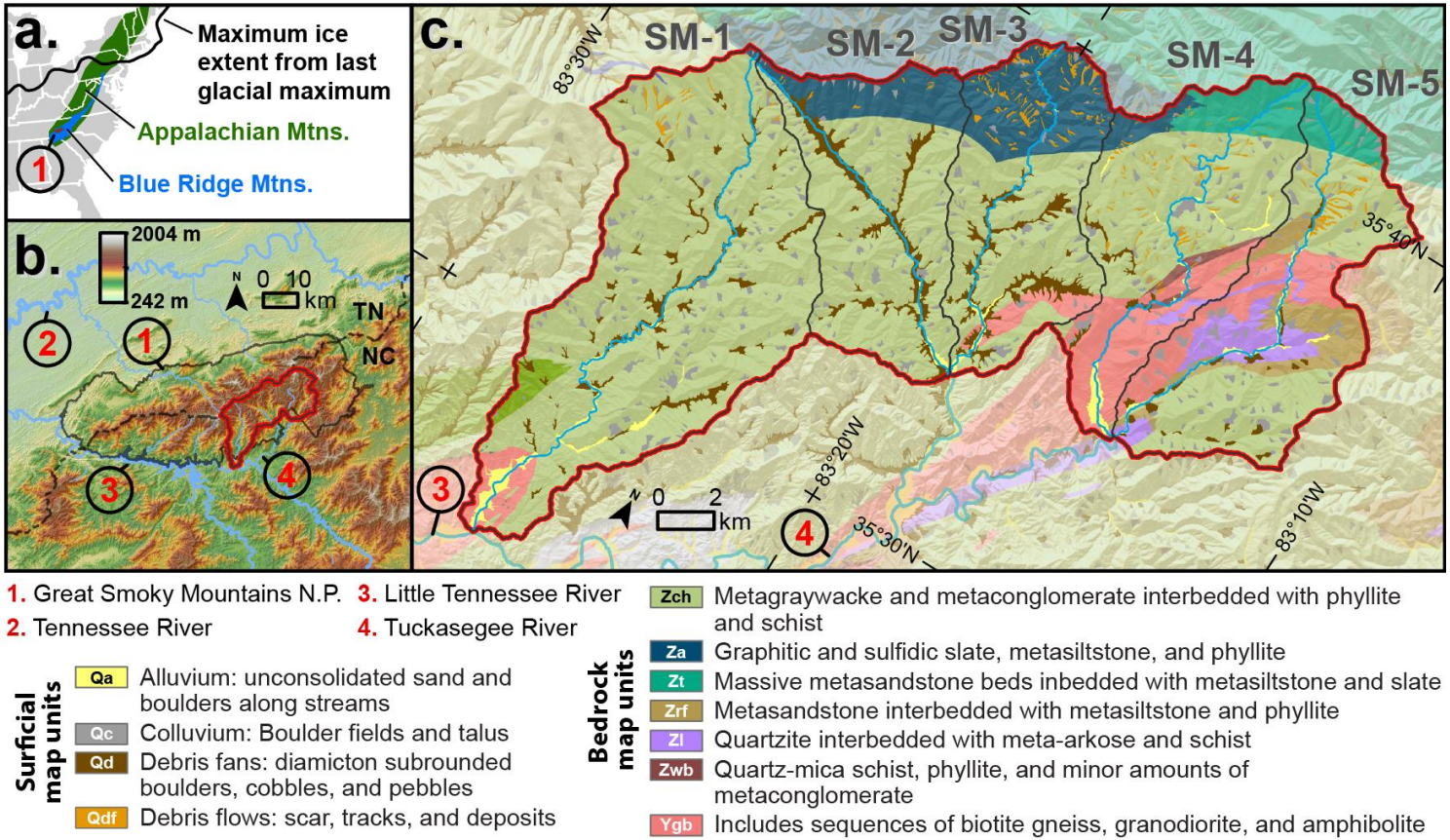

Figure 2.2. Study area bedrock and surficial deposits: (a) The study area is located south of the last glacial maximum (LGM; Dyke *et al.*, 2002). (b) The five study watersheds contain high relief. (c) Bedrock is dominantly metasedimentary rocks of the Ocoee Supergroup and gneiss of the Grenville Basement Complex. Surficial deposits include debris flows at higher elevations, colluvial deposits in hollows, debris fans in mid-elevation valleys, and alluvium in the lower, wider valleys.

Matmon *et al.* (2003b) examined the erosional history of the Smoky Mountains in terms of two classic landscape evolution models, the “Geographic Cycle” and “Dynamic Equilibrium” and concluded that this range contains characteristics of both. They propose that the dominance of slope processes in the Smoky Mountains is reminiscent of the centrality of relief variation throughout the Geographic Cycle proposed by Davis (1899), which states that relief increases in “young” landscapes as stream incise in uplifted terrain, then relief begins to decrease in a “mature” landscape as ridges erode. They emphasize that the erosion rate, 28 ± 8 mm·ky^{-1}, in large drainage areas does not vary widely, though does vary in small headwater drainages (Figure 2.3). This is consistent with Dynamic Equilibrium, the concept proposed by Hack (1960) where local landscape elements adjust such that they erode at the same rate. The highly variable erosion rates in small drainages exhibits a relict landscape that has not reached equilibrium throughout the highlands. Matmon *et al.* (2003a) conclude that the thick crustal root of the southern Appalachians permits the maintenance of high relief over millions of years by means of isostasically driven erosion. Implications of these models, both of which were developed in the tectonically quiescent central Appalachian Mountains, directly link to landsliding since an increase of relief leads to the possibility of increased landsliding until relief or slope magnitude is once again reduced.

2.2.2. Data

2.2.2.1. Digital Elevation Model, Topographic Derivatives, and Trunk Channels

Elevation data were obtained with a lidar (light, detection, and ranging) system and collected by the North Carolina Flood Mapping Program (NCFMP) in response to damages caused by Hurricane Floyd in 1999 (NCFMP, 2011). The collection for the third and final phase of the state of North Carolina, which contains the Smoky Mountains, began in the spring of 2005 and collection efforts for this phase were separated into six blocks. The Smoky Mountains is covered within two of these blocks (Figure 2.4). Block A, the western half, was flown April 5 to April 15,

2005. Block B, the eastern half which includes the study area, was flown between March 9 and the beginning of May, 2005. Chasm Prong watershed, the area of the classification training map, was captured May 1, 2005 flown at approximately 3600 m above sea level.

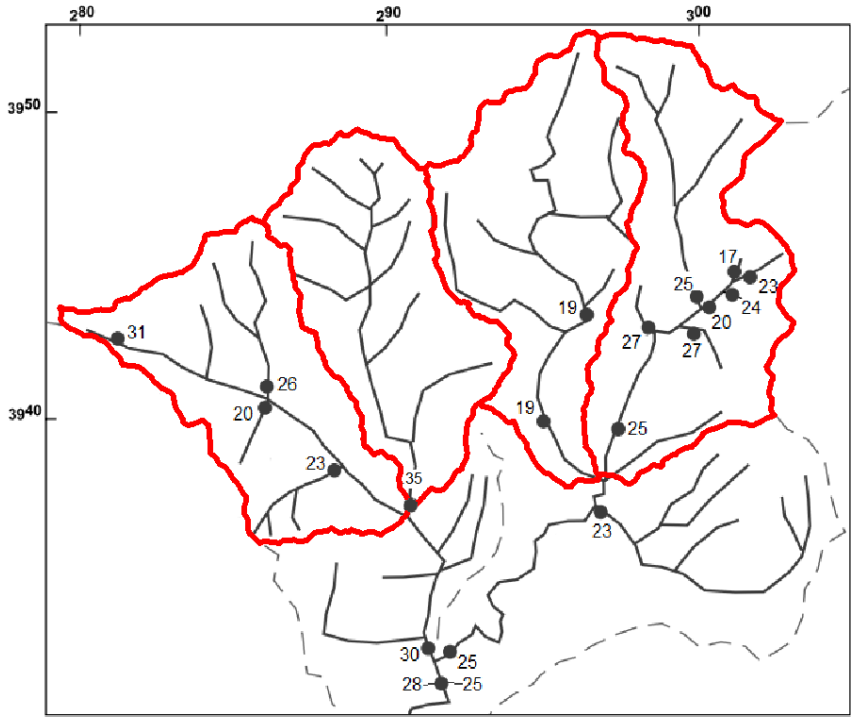

Figure 2.3. Modeled erosion rates ($mm \cdot ky^{-1}$) in the four easternmost watersheds of this study were calculated from ^{10}Be concentrations collected from alluvium. Figure is modified from Matmon *et al.* (2003b).

Lidar data is distributed in two datasets: (1) an all return point cloud, available from USGS (2011), which includes all the non-erroneous lidar pulses returned to the aircraft, and (2) a bare earth point cloud that is available from NCFMP (2011). The bare earth dataset represents a point cloud of the ground surface since data points that were classified as the elevations of vegetation and structures were removed by North Carolina state contractors during post-processing. The all return and bare earth point clouds have average density of 3.23 $points \cdot m^{-2}$ and 0.41 $points \cdot m^{-2}$,

respectively. These points are not equally distributed across the study area (Figure 2.5). Bare earth lidar points exist in higher densities in valley bottoms and some of the USGS mapped debris flows. The bare earth point cloud can be used to create a DEM for topographic analyses, while the all point return DEM is suited for analyses pertinent to vegetation. A lidar accuracy assessment of a bare earth DEM of Swain County was conducted after data collection (NCFMP, 2006). Vertical elevation error of 20 open terrain points had a mean of 0.03 m, a standard deviation of 0.11 m, and ranged from -0.17 to 0.21 m. Vertical elevation error of 20 forested area points had a mean of 0.01 m, a standard deviation of 0.44 m, and ranged from -2.43 to 0.56 m.

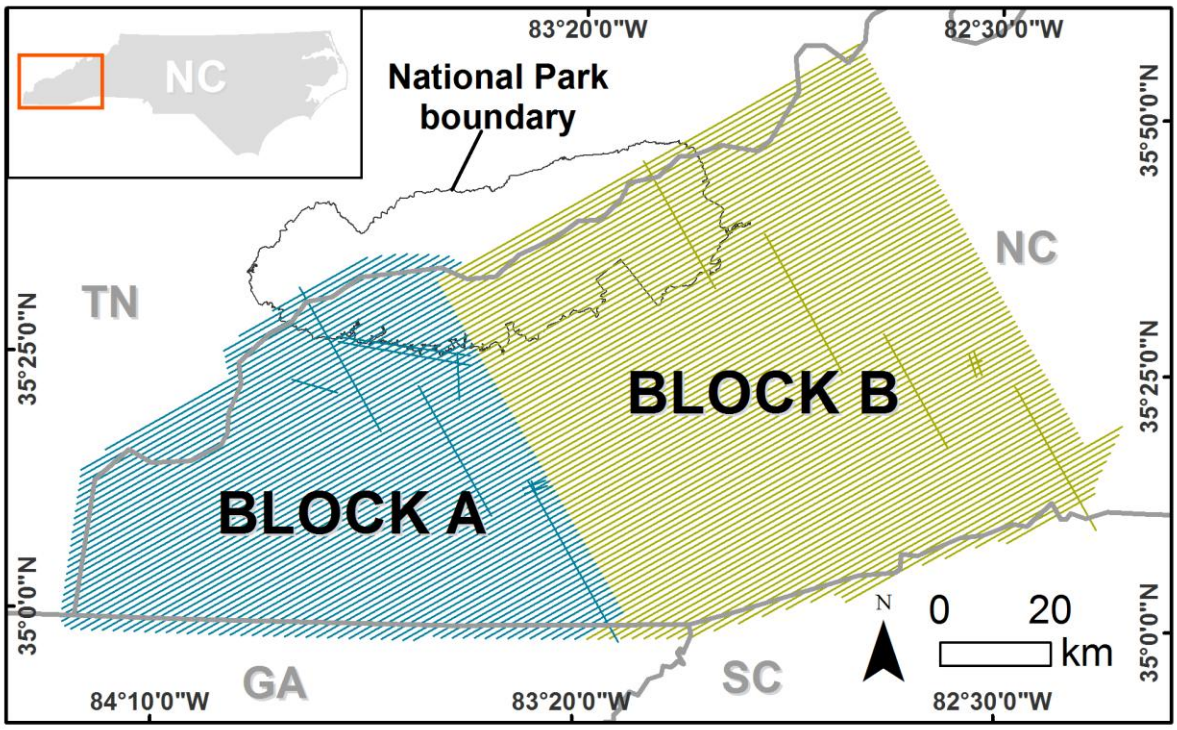

Figure 2.4. The majority of lidar flight paths were flown in a northeast-northwest direction. While the Smoky Mountains were flown in two blocks, the area of this study is all contained within Block B.

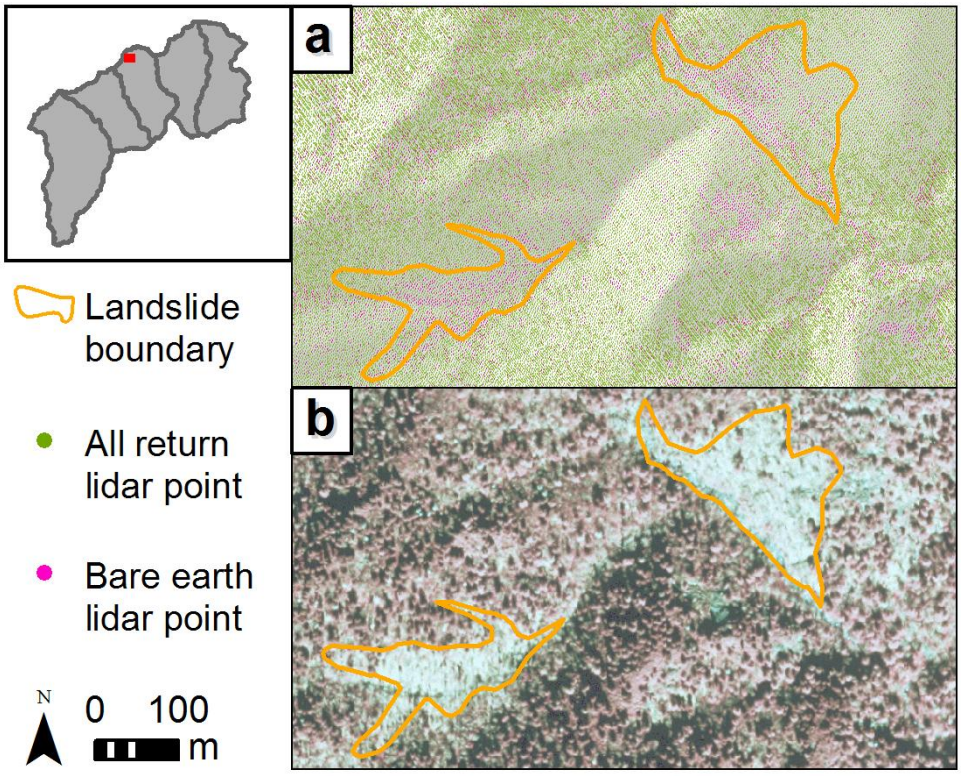

Figure 2.5. Lidar point clouds:(a) Lidar points and landslides mapped by the USGS in Frowning Rock watershed, a sub-watershed of SM-3; (b) A 1998 aerial photograph with the same extent as (a) showing landslides with sparse vegetation.

DEMs were created from the all return and bare earth lidar point clouds. Prior to creating the DEMs, the point clouds were reprojected from their native format, North Carolina State Plane [ft] and vertical datum NAVD88 [ft], to UTM Zone 17 [m] and NAVD88 [m]. Reprojection was necessary because other datasets where projected in UTM, including the geology and vegetation datasets, and calculations required that the inputs derived from the DEMs be in SI units. The DEMs were constructed by using the approximation function, regularized spline with tension (RST), to solve the bivariate function $z = f(x,y)$ in 4 m grid cells (Mitasova and Mitas, 1993). Smoothing and tension parameters were included in the approximation function to allow deviation of the surface from data points and to control the influence that individual points had upon the surface, respectively.

Slope, aspect, and profile curvature were computed during the creation of the bare earth DEM following the principles of differential geometry (Mitasova and Hofierka, 1993). Standard algorithms that compute topographic parameters in 3 by 3 neighborhoods of grid cells do not accurately represent topography in high resolution data and/or rough topography (Mitasova *et al.*, 2005). Additionally, in an evaluation of methods to compute slopes from DEMs, Warren *et al.* (2004) determined that the RST approximation method introduced lower error compared to many of the other methods evaluated. Partial derivatives of the RST function are calculated as vectors in the direction of the steepest slope. Following Mitasova and Hofierka (1993), slope angle, γ_{DEM} [degrees]; aspect, α_{DEM} [degrees]; and profile curvature, κ_{DEM} [m^{-1}]; were computed as:

$$f_x = \frac{\delta z}{\delta x} \ , \ f_y = \frac{\delta z}{\delta y} \ , \ f_{xx} = \frac{\delta^2 z}{\delta x^2} \ , \ f_{yy} = \frac{\delta^2 z}{\delta y^2} \ , \ f_{xy} = \frac{\delta^2 z}{\delta x \delta y} \qquad \textbf{(2.1)}$$

$$\gamma_{DEM} = arctan\sqrt{f_x^2 + f_y^2} \qquad \textbf{(2.2)}$$

$$\alpha_{DEM} = \arctan\frac{f_y}{f_x} \qquad \textbf{(2.3)}$$

$$K_{DEM} = \frac{f_{xx}f_y^2 - 2f_{xy}f_x f_y + f_{yy}f_x^2}{\sqrt{(f_x^2 + f_y^2)^3}} \qquad \textbf{(2.4)}$$

The topographic derivatives, like the DEMs, were created with GRASS GIS with a horizontal resolution of 4 m.

The trunk channels are defined as the primary channel that drains the study watersheds. A drainage area threshold of 0.05 km^2 for headward channel initiation of trunk channels was determined with field observations. Headwater intermittent channels, marked by colluvium accumulation in convergent topography with evidence of recent waterflow such as rills, were selected as the channel initiation points since debris flows can occur in these areas (Wooten *et al.*, 2008). Riverbark and Jackson (2004) determined an average drainage area of 0.08 km^2 for initiation of perennial flow in small basins of the southern Appalachians, which corroborates

field observations of channel initiation made in this study. The drainage network and upstream drainage area were computed with the ArcGIS hydrologic modeling toolset, Arc hydro (Maidment, 2002). The standard workflow in this toolset was followed: local depressions were filled, and flow direction and accumulation were computed. Drainage area was determined as the product of flow accumulation cell quantity and resolution. Sinks, which are local depressions that were likely caused by lidar point interpolation, were filled such that modeled flow would not be impeded by the depressions. Trunk channels were delineated at a minimum drainage areas of 0.05 km^2.

2.2.2.2. Imagery

Multiple aerial photographs were used during the preparation of input data for classification though only one was used as an input for classification. Aerial photographs were used in order to take advantage of the high resolution available in this type of imagery. A National Aerial Photography Program (NAPP) 3-band infrared color-composite photograph with a 1 m resolution was taken in 1998 during leaf-off conditions. The aerial photograph was scanned and rectified with ground surveyed tie-points and a DEM with a resolution of 30 m. The image has a native projection in UTM Zone 17 and vertical root mean square error is listed as ± 7 m. A National Agricultural Imagery Program (NAIP) aerial photograph was taken in 2008 and 2009 during leaf-on conditions. The 2008 image includes a fourth, infrared band (IR) and the 2009 is a 3-band natural color image. However, the 2008 image does not include an IR band in the entire area. The NAIP image is a rectified orthophotograph with native projections in UTM Zone 17 with error listed as ± 6 m to the true ground horizontal location. Orthoretrification was accomplished with the USGS National Elevation Dataset at 1 m resolution.

2.2.2.3. NDVI Map

NDVI maps were created from the 1998 NAPP and the 2008 NAIP photos. NDVI has been successfully used for classification since it is able to discriminate

between vegetation and landslides (Barlow *et al.*, 2006; Martha *et al.*, 2010). NDVI values between 0.2 and 0.8 typically indicate vegetation. This index is calculated from imagery's bands and ranges from -1 to 1:

$$NDVI = \frac{near\ infrared - red}{near\ infrared + red} \quad \textbf{(2.5)}$$

2.2.2.4. Georeferenced Geologic Data

A surficial geology map of the Smoky Mountains was created prior to this study by the USGS that includes a debris flow map unit that was delineated with the 1998 NAPP photograph (Southworth *et al.*, 2005). Geologic map units were drawn on basemaps with a scale of 1:24,000 from a compilation of previous maps, aerial photography, landform interpretation, and observations from field traverses. Scale was reduced to 1:100,000 when the mapped data were digitized by the USGS.

Mapped debris flows and the 1998 NAPP photo do not align with debris flow scars and other features in the 2008 and 2009 NAIP photos. The misalignment ranges from approximately 1 to 30 m between the 1998 and 2009 photos (Figure 2.6). The offset appears to be intensified by high slopes given that the highest offsets are on hillslopes and the lowest are on ridges and valley floors. The misalignment is likely due to the coarser scale used in the 1998 photo that was used during the production of the USGS map, and that this photo was then not geographically rectified (Southworth, personal communication, 2011). A systematic offset between the two photos was not determined nor could an error in projection be traced back to its source. The 1998 photograph was rectified with a 30 m DEM, which could be the cause for the offset given that the maximum offset vector is 30 m. Debris flows were manually digitized for this study since the USGS mapped debris flows do not align with the 1998 image, and the USGS debris flows are used during the inventory technique.

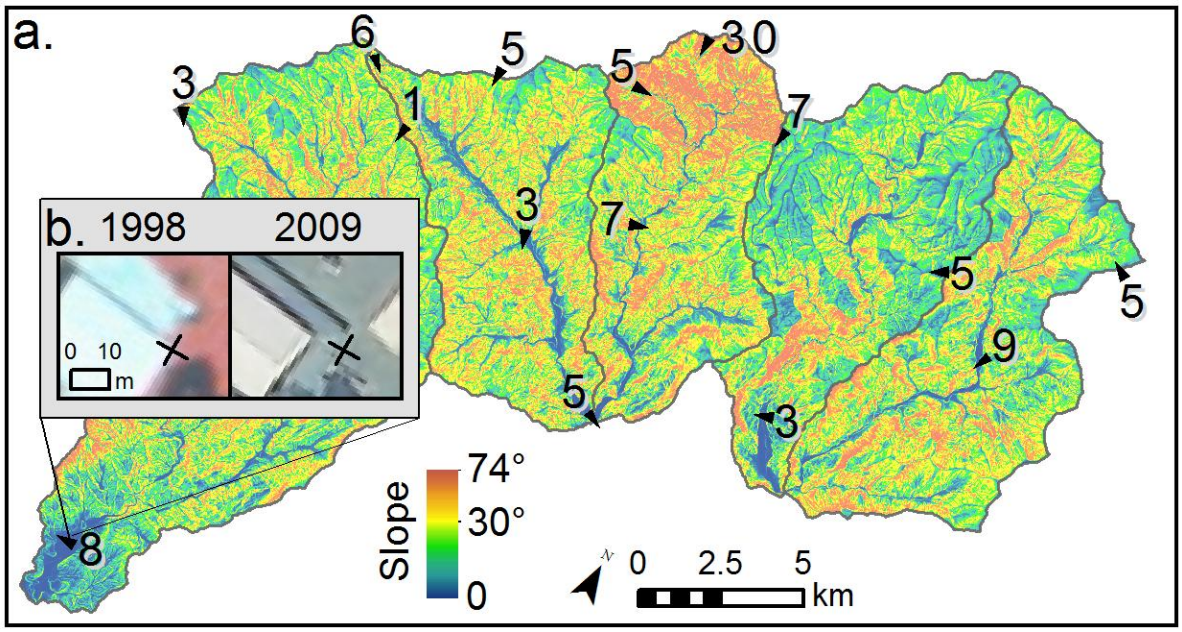

Figure 2.6. Offset vectors of 1998 and 2009 aerial photographs: (a) The offset vectors [m] were determined by comparing identifiable objects in the two images using the 1998 photo as the baseline. The majority of points compared were on areas with low slopes since areas with high slopes had few features that could be identified in both photos. (b) This vector was determined at the corner of a building where the 2008 photo was offset 8 m to the northeast from the 1998 photo.

2.2.3. Location and Origin of Debris Flow-Dominated Channels

Models that express the form taken by watersheds and drainage networks in response to environment factors have been under development for decades, but an expression has not been determined for channels above the transition to debris flow dominated channels (Stock and Dietrich, 2003). Below the transition, Whipple and Tucker (1999), for example, related the stream power law to drainage area and slope to describe stream incision:

$$\frac{\delta z}{\delta t} = U - KA^m S^n \qquad (\mathbf{2.6})$$

where z is elevation [m], t is time [y], U is rock uplift rate relative to base level [m·y^{-1}], K is rock erodibility [L^{1-2m}·y^{-1}], A is drainage area [m^2] substituting for discharge, L is total bedrock stream length [m], and m and n are empirically determined values

often referred to as the area and slope exponents, respectively. In steady state landscapes, where δ*z* / δ*t* = 0, channel slope is approximated with:

$$S = \left(\frac{U}{K}\right)^{1/n} A^{-m/n} \quad \textbf{(2.7)}$$

and in areas of uniform uplift and rock erodibility:

$$S = k_s A^{-\theta} \quad (\textbf{2.8})$$

where k_s, $(U/K)^{1/n}$ in Equation 2.7, is referred to as the steepness index and θ, m/n in Equation 2.7, as the concavity index. In the Smoky Mountains, uplift is likely nonexistent or uniformly negligible that is due to isostatic rebound, which permits the assumption of uniform uplift required for Equation 2.8. However, the existence of a steady state condition in the Smoky Mountains is debatable, though the existence of this state occurring anywhere is also debated (Pazzaglia, 2003). Erosion rates of 28 ± 8 mm·ky^{-1} in this Range (Matmon *et al.*, 2003b), and negligible uplift approximate steady state over the short times scales considered in this study. Further, rock erodibility varies widely in the study watersheds, thus variations in the channels' profile due to rock erodibility variations and areas that deviate largely from local steady-state conditions will be reflected in anomalous k_s and θ values. Also, as can be seen in Figure 1.1, θ becomes increasingly negative over small reaches. Interpretations of steady-state conditions barring rock erodibility variations, expressed through anomalous θ and k_s and values, as well as observations of debris flow and fan deposits, provide spatial limits upon the transition from the fluvial power law region to the curved debris flow region in log-log plots of drainage area versus channel slope (DS plots).

2.2.3.1. DS Plots

DS Plots of the five trunk streams were created to locate the scaling break between debris flow and fluvial dominated channels. Drainage area and slope for the DS plots were extracted from the DEM along trunk channels of each of the study watersheds. Data points where extracted up the channel at every 10 m increase in

elevation. This interval was chosen so that log jams, foot bridges, and lidar vertical accuracy minimally affected the DS plot values. Multiple regressions of DS Plot data points were conducted in order to account for hydraulic jumps where large changes in drainage area and slope occur on the trunk stream at tributary junctions. Single regressions in DS Plots are not applicable when attempting to locate the stream section affected by debris flows due to stream power contrasts at tributary junctions (Stock and Dietrich, 2006). The limits of the regressions in the DS Plots were selected if one of the following were true: (1) the regression crosses hydraulic jumps greater than $10^n / 10$ where n is the magnitude of the drainage area in m^2, or (2) where the regression slope changes sign. Plots were created with the aid of the ArcGIS and MATLAB extension, StreamProfiler (Whipple *et al.*, 2007), which was used to extract channel parameters.

The scaling break in the DS Plot, indicating the transition between the dominant channel processes, was defined as the location of the most downstream positive regression slope, a negative θ in Equation 2.8. This point additionally represents the most downstream, large-scale knickzone that separates the curved region and the power law region, representing debris flow and fluvial-dominated channels, respectively, as shown in Figure 1.1. The most downstream negative θ was selected in order to be conservative in selection of the debris flow-dominated drainage areas to account for the ambiguous transition zone between the channel process transitions. Further, the relative position of the lowestmost debris flow deposit and uppermost fan deposit is determined to provide further context of the geomorphical significance of the defined scaling break.

The uppermost point of debris fans is significant to the location of the scaling break for following reason. The fan deposits, primarily attributed to debris flows in the late Pleistocene and early Holocene, show evidence of having been reworked by fluvial action (Leigh and Webb, 2006; Southworth *et al.*, 2005). The historical mapped debris flows in the area occur in tributary streams, though the track sometimes extends into the trunk stream. Thus, the fans represent the debris flow

material storage site, in large volumes in the area, but not the initiation or deposition site of recent debris flows.

2.2.3.2. Watershed Parameters

Stream knickpoint distribution, watershed slope distribution, and hypsometry analyses are also presented here corroborate the spatial extent of debris flow dominated channels. The locations of knickpoints on the trunk channels of the study watersheds were determined with StreamProfiler (Whipple *et al.*, 2007). Knickpoints were identified at points along the channel longitudinal profile with a noticeable convexity, change in slope of at least 0.02 over 500 m, and a k_{sn} that peaked at a minimum of 70 following Equation 2.8. Profiles were smoothed prior to knickpoint detection in sampling windows of 50 m to reduce the impact of lidar false returns and artifacts of lidar post-processing and DEM creation. Watershed hillside slope was averaged in 50 m elevation bins for all surfaces in the study area. Hypsometry was calculated separately in each of the study watersheds with the 4 m bare earth DEM.

Characteristics of the landscape in the Smoky Mountains implicate a long history and adaption to debris flows: highly dissected valleys and thick sequences of bouldery diamicton in debris fans coupled with evidence of adaption to high volumes of water (Bogucki, 1976; Kochel, 1990; Leigh and Webb, 2006). Gallen *et al*. (2011) asked the question of how tectonically quiescent mountain ranges retain high relief for millions of years, concluding that hillslope evolution is largely dependent upon knickpoint migration through fluvial networks. Limits in the spatial extent of debris flow activity will impede the expanse of downwasting, which can be caused by limited knickpoint propagation through a watershed. These factors control the shape of DS Plots and result in the location of the scaling break indicating the dominant channel process, upstream from which the inventory of debris flow dominated channels will be created.

2.2.4. Landslide Inventories

Inputs that were evaluated for use in classification were topographic derivatives determined from the bare earth DEM, and vegetation parameters determined from NDVI and the all point return DEM. The difference between DEMs created from the all return point cloud, representing the top of the vegetation canopy, and the bare earth point cloud represents canopy thickness. Canopy thickness can then be used as a criterion to locate debris flow scars. Input segmentation and landslide classification was conducted with GRASS GIS.

2.2.4.1. Input Texture Maps for Classification

Texture maps of inputs for classification, instead of inputting raw data, were used in order to emphasize the spatial structural variations in small neighborhoods of the study area (Haralick *et al.*, 1973). Moine, *et al.* (2009) and Martha *et al.,* (2010) computed textural features of imagery since local variations, such as shadows and vegetation communities, may have an unintended influence upon the statistical characterization of classes throughout the entire study area. Textural features, as applied and defined by Haralick *et al*. (1973), are computed as the occurrence frequency of gray level pixel value pairs separated by a given distance in a matrix of a given size. The pairs within the moving neighborhood matrices are assigned by a displacement vector between two pixels as a direction, commonly 0°, 45°, 90°, and 135°. The texture algorithm used in GRASS GIS uses these directions and allows for numerous textural feature types to be calculated.

The following texture maps of these inputs were computed in 144 m^2 matrices containing 3 by 3 arrays of 4 m^2 cells in the study area: slope, aspect, and profile curvature entropy, a measure of the uncertainty of a variable, and the sum average of the NDVI maps. The computational matrices have a quality called spatial-dependence since the relationship of gray level tones between neighboring matrices determines the texture. These textual features were calculated as:

$$Entropy = -\sum_i \sum_j p(i,j) \log\left(p(i,j)\right) \quad \textbf{(2.9)}$$

and:

$$Sum\ average = \sum_{i=2}^{2N_g} ip_{x+y}(i) \quad \textbf{(2.10)}$$

where *p(i, j)* is the spatial-dependence matrix with paired values *i* and *j*, N_g is the number of distinct gray levels in the raster, and *x* and *y* are the number of columns and rows of the matrix, respectively (Haralick *et al.*, 1973). Lastly, texture maps were equally weighted and scaled from 0 to 255 for classification. This scale was necessary since the GRASS GIS texture algorithm was designed for 8-bit imagery input.

2.2.4.2. Classification Training Map

The training map was created in Chasm Prong watershed, a 4.9 km^2 sub-watershed of SM-3 (Figure 2.7). This area was chosen for its clarity of debris flow scars in aerial photos and the close alignment between the 1998 photo and USGS debris flow map discussed in section 2.2.2.2. Debris flows were located using the 2005 USGS map and debris flow polygon boundaries were digitized using the 2009 NAIP and 1998 NAPP photos, and a shaded relief map derived from the bare earth DEM. The 1998 NAPP photo was used to locate the boundaries of debris flows that were not apparent in the 2009 photo, likely due to revegetation of some debris flow scars. Only USGS mapped landslides that have a track that is perpendicular to contour lines were digitized in order to create a training map of only debris flows.

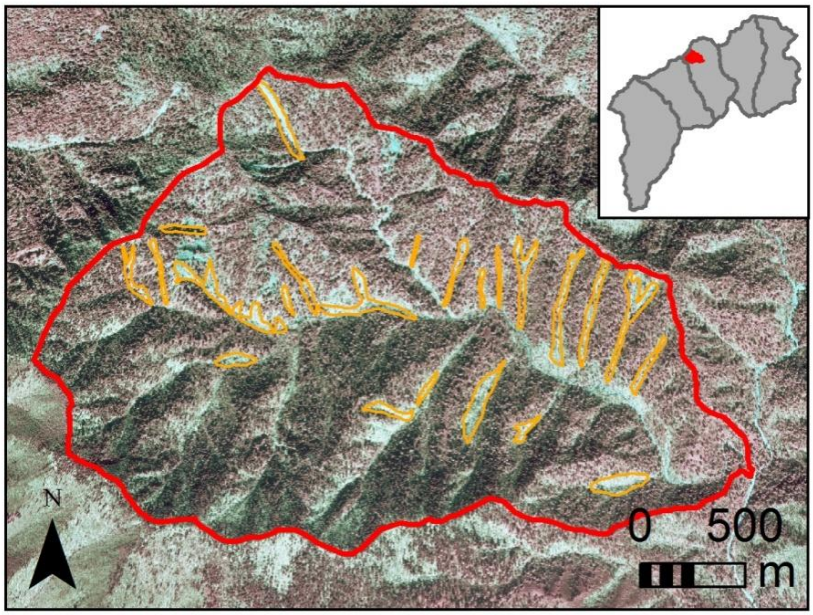

Figure 2.7. The training map was created in the Chasm Prong watershed, a sub-watershed of SM-3. Redigitized debris flow polygons were assigned 'true positive' status in this sub-watershed since the majority of USGS mapped landslides here have a debris flow shape, occur in convergent topography, and extend downslope.

2.2.4.3. Segmentation and Classification

Debris flow geomorphic signatures, necessary for supervised classification, were defined by the means and covariances of the NDVI and topographic derivative texture maps in the locations of the digitized debris flows in the training map. Subclass signatures contained within the two training map classes, "is" and "is not a debris flow", were determined with a clustering algorithm employing a Gaussian mixture distribution model similar to Bouman and Shapiro (1994). Classes in this algorithm are a probabilistic combination of subclasses. The subclasses are defined by their means and covariance among inputs and the algorithm began testing clustering at 10 subclasses for each class, reducing the number of classes until an optimal number of subclasses that represented the class are determined.

The segmentation method employed sequential maximum *a posteriori* (SMAP) estimation, a method typically applied to multi-spectral image analysis (McCauley and Engel, 1995). SMAP was chosen for its ability to minimize continuously large misclassified areas and its ability to incorporate neighboring pixel values in segmentation, thus incorporating contextual information. SMAP performs in multiple resolutions where in each successively finer resolution segmentation optimization is guided by prior miscalculations at courser resolutions. Considering a quadtree model, each raster value, $x_s^{(n)}$ where n is the scale and s is the position in a two-dimensional lattice:

$$\hat{x}_s^{(n)} = \arg \max_{1 \le k \le M-1} \left\{ \log p_{\mathrm{y}|\mathrm{x}_s^{(\mathrm{n})}}(\mathrm{y}|\mathrm{k}) + \log p_{\mathrm{x}_s^{(\mathrm{n})}|\mathrm{x}_{\partial s}^{(\mathrm{n}+1)}}\left(\mathrm{k}\middle|\hat{\mathrm{x}}_{\partial s}^{(\mathrm{n}+1)}\right) \right\} \quad \textbf{(2.11)}$$

where k is the class number, M is the number of possible classes, ∂ is the neighborhood of pixel s, y is the number of points or calculations in a quadtree segmentation branch, and $p_{\mathrm{x}_\mathrm{s}^{(\mathrm{n})}|\mathrm{x}_{\partial s}^{(\mathrm{n}+1)}}$ is the probability density for $x_s^{(n)}$ given values in the neighborhood with a coarser scale $\hat{\mathrm{x}}_{\partial s}^{(\mathrm{n}+1)}$ (Bouman and Shapiro, 1994). Equation 2.11 determines which of the classes contains the maximum probability of a pixel's ownership given the increased probability that the pixel is contained in the same class as neighboring pixels.

False positives were iteratively removed from the classification results by removing candidates that fell outside the bounds of debris flow morphometric parameters. Debris flow surface area varies by orders of magnitude, thus conservative bounds, 0.5 ha to 20 ha, were chosen based upon the range of digitized debris flows. Barlow *et al*. (2006) used a lower limit of 1 ha since smaller scars are difficult to detect with the DEM and satellite imagery they used. However, the higher resolution of the lidar DEM and aerial photography of this study permits a smaller minimum area. Further, the smaller size of debris flows in this study demands a lower minimum debris flow area in order to identify many of the flows. The ratio of length to width of debris flow candidates was also determined for

delineated debris flows. The range was 1.8 to 16, thus candidates outside this range were deemed false positives. Length was determined by locating the maximum distance perpendicular to contours from the minimum elevation cell in each debris flow candidate. Surface distance, not planimetric distance, was calculated, an important consideration that is rarely made when calculating lengths of landslides. Width was defined as the average length of contour lines contained within the debris flow candidates.

The process outlined above: multi-resolution segmentation of sites with similar topographic derivatives and NDVI textures, classification of segments into two classes, and removal of false positives; will result in a map that contains debris flow candidates that then can be evaluated with the USGS inventory. As mentioned above, this inventory does contain positional error, thus debris flows were digitized following the method outlined in section 2.2.4.2. for evaluation of classification results.

2.3. Results

2.3.1. DS Plots and Watershed Parameters

The transition from debris flow to fluvial dominated channels, the scaling breaks, were determined as the most downstream negative θ of stream segment regressions in DS plots of the study watersheds' trunk channels (Figure 2.8). The drainage areas of the scaling breaks for trunks channels SM-1 to -5 are similar to the typical values found in streams across the world: slopes of 0.03 to 0.10 and drainage areas between 0.1 to 1 km^2 (Table 2.2; Stock and Dietrich, 2003). Debris flow and fan deposits are located upstream from all of the scaling breaks of trunk streams.

Table 2.2. Scaling break parameters of the study watersheds.

	Drainage area (km^2)	Slope ($m \cdot m^{-1}$)	Elevation (m)	Upstream trunk channel length (km)
SM-1	3.36	0.07	1138	2.97
SM-2	3.58	0.08	1149	2.90
SM-3	15.60	0.03	989	5.63
SM-4	37.23	0.05	1083	14.92
SM-5	31.60	0.03	927	11.04

Figure 2.8. Drainage area and slope plots used to locate the scaling break between dominant channel processes in the study watersheds SM-1 through SM-5. (a) Regressions (blue lines) of DS plot points (magenta crosses) of stream reaches are compared with USGS mapped surficial geologic deposits to locate the scaling break. (b) The slope of the regressions, the concavity indices [θ] in Equation 2.8, are shown below the corresponding regression in (a).

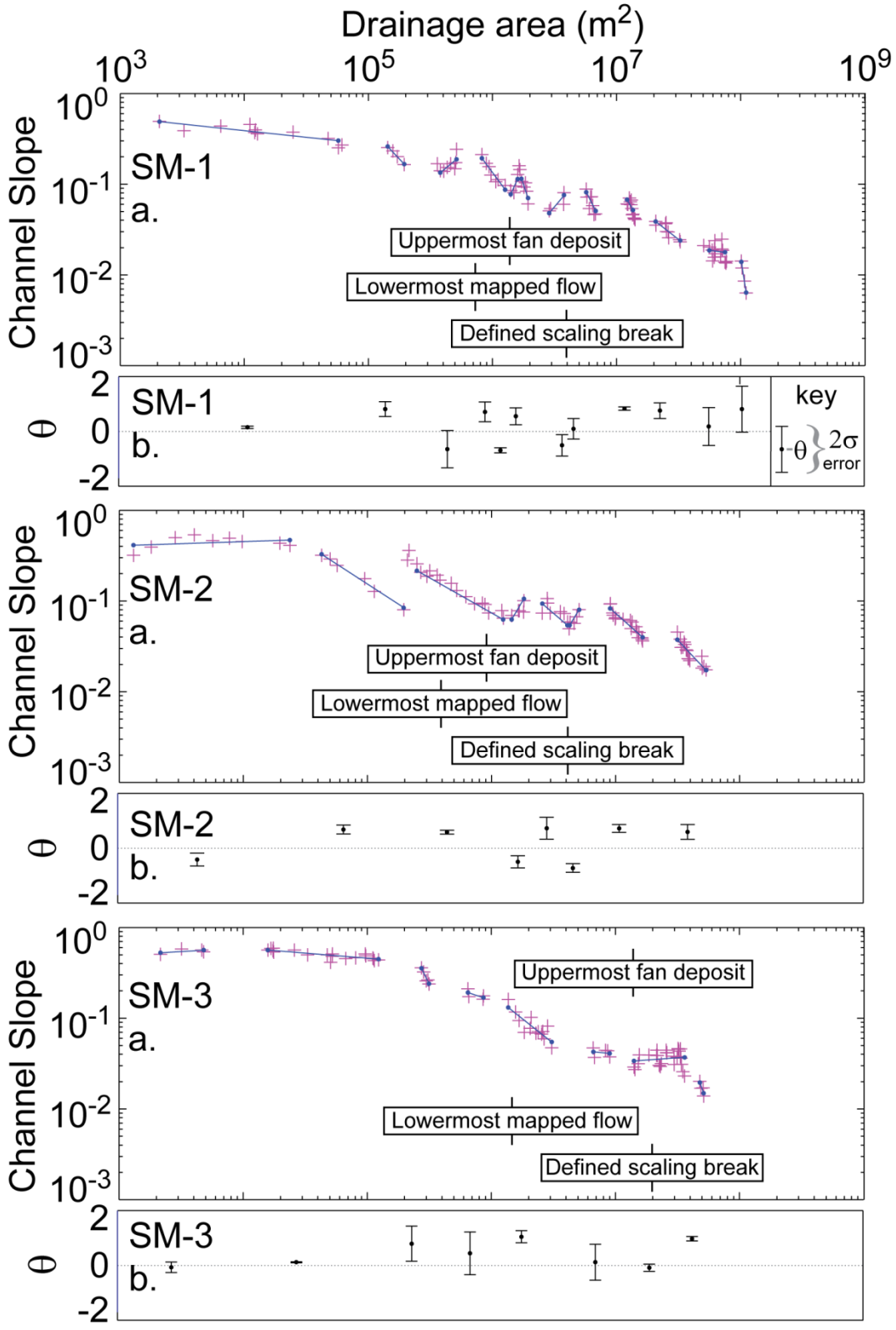
Drainage area (m2)
10^3
10^5
10^7
10^9
Channel Slope
10^0
10^-1
10^-2
10^-3
SM-1
a.
Uppermost fan deposit
Lowermost mapped flow
Defined scaling break
θ
2
0
-2
SM-1
b.
key
θ
2σ error
SM-2
a.
Uppermost fan deposit
Lowermost mapped flow
Defined scaling break
SM-2
b.
SM-3
a.
Uppermost fan deposit
Lowermost mapped flow
Defined scaling break
SM-3
b.

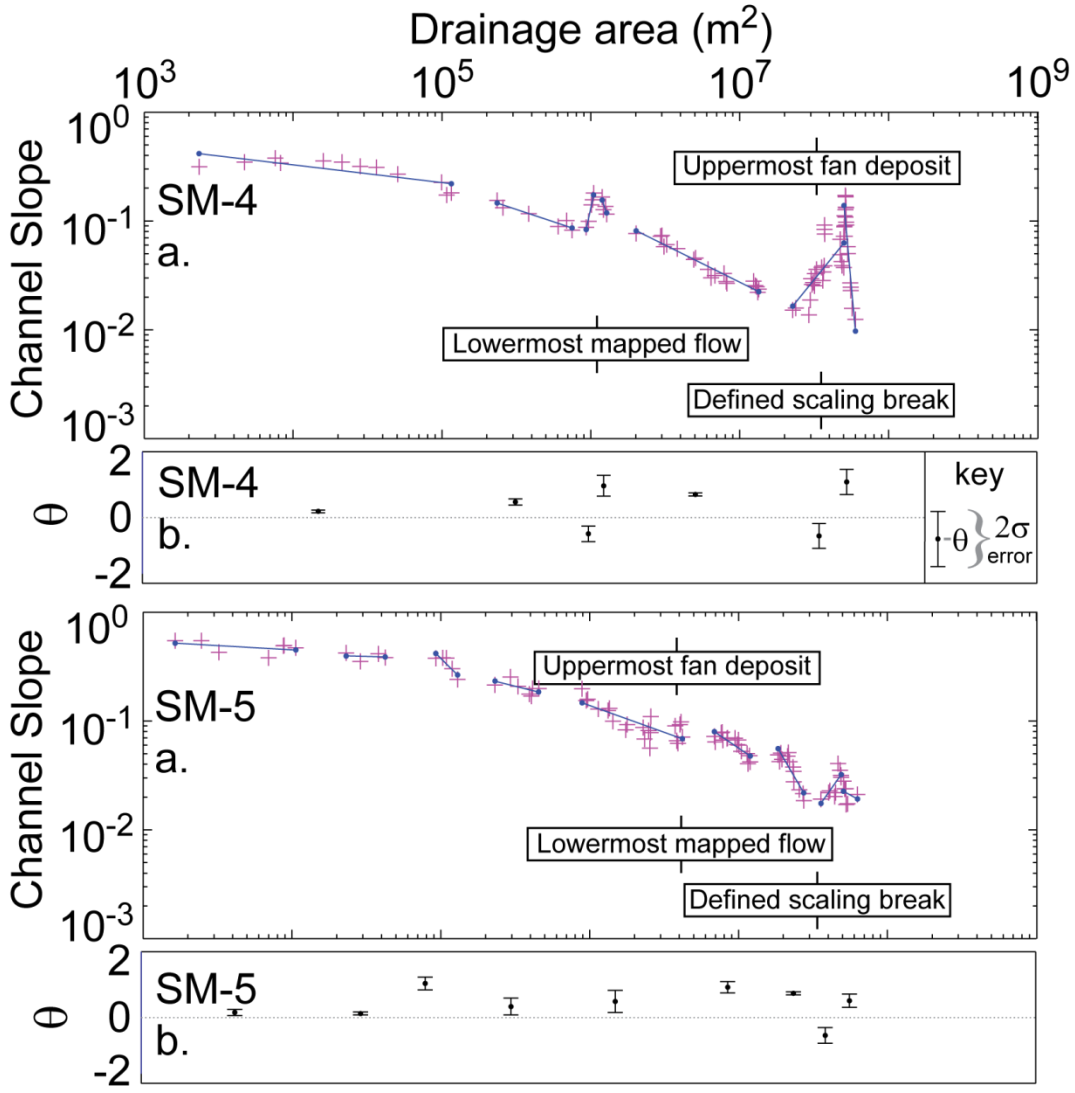
Drainage area (m2)
10^3
10^5
10^7
10^9
Channel Slope
10^0
10^-1
10^-2
10^-3
SM-4
a.
Uppermost fan deposit
Lowermost mapped flow
Defined scaling break
θ
2
0
-2
SM-4
b.
key
θ
2σ error
Channel Slope
SM-5
a.
Uppermost fan deposit
Lowermost mapped flow
Defined scaling break
θ
SM-5
b.

Delineation of the areas upstream from the scaling breaks along the trunk channel results in a total area of 127 km^2 for all watersheds, which represents the areas that drain to debris flow-dominated channels (Figure 2.9). This area is 37% smaller than the entire study area of 343 km^2. All of the USGS mapped debris flows are confined within the 127 km^2 area. A total of 15 major knickpoints or zones were identified and they cluster at elevations between approximately 950 to 1200 m (Figure 2.10). SM-1 and 2 have well defined concave up profiles throughout. WS-3 thru 5 have noticeable convex portions near the lowestmost knickpoint. The maximum value in bin-averaged slope of all the initial study area also exists at approximately 1100 m corresponding with the minimum elevation of a USGS mapped debris flows at approximately 1130 m (Figure 2.11).

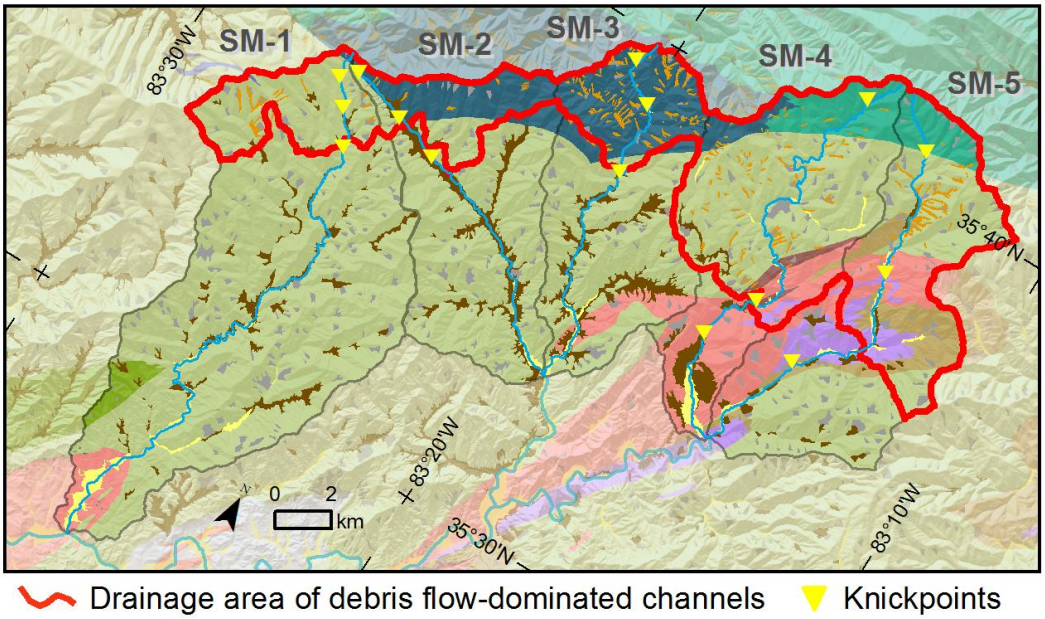

Figure 2.9. Drainage area of debris flow-dominated channels. The legend for bedrock and surficial deposits follows Figure 2.2.

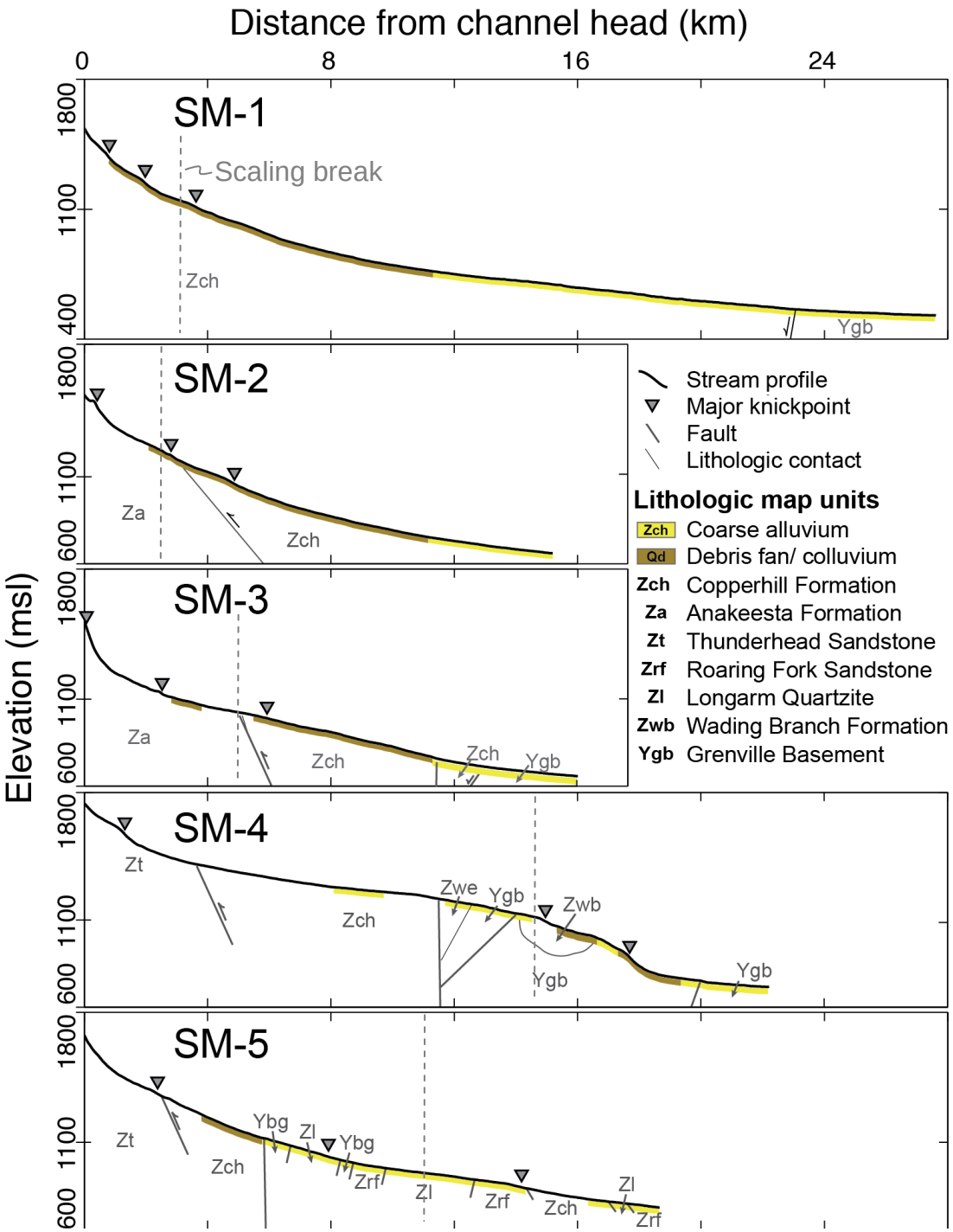

Figure 2.10. Stream longitudinal profiles were constructed from evaluation stations every 10 m. Lithologic map units, faults, and cross-sections are from Southworth, *et al*. (2005) and Matmon, *et al*. (2003b). See Figure 2.2 for bedrock and surficial deposit description.

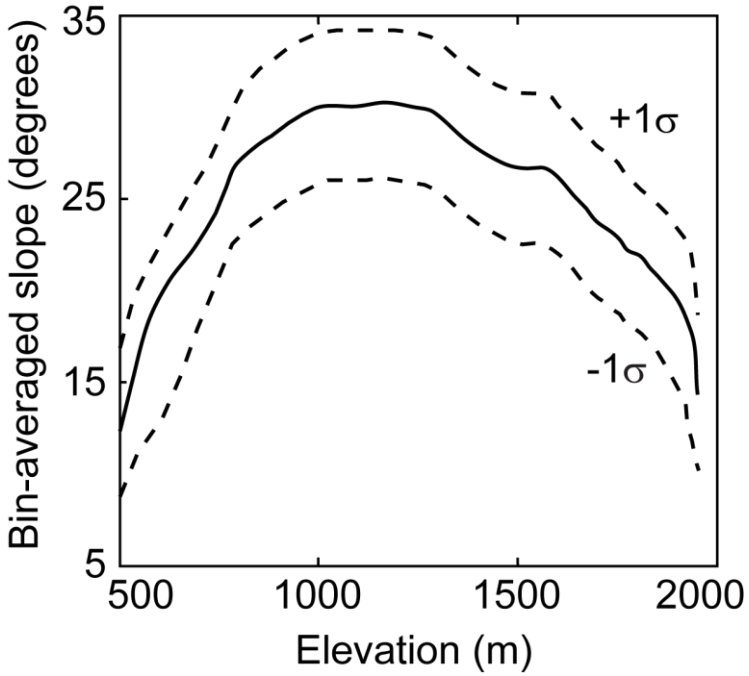

Figure 2.11. Elevation versus study area-wide slope. All cell values of slope, calculated with Equation 2.3, in the study area were averaged in 10 m elevation bins. Dashed lines are ± 1 standard deviation, σ.

The variation in the study watersheds' elevation distribution relative to area is apparent by observing the hypsometric curves of the study area (Figure 2.12). Resistance to downwasting of the two easternmost watersheds is further supported by these watersheds lower hypsometric index compared with the other watersheds. The elevation of these two watersheds, especially SM-4, largely is composed of low and high elevations, with mid-elevations limited to areas adjacent to the watersheds' trunk channel. SM-4 especially contains a low hypsometric index compared to the other watersheds corresponding with the higher elevations of the trunk channel's longitudinal profile upstream from the lowest knickpoints. These parameters and their relationship to debris flow and knickpoint distribution corroborates the lower elevation of USGS mapped debris flows that is likely influenced by knickpoint propagation in SM-4.

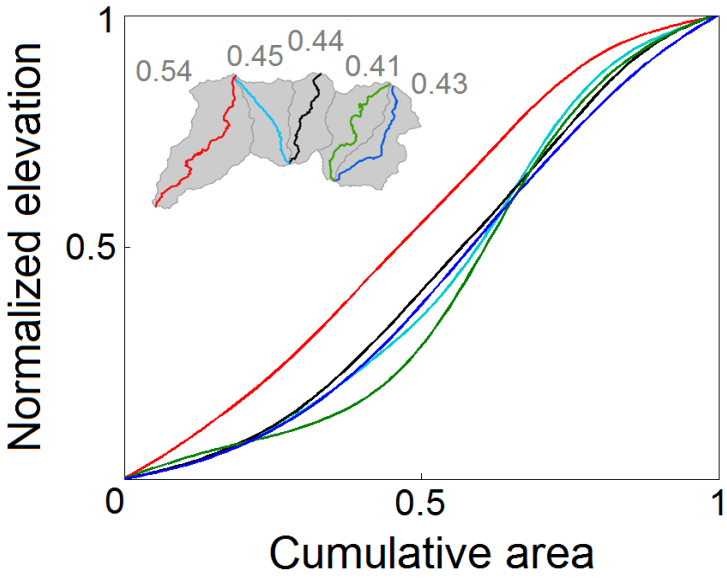

Figure 2.12. Hypsometric indices (values adjacent to map inset) and curves were determined separately for each of the study watersheds.

The effect that the distribution of debris flow-dominated channels has upon vegetation is apparent (Figure 2.13). Northern hardwood and spruce/fur forest types are the dominant type in areas upstream from the scaling break in each watershed and are rarely found downstream from it. Elevation controls the distribution of these forest types, which typically are found at elevations above 900 to 1300 m (Madden *et al.*, 2004).

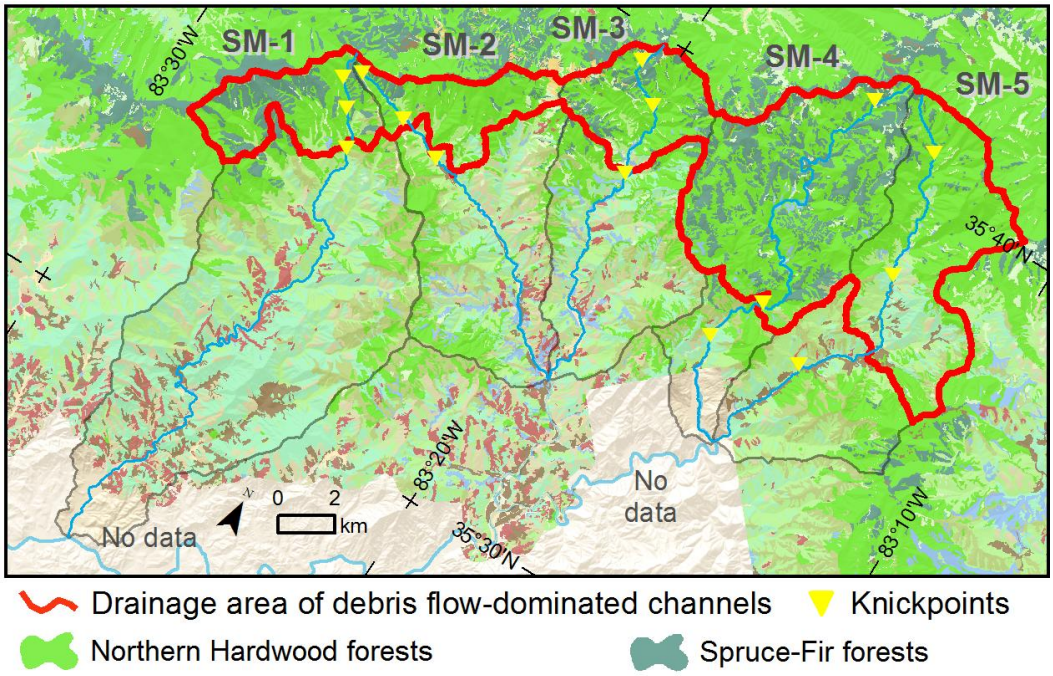

Figure 2.13. Vegetation in drainages of debris flow-dominated channels. Vegetation classes not in legend are defined in Figure 1.5.

2.3.2. Classification Input Maps

Texture maps of topographic derivatives and NDVI were used in segmentation and classification. The use of vegetation canopy thickness as a criterion, calculated from the difference between DEMs created from the all return point cloud and the bare earth point cloud, proved problematic. Elevation shifts up to approximately 3 m at swath edges are apparent in relief shaded maps (Figure 2.14). Additionally, canopy thickness on many of the USGS mapped debris flows is similar to areas outside of debris flows, indicating that regrowth since the debris flow can obscure the scar in canopy thickness maps. Nevertheless, vegetation canopy thickness calculated from lidar data may be a viable technique in areas with minimal elevation shifts at swath edges and less rapid vegetation growth on landslide scars.

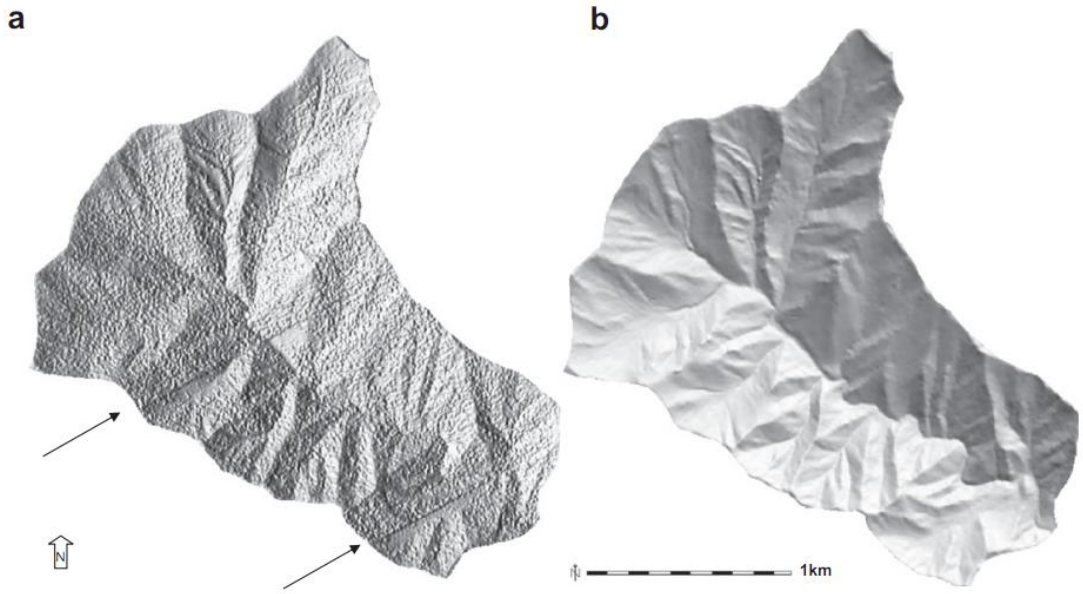

Figure 2.14. All returns lidar error at swath edges are observed in relief shaded maps of the Frowning Rock watershed, a sub-watershed of SM-3. (a) Two elevation shift errors are visible parallel to swath edges in the relief shaded map created from the all return DEM. (b) Elevation shifts errors are not apparent in the relief shaded map created from the bare earth DEM. Figure is from Mitasova *et al.* (2011b).

NDVI maps were used as an input for classification in order to locate areas with no or sparse vegetation indicated by low NDVI values. It is difficult to distinguish between digitized USGS debris flow scars and ridges in the 1998 aerial photo (Figure 2.15.1a) and NDVI map (Figure 2.15.1b). However, digitized debris flows coincide with low sum average values in the texture maps of NDVI from the 1998 photo (Figure 2.15.1c). Ridges are less apparent given the texture feature neighborhood size that is larger than many ridges in the study area are wide. Exposed soil and bedrock resulting from debris flow induced vegetation removal is responsible for the low NDVI values in the 144 m^2 neighborhoods. Channels also contain low sum average values where there is a break in vegetation density and accumulations of boulder deposits. Sum average values also infer the vegetation class type, with high values coinciding with spruce/fir and northern hardwood forests,

which exist at higher elevations, low values coinciding with oak/hickory and montane cove forests, which exist at lower elevations.

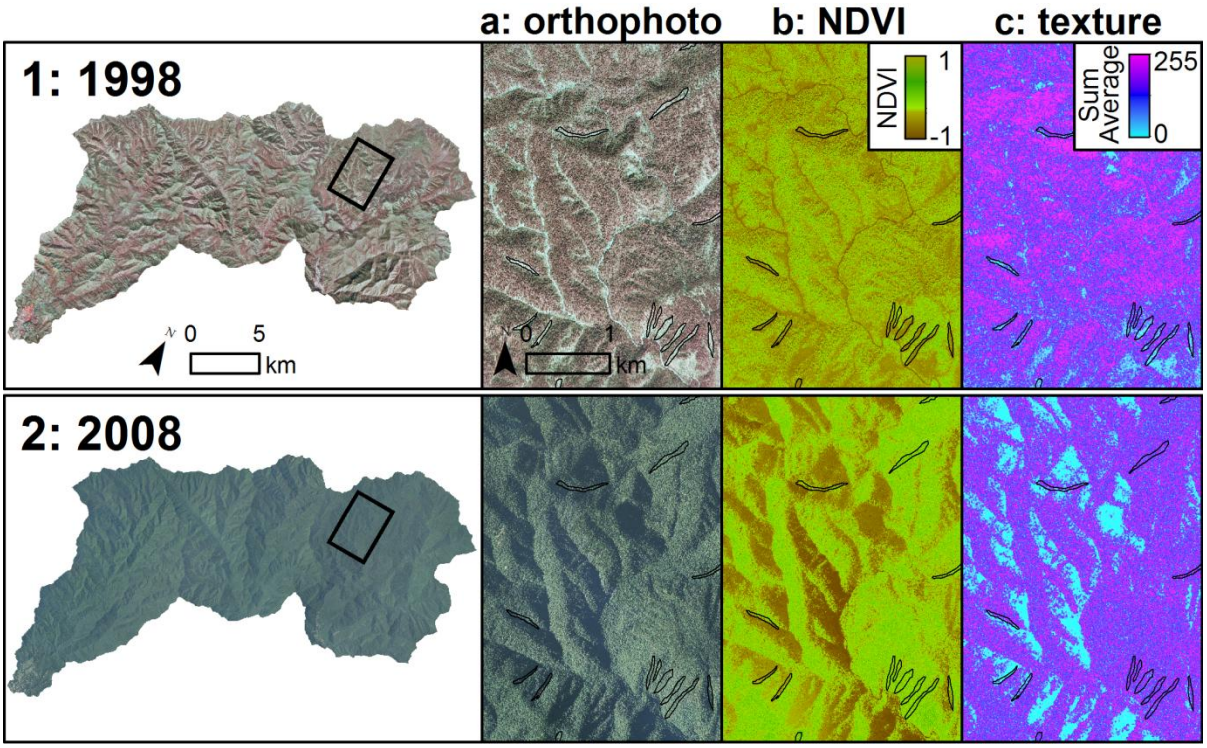

Figure 2.15. NDVI maps created in the study area. The influence of shadows was used to determine that the NDVI map created from the 1998 aerial photo (top row), composed of and shown here with infrared, red, and green bands, was used as a classification input. The 2008 image (bottom row), shown here with red, green, and blue bands, has extensive shadows, affecting the NDVI and texture maps.

The 1998 image contains much less shadow than the 2008 image (Figure 2.15.2a) that results in low NDVI (Figure 2.15.2b) and sum average values (Figure 2.15.2c) in areas with shadows despite the appearance of vegetation in these areas. Further, the intense illumination coupled with extensive shadows in the 2008 photo causes USGS mapped debris flows to have higher spectral values when they are not in shadows, so their boundaries between adjacent areas are difficult to distinguish. For this reason, the NDVI texture map from the 1998 photo is used for classification.

The classification input maps vary across watersheds. Topographic slope in SM-1, SM-2, and atop the Copperhill Formation in SM-3 is at its steepest on hillslopes near ridges (Figure 2.16.1a). These areas contain few USGS mapped debris flows and they are relegated to headwater channels. The area surrounding upper reaches of SM-3 atop the Anakeesta Formation has the steepest sub-watershed slopes which extend from channels to the ridges (Figure 2.16.1b). Conversely, the steepest slopes of SM-4, and to a lesser extent SM-5, are adjacent to channels (Figure 2.16.1c).

Debris flows preferentially initiate upon eastern and southern hillslope aspects (Figure 2.16.2). This phenomenon appears to reflect bedrock orientation. Bedrock orientation data, included in the USGS georeferenced bedrock dataset, indicate that planes of weakness parallel to bedrock bedding control the aspect at which debris flows initiate. Bedrock strike azimuth, the geographic direction of a plane placed tangentially to rock bedding surface, in the randomly selected points outside of the debris flow population show a trend that expresses the underlying geologic structure (Figure 2.17a). The dominant structure in the region is the Alum Cave Synclinorium, which trends northeast-southwest, and is accompanied by numerous parallel, smaller folds (Figure 1.3). The ground aspect of points outside of debris flows show a small trend to the south though it is well distributed throughout the southern hemisphere (Figure 2.17b). Unsurprisingly, bedrock strike outside debris flow areas is similar to bedrock strike inside debris flow areas since bedrock is continuous throughout these areas (Figure 2.17c). Ground aspect of debris flow cells trend strongly to the south, perpendicular to bedrock azimuth, indicating that debris flows fail atop bedrock dip slopes (Figure 2.17d).

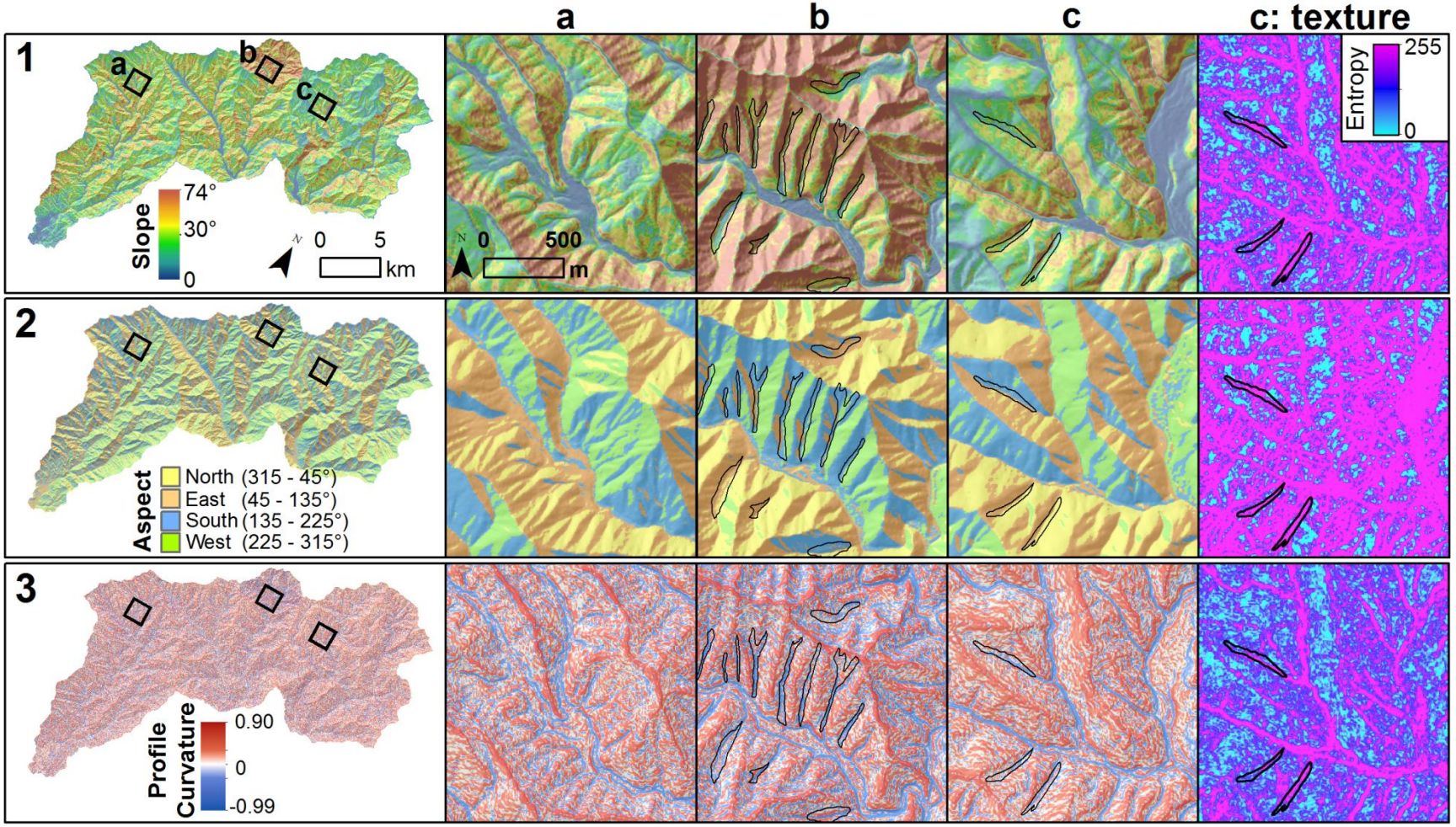

Figure 2.16. Topographic Derivative Maps: Insets (a), (b), and (c) show areas within maps (1), (2), and (3).

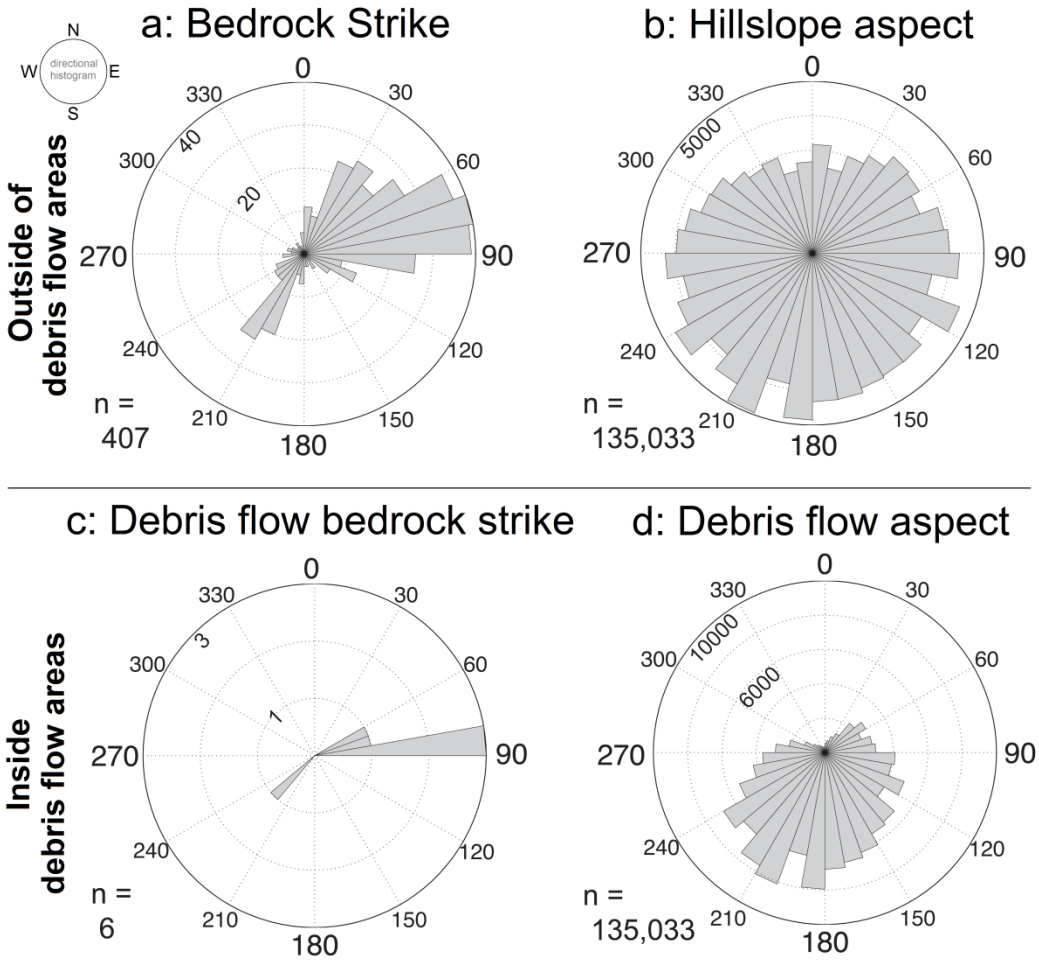

Figure 2.17. Bedrock strike and ground aspect rose diagrams: (a) Bedrock strike in the study area (Southworth *et al.*, 2005) outside of USGS mapped debris flow areas. (b) Hillslope aspect derived from the DEM of areas outside of USGS mapped debris flow areas. (c) Bedrock strike atop USGS mapped debris flow areas. (d) Hillslope aspect derived from the DEM in USGS mapped debris flow areas.

The characteristic profile curvature of the study area is highly concave channels and alternating profile curvature on hillslopes (Figure 2.14.3a). Digitized USGS debris flows and channels often coincide with negative, concave profile curvature (Figure 2.14.3b). Areas with concave profile and concave tangential curvatures are more prone to debris flows since flow is convergent here. The

majority of other areas contain low to moderate entropy values. WS-4 has a slightly more planar curvature than the other watersheds (Figure 2.14.3c).

Texture maps of topographic derivatives that appear to coincide with digitized USGS mapped debris flows were used for input. Entropy within digitized USGS debris flows is high for all derivatives, indicating homogenous, smooth surface (Figure 2.16.1a, 2.14.2a, and 2.14.3a). However, much of the aspect texture map contains a high value providing little use as an input for classification, so it was not used in classification.

2.3.3. Classification Evaluation

The digitized debris flows created from the USGS map of debris flows, orthophotos, and hillshade map were used to evaluate the results of segmentation by calculating the percent of area that intersected debris flow or non debris flow map areas as well as the percent of debris flows that were identified. Debris flows were deemed correctly identified if more than 25% of its area was classified as a debris flow. A comprehensive evaluation value of 79% was calculated as the total debris flow area that was correctly identified in the inventory created of drainage areas of debris flow-dominated channels compared with 61% of the area in the initial inventory (Table 2.3).

Table 2.3. Evaluation assessment results.

Inventory	Correctly identified		
	Debris flow area		Areas outside debris flows (%)
	area (%)	count (%)	
Entire study area	61	60	64
Drainage area of debris flow-dominated channels	79	67	88

Variation between the two inventories is largely in low slope areas. Errors of omission are high in the entire study area, especially in digitized USGS debris flows that have lower slopes (Figure 2.18.1a). Large tracts of errors of commission that are in adjacent valleys as mapped debris flows mimic the shape of debris flows (Figure 2.18.1b). Entire debris flows that were omitted tended to be slightly below the lower length to width ratio of 1.8 (Figure 2.18.1c). Errors of omission are lower in the reduced study area and flows that contain multiple tracks were often identified (Figure 2.18.2a). The large tracts of errors of commission are reduced in the reduced study area due to the tendency of lower slope subareas to be erroneously classified as debris flow areas in the initial study area classification. Errors of omission were most common as extensions of correctly identified debris flows at the head of the flow (Figure 2.18.2c).

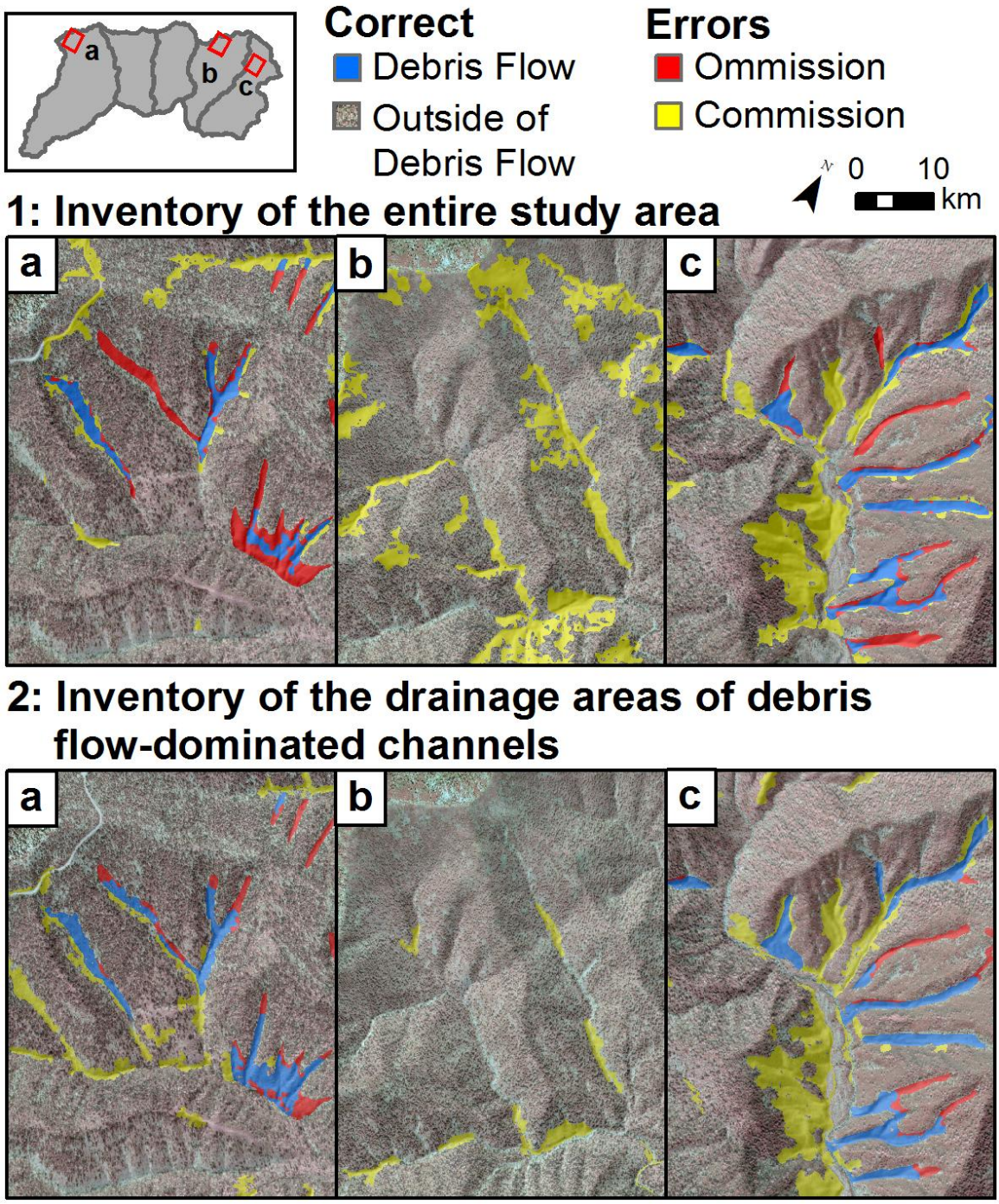

Figure 2.18. Evaluation of model results. The extent in each of the insets of the two inventories, inset rows (1) and (2), are the same as the reduced study area (bottom row). The areas shown in insets (a), (b), and (c) were selected since they contain classification features that are common throughout the study area. Basemaps are the 1998 aerial photo and hillshade map.

2.4. Discussion

2.4.1. Landscape Evolution of the Study Area

The variations amongst channel and hillslope form, as expressed through the extent of debris flow-dominated channels, hypsometry, and debris flow and knickpoint distribution, implicates an evolving landscape in the long tectonically quiescent Smoky Mountains. Evidence from the DEM, bedrock distribution, and inferences from previous studies indicate that rock strength variations are in part controlling headward stream incision rates and are among the primary factors causing differences in debris flow occurrence across the study watersheds.

The nonequivalent distribution of debris flows across the five study watersheds provides insight into hillslope response to regional landscape evolution. All study watersheds are largely underlain by the metagraywacke and metaconglomerate of the Copperhill Formation. While this unit does contain siltstone, slate and high dip planes susceptible to failure, none of the USGS mapped landslides are present on this unit in SM-2 and 3. Conversely, debris flows occur almost exclusively on the Copperhill Formation in SM-4 and 5, as well as upon the metasedimentary rocks of the Thunderhead Sandstone, indicating that there is an additional spatial control upon landslide initiation. The following paragraphs elucidate the potential mechanisms of the channels' headward incision with the intent to synthesize knickpoint and debris flow distribution relative to the landscape's evolution.

The first mechanism relates rock erodibility variations to the concentration of knickpoints near elevations of 1100 m. The lowest knickpoints in SM-4 and 5, existing at approximately 950 msl, coincide with outcroppings of highly resistant gneiss and quartzite of the Grenville Basement Complex. The coincidence of these outcroppings and knickpoints at more downstream locations than knickpoints in other watersheds indicate that the knickpoints are propagating upstream and that the outcropping of Mesoproterozoic gneiss is slowing knickpoint propagation and stream incision. The Mesoproterozoic gneiss outcrops in the course of all study

streams, though outside of the study area in the case of SM-2, but the stream length over these rocks is the longest for WS-4 and 5. The resistance of gneiss to stream power is further evident by noting the lower stream sinuosity over this map unit in Figure 2.2. Matmon *et al.* (2003b) came to a similar conclusion in their analysis of Raven Fork watershed, the higher order watershed that includes SM-2 thru 4, but suggested that knickpoint development appears only correlated with lithology in this watershed, but not other watersheds in this area. Intraformational variations present in the other watersheds are high and also may have influence upon the knickpoint propagation, though impeding upstream propagation less, in the westernmost watersheds. Throughout all of the study watersheds, it appears that stream incision is most advanced below knickpoints, though the legacy of previously propagated knickpoints and other modes of stream incision may still exist in upper hillslopes.

The second mechanism is suggested by differences between the relative positions of knickpoints and debris flows in each of the watersheds in this area and in a study by Gallen *et al.* (2011) in an area approximately 60 km south of the Smoky Mountains and by Crosby and Whipple (2006) in New Zealand. In these studies, many landslides are located close to and below knickpoints and more directly result from adjusting hillslopes to incising channels. In the Smoky Mountains, however, debris flows are all above the most downstream knickpoints. These debris flows provide a sediment source for aggradation zones upstream from propagating knickpoints where lower slopes exist. Korup *et al*. (2010) proposed a feedback mechanism between debris flows and fluvial systems such that stream incision causes hillslope susceptibility to landslides, and that debris and sediment delivered by landslides can create a convex zone in an otherwise concave channel longitudinal profile. This phenomenon can be observed in the channels' longitudinal profiles (Figure 2.10), and appears to be related to the large Pleistocene debris fans. The debris fans, comprised of unconsolidated material, contain slopes of 0.17 to 0.30 (Kochel, 1990), and have been in a phase of incision, along with lower alluvial floodplains, for about 6000 years tending towards the slope magnitudes of channels

without fans (Leigh and Webb, 2006). Knickpoints can be further accentuated due to downstream incision and upstream aggradation, which may prolong its erosion.

The last mechanism proposed here is analogous to the conclusion of Crosby and Whipple (2006) who observed that knickpoint formation can be the result of channel incision thresholds in small drainage areas. Below the drainage area threshold, again using drainage area as surrogate for discharge, streams incision is hindered by low stream power, but above the threshold stream incision is rapid. Knickpoints then are maintained at a threshold drainage area where contrasts of stream incision rates interface.

Any one of these three mechanisms by itself cannot fully explain the study streams' form, though a combination of these mechanisms does put forth a viable landscape evolution model explaining knickpoint distribution, hypsometry and debris flow-dominated channel extent. The unequivocal knickpoint distribution across drainage area size in the study area, as proposed in the first mechanism, results from the outcroppings of the Grenville Basement Complex, which retard upstream knickpoint propagation in the two easternmost watersheds. Minor amounts of Grenville Basement Complex outcroppings along the trunk channels in the three westernmost watersheds permitted knickpoint propagation up to the threshold of the stream power necessary to downgrade the knickpoint. The uppermost knickpoint in the two easternmost watersheds surpassed the Grenville Basement Complex outcroppings and also seemingly resides at this threshold. The transitory knickpoints, those whose propagation is inhibited by the Grenville Basement Complex in SM-4 and 5, cause unstable hillslopes adjacent to the trunk streams. Debris flows are still located upstream of the inhibited knickpoints of these watersheds, though it is hypothesized here that the uppermost knickpoint of these watersheds has propagated to the drainage area threshold more recently than SM-1 thru 3, thus debris flows proximal to the trunk streams throughout the watershed indicate that the landscape is still responding to downstream base level lowering or another mechanism that initiates upstream knickpoint propagation.

Hillslope steepness initially increases due to knickpoint formation in higher drainage areas which then causes steepness increases in lower drainage areas, areas that drain to debris flow-dominated channels. The ability of knickpoints to propagate up the trunk channels of SM-1 thru 3 has allowed hillslopes to respond to channel incision such that only headwater areas now have hillslopes at slope angles above thresholds for mass wasting. The stream power component of stream incision is much smaller in these areas due to the smaller discharge, meaning that debris flows have the potential to be the dominant channel incision process here. The slate and phyllite of the Anakeesta Formation in the headwaters of SM-3 that nearly coincides with this watershed's scaling break and lowest extent of USGS mapped debris flows, is more resistance to fluvial erosion as evident by knickpoint propagation, but is more prone to mass failure due to its thin bedding and intraformational composition layering (Bogucki, 1976). The majority of streams in SM-4 and 5 are debris flow-dominated which is reflected in the high proportion of high elevation topography in SM-4 and -5, indicated by the low hypsometric index of these watersheds; and upstream from the scaling break, less entrenched valleys and lower relief. Less entrenched valleys and low relief are typically indicators of areas without debris flows, but comparison of knickpoint and hypsometry of these watersheds with the three westernmost watersheds indicate that these hillslopes are presently responding to knickpoint propagation.

2.4.2. Inventories of Debris Flow-Dominated Channels

Classification results were improved by reducing the study area to subareas that were deemed susceptible to debris flows, which were the areas that were determined to drain to debris flow-dominated channels. The improvement between the inventories created of the two areas, the entire study area and drainage areas of debris flow-dominated channels, is largely due to reducing the areas where false positives could be introduced. The statistical characterization of debris flows changed little given that this study used supervised classification, which limited the

area that was characterized, and that little of the training map was removed from the initial study area. The removal of low and high slope areas was the majority of the eliminated area from the training map since the lowest elevation of the training map area is near the highest debris fan deposits and the DS plot scaling break. Assigning a training area that is affected by more significant subarea removal by the scaling break may show a larger difference between classification results between initial and reduced study areas. Removal of lower slope areas in the training map removed the depositional area of several digitized USGS debris flows where NDVI is typically higher, possibly due to more rapid revegetation in the depositional area (Bogucki, 1976). The resulting lower NDVI sum average contained within the class, "is a debris flow," resulted in narrower tracts of errors of commission where NDVI sum average was lower.

Removal of false positives eliminated many of the areas incorrectly identified by classification, though numerous errors of commission remained. Small gullies adjacent to tributaries are the largest source of this type of error. These features have similar profile curvature, slope, and NDVI values of debris flows. The small size of gullies and the length of the valley that connects them place these features within the range of length to width ratio and planimetric area. Borghuis *et al.* (2007) noted a analogous phenomenon when they found that the differences between mean size and the number of landslides produced from automated and manual methods is often due to differences in how landslides are grouped. Multiple landslide tracks from adjacent valleys that intersect in the trunk valley typically comprise one landslide in manual delineation. However, patches of vegetation, false positive removal, or cell size and neighbor statistics can divide landslides into numerous segments. It is also possible that some of these features are debris flows that were not identified during the USGS mapping effort. The large size and remoteness of some areas within the National Park, the thick forest canopy, the time since the last mapping effort, and the subjectivity of aerial photograph interpretation introduce opportunities to omit debris flows. New techniques, field verification, and

improved understanding of an area's landscape evolution may expose previously unmapped debris flows.

The uppermost area of many debris flows was not delineated with the track and toe, the majority of the errors of omission, which appears to be explained by observations made by Glenn *et al*. (2006) who also observed with lidar DEMs, a decrease in surface roughness up slide scars. These uppermost areas of debris flows where regolith detached from underlying bedrock contain relatively low surface roughness compared to lower parts of the debris flow where material is deposited. The classification algorithm was able to detect roughness by proxy of the input, slope entropy, which appears slightly higher on the head of debris flows, indicating less heterogeneity in these areas.

Recent attempts have shifted from employing aerial to satellite data in order to take advantage of increased temporal resolution at the cost of spatial resolution. This shift is a necessary one in areas of frequent landscape adjustment and landsliding. However, in tectonically stable environments such as the Smoky Mountains, temporal resolution in the range of months may not be worth the cost of decreased spatial resolution. Hence, multi-resolution segmentation and supervised classification of DEM derivatives and NDVI produced from aerial imagery was conducted to take advantage of the high resolution of these datasets to produce the inventories.

2.5. Conclusions

Creation of a landslide inventory in the Great Smoky Mountains only in subsareas that are susceptible to debris flows was conducted and evaluated. The results indicate that this technique dramatically removes overestimation of potential debris flow scars. Many of the errors were systematic, for example small gullies adjacent to streams and omission of debris flow heads, thus refinements to the classification algorithm and false positive removal can further improve the delineation success of this proposed technique. It appears that removal of

geomorphically stable areas improves characterization of surfaces, though a training map area that is more affected by the area removal and an analysis of the statistical characterization before and after the analysis will provide more insight. Field verification of errors of commission may also benefit evaluation of this technique since it is likely that the USGS landslide map, used for evaluation, does not contain all historical landslides.

Creation of inventory maps based upon known debris flows, without understanding the controls upon their parameters, is short sighted. Determining a landscape's evolution provides insight into the mechanisms that shape the area's geomorphology. The evolution of this study's hillslopes and it connectivity to fluvial incision remains enigmatic. Further work with the intent to resolve the timing and mechanisms of knickpoint retreat, hillslope response, and importantly the coupling of these two processes can further improve preparation for debris flows. The suggested refinements to this landslide inventorying technique as well as applying it to other areas will further assist the evaluation of this technique.

CHAPTER 3: A POTENTIAL IMPACT OF DOWNSTREAM COARSING IN DEBRIS FLOW-DOMINATED CHANNELS: A REFUGE FOR NATIVE SOUTHERN APPALACHIAN SALMONIDS

3.1. Background

The seemingly ubiquitous trend of gradual downstream grain size fining is the result of fundamental processes in geomorphology including selective transport of finer grains, particle abrasion, clast weathering during streambed storage, and escalated channel-hillslope coupling in headwater streams (summarized by Brummer and Montgomery, 2003). The reverse trend has been observed less frequently upstream from the transition from fluvial- to debris flow-dominated channels. Downstream grain coarsening may occur in debris flow-dominated channels due to a systematic increase in unit stream power along with a second-order control from mass wasting lag deposits (Figure 3.1; Brummer and Montgomery, 2003). Downstream coarsening, if it is a common trend in debris flow-dominated channels, has geographically widespread implications for sediment transport, landscape evolution, and fluvial ecosystems.

A frequent area of research with regards to the overall health of fluvial ecosystems is the habitat of salmonid species, which includes chars, salmon, and trout. Sediment bedload grain size availability is a control upon salmonid species fecundity since these fish use sediment to construct redds, the streambed mounds in which salmonids deposit their eggs (Kondolf and Wolman, 1993). The viability of a stream reach to sustain a salmonid population may be linked to grain size trends in fluvial networks dependent upon the species' grain size requirement, which is species-specific. Some researchers have investigated the distribution of multiple species that use different grain sizes in fluvial networks, which provide the opportunity to explore sediment transport dynamics (Buffington *et al.*, 2004; Wilkins and Snyder, 2011).

The southern extent of salmonid habitat has reached to the southern Appalachians since at least the Pleistocene (Fausch, 2008). However, salmonid

species composition in this region is in a state of rapid transition directly due to human impacts upon fluvial ecosystems and watersheds (Fausch, 2008; Larson and Moore, 1985). Previous studies have investigated the hydrologic, biologic, and land use controls on the distribution of the only native salmonid species in the Smoky Mountains, brook trout *Salvelinus fontinalis* (Fausch, 1989; Larson *et al.*, 1995). Recent research conducted in the Pacific Northwest of the United States (Buffington *et al.*, 2004) and northeastern North America (Wilkins and Snyder, 2011) has examined a streambed grain size availability control on salmonid distribution. The native and nonnative salmonid species in the Smoky Mountains, which use different grain sizes to construct redds, contest for limited reproductive stream reaches in the Smoky Mountains, providing incentive and a natural laboratory to study this topic (Kondolf and Wolman, 1993).

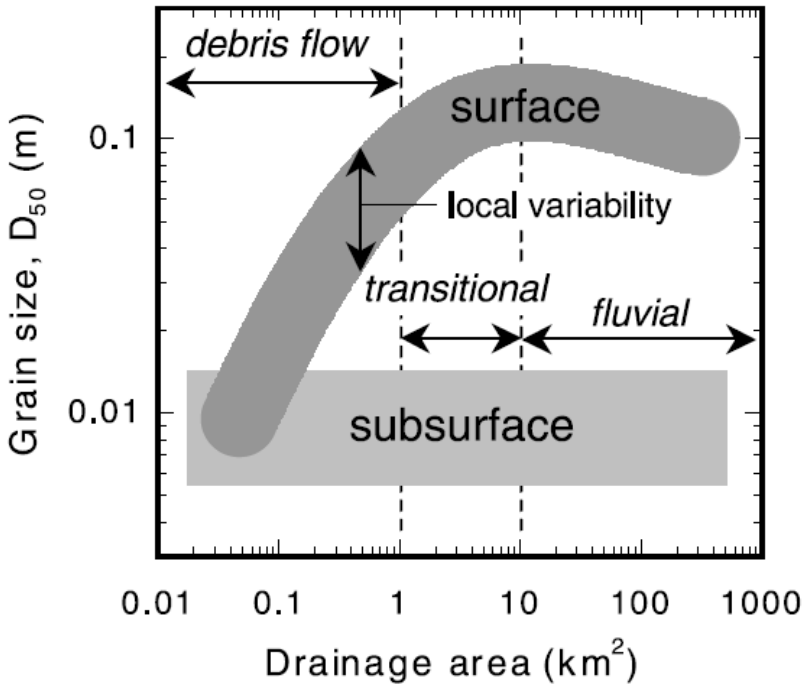

Figure 3.1. Grain size relative to channel process domains. The trend of channel surface grain size relative to drainage area has been observed to change within the transition of debris flow- and fluvial-dominated channels. Figure is from Brummer and Montgomery (2003).

Lastly, a potential, additional source of recently detached large woody material and sediment that can be entrained into streams is investigated. This case study examines a debris flow that contains numerous eastern hemlock (*Tsuga Canadensis*) trees at its initiation zone. Documenting a potential new hillslope failure trigger due to hemlock wooly adelgid (HWA, *Adelges tsugae*), an aphid that can cause mortality to eastern hemlocks (Johnson *et al.*, 2008), is the motivation behind investigating this case. Previous work in sediment transport and channel hydraulics suggests that increases in delivery of woody debris to streams produced by debris flows may alter grain size distribution (Hart, 2002; Nakamura and Swanson, 1993; Pearce and Watson, 1983). Salmonids rely upon large woody debris accumulation in stream channels for spawning substrate and provide refuges during high flow events. Processes that deliver wood to channels, such as tree throw and debris flows, have likely existed in parallel, and perhaps impacted, salmonid distribution and evolution. Documenting a case of HWA-induced landsliding will provide more insight into the swath of consequences of this pest and may be a forecast of grain size alterations due to increases in large woody debris channel entrainment.

The objectives of this chapter are:

(1) investigate grain size trends relative to the dominant channel types,

(2) determine if trout habitat can be explained in part with the modeled grain size distribution across channels, and

(3) investigate a potential new source of sediment resulting from landslides induced by HWA infestation.

3.1.1. Models and Controls of Grain Size Distribution in Drainage Networks

Variations in basin geology and flow regime have elicited region-specific sediment transport research that draws upon decades of sediment transport and hydraulic modeling efforts to predict grain size distribution in scales from a reach segment to several watersheds (reviews by Buffington and Montgomery, 1997;

Merritt *et al.*, 2003). Hydraulic feedback mechanisms stochastically vary in scales across space and time and modeling efforts are complicated by heterogeneity in soils, flow regimes, wood loading, and surficial geology. For this reason, as well as limits in data availability, some researchers have developed empirical models instead of conceptual or physics-based models in attempts to predict reach scale stream metrics and hydraulics (Merritt *et al.*, 2003). The need to understand grain size distribution in fish habitat studies has motivated recent attempts to extrapolate channel metrics collected in the field to the larger scales only attainable with DEMs (Buffington and Montgomery, 1999a; Snyder *et al.*, 2008; Wilkins and Snyder, 2011). Present habitat suitability is evaluated in terms of the median grain size (D_{50}) that acts as a species substrate and results from local stream competence, and is predicted from reach-averaged stream metrics with a series of sediment transport and geomorphic relationships.

Broadly, grain size distribution is a function of sediment supply and stream transport ability. Sediment sources and entrainment mechanisms include remobilization of streambed sediment, soil erosion due to overland flow, subsurface weathering, tree throw, soil creep, and mass wasting (Benda, 1990; Dietrich and Dunne, 1978; Horton, 1945). Snyder *et al.* (2008) concluded, with the use of painted rocks as sediment tracers, that channel sediment entrainment is controlled by reach scale channel geometry, upstream sediment supply, bankfull flows, and in their case, seasonal flows. The grain size delivered from the sediment source can affect channel competence since fine grains can tightly pack streambeds and saltation can loosen and assist entrainment (Sear, 1996; Snyder *et al.*, 2008). Sear (1996) observed that coarse grains are transported further distances in pools than riffles during bankfull discharge due to more frequent, turbulent flows in riffles that tightly pack sediment. Streambed grains can become immobile when finer sediments fill gaps between coarser grains, strongly embedding the sediment, and streambed armoring, the situation where the magnitude of frequent flow events is able to remove finer sediment but unable to move coarser sediment.

Channel hydraulics and competence is largely affected by hydraulic roughness, the resistance to shear stress caused by streambed sediment and large woody debris in the channel (Buffington and Montgomery, 1999a; Leopold, 1964). Equivalent rates of sediment supply and bedload transport cause bedload size selective erosion and deposition eliciting variations in bed roughness and the critical shear stress required to move grains of a given size (Buffington and Montgomery, 1999b). Further, bankfull flow is often the stage used in modeling efforts since channel morphology of gravel and cobble bedded streams largely results from bankfull discharge events (Andrews, 1984), and the channel geometry of this stage is apparent in the field.

Buffington and Montgomery (1999b) noted the importance of hydraulic roughness in controlling stream competence and channel morphology both resulting from alterations of streambed shear stress. Fluvial bars are often the dominant source of roughness in lower reaches, while wood loading is often the source in upper reaches (Buffington *et al.*, 2004; Hart, 2002). Roughness in pool-riffles, plane-beds, step-pools, and cascades sequentially increase in these generalized channels types that are frequent in upper reaches of mountainous regions (Buffington *et al.*, 2004).

Debris flows contribute to sediment supply and transport in montane environments when landslides translate into debris flows. Fallen trees are delivered to the stream during the flow or some time thereafter, resulting in altered flow regimes that locally alter bedload grain size (Hart, 2002). Additionally, debris flows are a central mechanism of wood recruitment in headwater streams and important contributors in log transport longer than bankfull width to channels, the length that effects channel morphology. Hart (2002) documented logjams over 100 years old in the low order streams of the Smoky Mountains where some logjams impound up to 4000 m^3 of sediment upstream from the jams. Additionally, log jams in reaches subjected to recent debris flows are less frequent, more complex, and have a shorter residence time, an average minimum residence time of 49 years compared with 81

years in non-debris flow reaches, which Hart (2002) attributed to more frequent flushing of logjams due to later debris flows.

Large woody debris (LWD) is delivered to channels through bank erosion, mass wasting, wind, and disease or senescence (summarized by Hart, 2002). LWD in a channel decreases stream competence, alters pool spacing, locally fines streambed grains, and is an important process in salmonid habitat formation and maintenance (Buffington and Montgomery, 1999a; Hart, 2002; Kondolf and Wolman, 1993). LWD allows formation of active alluvial reaches on channels with slopes reduced by logjams (Montgomery *et al.*, 1996). Median grain size also follows trends of the channels' geomorphic type, often influenced by LWD, which is in turn a control of the preferred spawning grain size of trout species that exist in the Smoky Mountains (Figure 3.2). The preferred sizes of Brook, Rainbow and Brown trout are 8 mm, 22 mm, and 18 mm, respectively (Kondolf and Wolman, 1993). Therefore, stream LWD is an important mechanism in the formation and maintenance of salmonid habitat due not only to local fining, but also flow velocity changes in which some species are better adapted (Larson *et al.*, 1995).

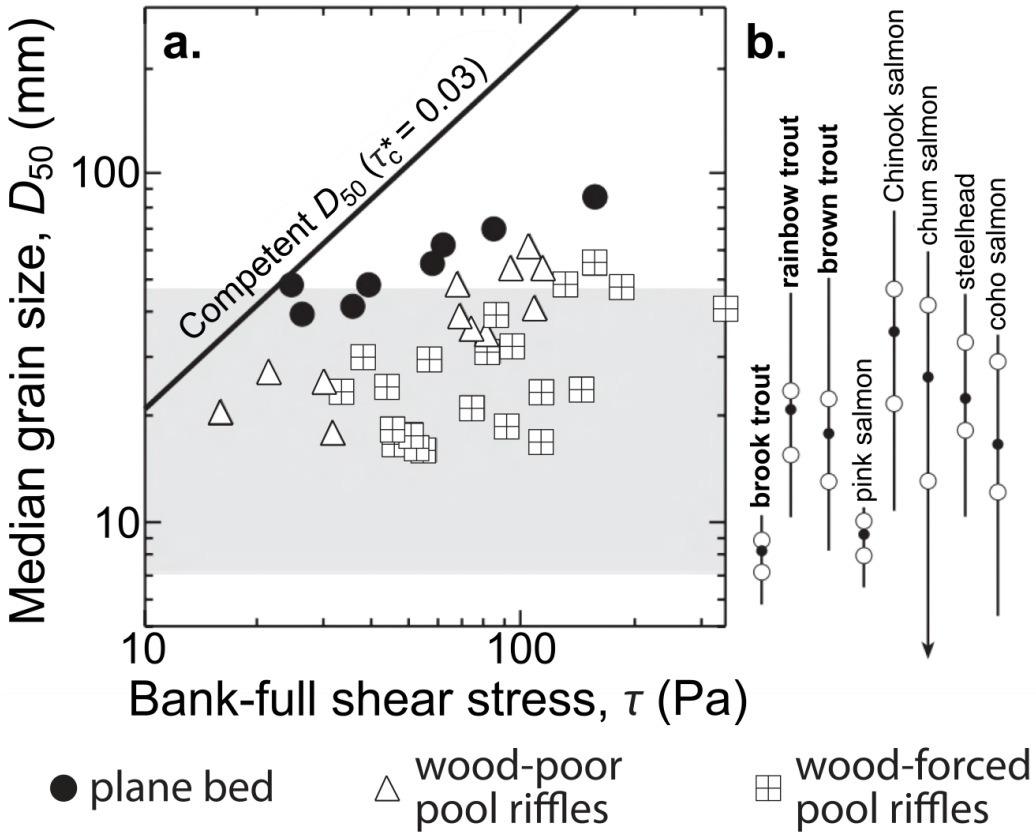

Figure 3.2. Salmonid substrate size and reach-average median grain size as a function of bank-full shear stress and channel type. The competent D_{50} at the critical Shields value, τ_c^* of 0.03 was observed in the mountainous streams in northwestern Washington State and Alaska. Figure is modified from Buffington *et al.* (2004).

3.1.2. History of Salmonids in North America and the Southern Appalachians

Two prevalent salmonid species in the United States continue to expand their range by invading the southern extent of habitats of the native salmonid species facilitated by human transplantation of species (Figure 3.3; Fausch, 2008). Brook trout are displacing cutthroat trout *Oncorhynchus clarkia* in their native range, the Rocky Mountains, originating from anthropogenic introduction in 35 states in the late 1800's that continues today in at least 7 states where it seems apparent that brook trout will not come into contact with native species (Dunham *et al.*, 2002). Rainbow trout are displacing native Brook trout in the southern Appalachians following the

anthropogenic introduction of this invasive species in the early 1900's (Larson and Moore, 1985).

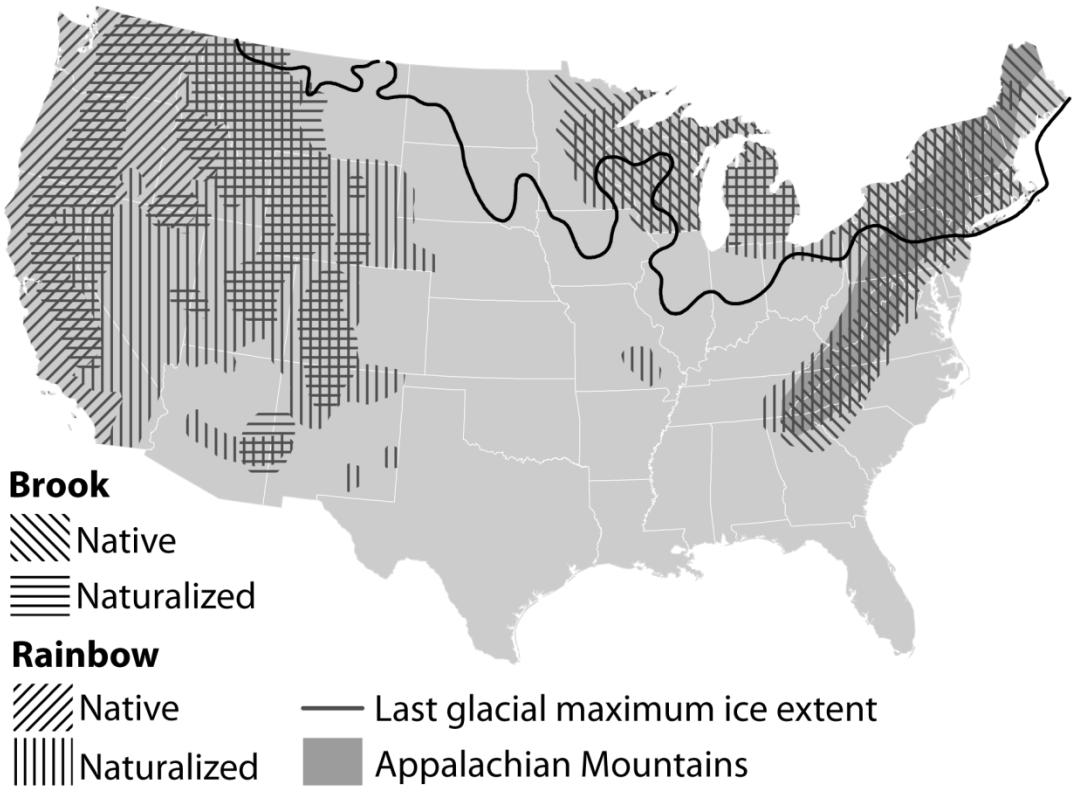

Figure 3.3. Salmonid distribution and the last glacial maximum. Recent distribution of brook and rainbow trout (after Fausch, 1989) and the southernmost extent of the last glacial maximum (after Dyke *et al.*, 2002) in the conterminous United States.

Multiple hypotheses have been developed in attempts to explain why native salmonids that have the benefit of time to adapt can be rapidly displaced by invasive salmonids. The advancement of the Laurentide ice sheet from approximately 100,000 ybp to it maximum extent 21,000 ybp drove numerous brook trout clades, organisms that share a common ancestor, to take refuge far south of their northeastern North American evolutionary range (Dyke *et al.*, 2002; Fausch, 2008). Mitochondrial DNA indicates that the clade that took refuge in the southern Appalachians genetically diverged from other clades in the early Pleistocene (1.6

million years ago) and is the most divergent such that it could be considered another species. Southern Appalachian Brook trout are syntopic, sharing the same habitat, with three to four other species in the downstream areas of their range. Relative isolation and low biotic resistance is believed to have made this clade susceptible to invasions.

Physiological processes cued by seasonal temperature changes retained from the ancestral native range of brook and rainbow trout result in a competitive edge to the latter species in the southern Appalachians (Fausch, 2008). Spawning is cued by a decrease and increase in temperature for brook and rainbow trout, respectively (Figure 3.4). Winter in the northeastern North America is typically the driest season, thus it is less likely that redds are excavated during this time. However, winter is the wettest season in the Smoky Mountains, thus rainbow trout incubation during spring precipitation decreases is preferable. Additionally, freezing of eggs can further limit fecundity, redds are constructed in areas with upwelling groundwater, thus incubation during warmer months is also preferable (Fausch, 2008).

The spawning habitat of native brook trout in the Smoky Mountains continues to withdraw upstream in ebb and flow cycles as it has done so for the last century (Hayes *et al.*, 1996; Kelly *et al.*, 1980; Larson *et al.*, 1995). Initially logging and overfishing were the causes of habitat degradation, though logging was ceased in 1936 and fishing restrictions began with the establishment of the Great Smoky Mountains National Park in 1936 (Moore *et al.*, 1983). Upstream encroachment by rainbow trout *Salmo gairdneri*, introduced into stocked streams in the early 1900s has prohibited brook trout expansion back to lower gradient streams after park establishment (summarized by Larson *et al*., 1995).

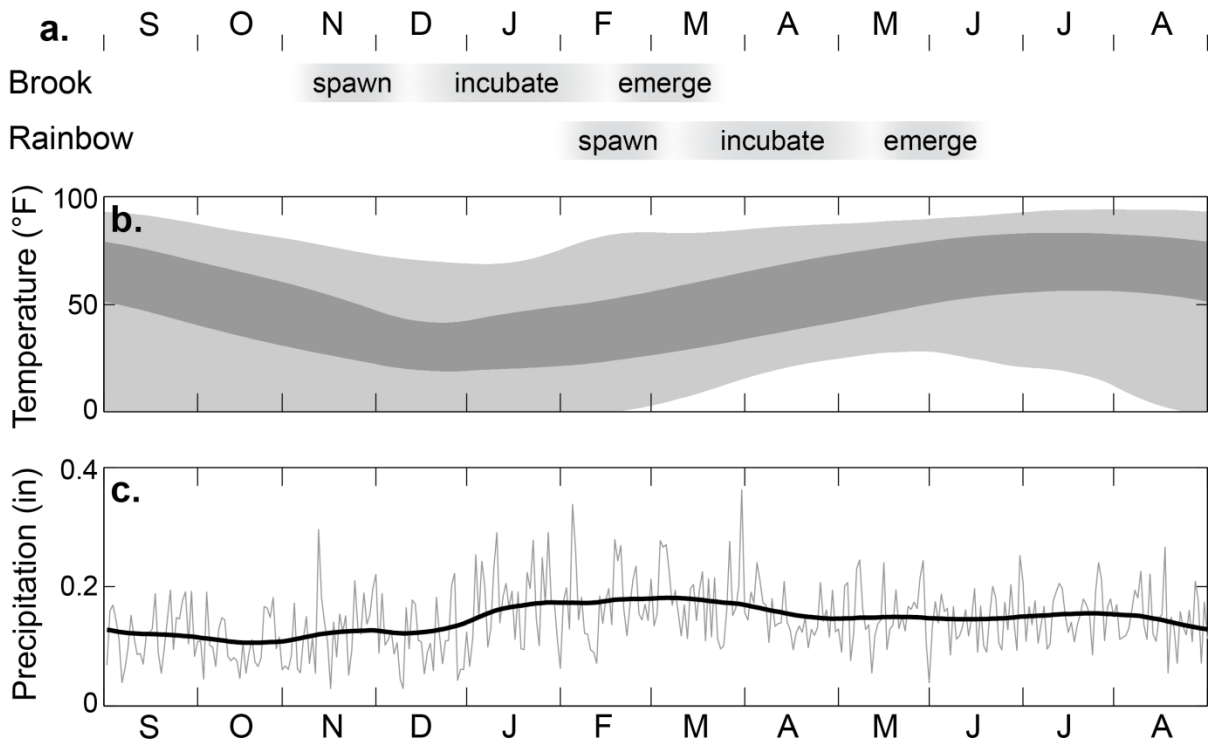

Figure 3.4. Relation of salmonid life histories (Fausch, 2008) and climate data from 1959 to 2010 recorded at the Oconaluftee River station (NCDC, 2011). (a) Brook trout typical life histories by month. (b) Bounds of daily average low and high temperature (dark gray) and maximum and minimum daily average high and low (light gray) for the 52 year period smoothed over 30-day window. Water temperature was not available in this location. (c) Daily precipitation (gray) and 30-day window smoothed daily precipitation (black) for 52 year period.

Many areas in this region that contain salmonid habitat are under state or federal land management direction, thus contain mandates and initiatives to maintain habitats as they were or believed to be prior to human influence. The National Park Service prioritizes protection of native species first, and further, enhancement of fisheries. Popularity of fishing grows as does a desire to restore trout habitat, though despite numerous management attempts, limits upon salmonid fecundity in the region has limited increases in salmonid populations and the population of the native species continues to decline (Kulp and Moore, 2005).

The range of brook trout in the Smoky Mountains prior to logging spanned between the approximate elevations of 500 m and 1550 m near stream headwaters

(Kelly *et al.*, 1980). Sympatric stream reaches that contain both rainbow and brook trout separate allopatric zones that contain only rainbow trout in lower elevations, or only brook trout in headwaters. Larson and Moore (1985) attribute the rainbow trout's ability to outcompete brown trout to habitat preferences, larger size of rainbow trout, and sex ratio of both species.

Elevation, latitude, and temperature are only weakly correlated with brook trout and other salmonids habitat selection when competition with other trout species is not a factor (Fausch, 1989). However, stream length, elevation and channel slope become important for competing trout species (Figure 3.5). Larson and Moore (1995) found that the mean elevation and slope occupied by allopatric trout significantly differ ($P < 0.05$). Mean elevation of reaches occupied by allopatric brook trout is about 1250 m and mean slope is 15.5 percent. Mean elevation of reaches occupied by allopatric rainbow trout is 780 m and mean slope is 10 percent.

Brook trout prefer low gradient streams though are better adapted to step-pool sequences than rainbow trout where they are at highest density in the pool portions of step-pool sequences where turbulence and gradient are at the minimum (Larson *et al.*, 1995). Periods of low flow may also allow rainbow trout to extend their habitat upstream (Larson *et al.*, 1995).

Elevation, pH, temperature, channel slope, and competitive disparity between salmonid species resulting from different evolutionary backgrounds are the controls upon salmonid distribution that have been observed in fluvial networks of the southern Appalachians. A grain size control has been observed in other regions, though not studied directly or through models in the Smoky Mountains. More specifically, the control of grain size trends in debris flow-dominated channels upon salmonid distribution has not been documented in the area.

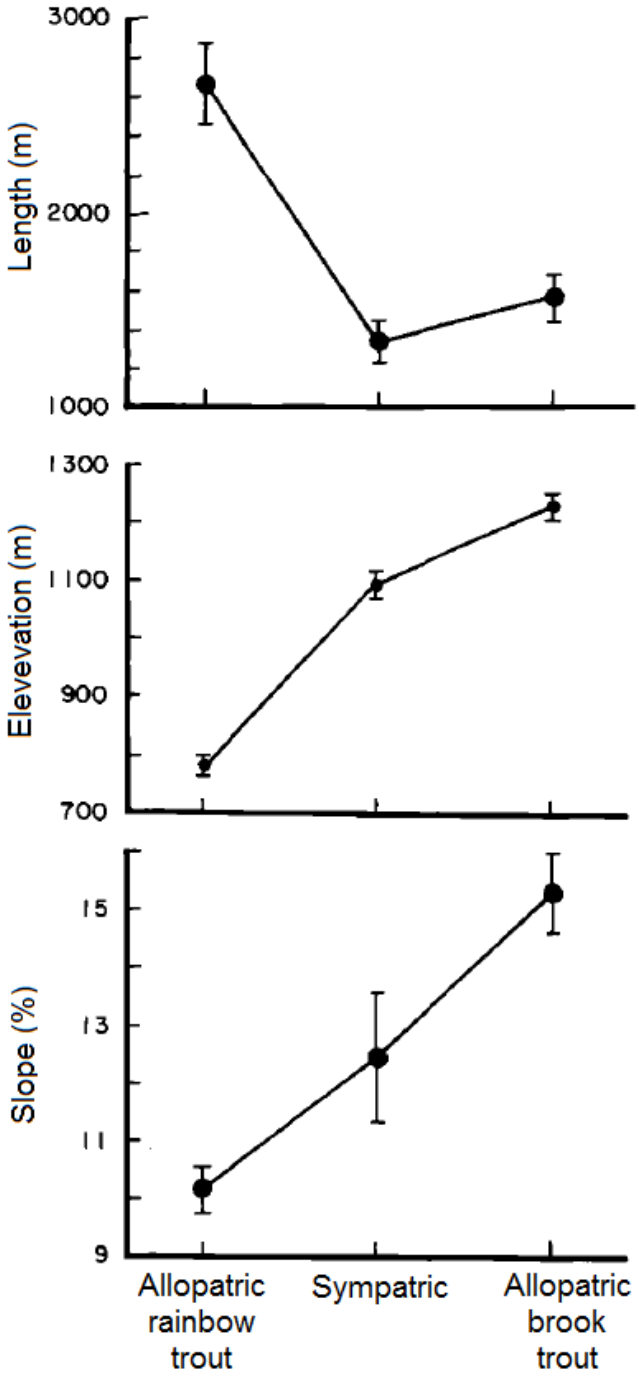

Figure 3.5. Mean channel length, slope, and elevation occupied by trout species in the Smoky Mountains. Bars are standard error of mean values. Figure is from Larson and Moore (1985).

3.1.3. Potential Recent Increase of Debris Flow Activity

Slope stability is threatened through rapid loss of eastern hemlock *Tsuga Canadensis* due to an infestation of hemlock wooly adelgid *Adelges tsugae* throughout the Appalachians (Johnson *et al.*, 2008; Orwig *et al.*, 2002). Tree roots provide slope stabilization, and root strength can control landslide occurrence and size (Dietrich *et al.*, 1995; Roering *et al.*, 2003). Precedence of deteriorating tree health and slope stability exists in the Smoky Mountains. Charlies Bunion, a summit of bare bedrock in the Smoky Mountains, was stripped of vegetation when a debris flow occurred in the area of burnt trees caused by an earlier forest fire (Southworth *et al.*, 2005).

HWA is indigenous to Japan, entered the United States via the Pacific Northwest in the 1920's, then was first discovered in Virginia in the 1950's and the Smoky Mountains in 2002 (Annand, 1924; Johnson *et al.*, 2008; Souto *et al.*, 1996). HWA, similar to other adelgids, feeds upon ray parenchyma cells of their host with the insect's elongated mouthparts that can penetrate tree bark (Young *et al.*, 1995). Hemlock trees increasingly deteriorate after infestation until mortality is reached, taking up to 12 years after infestation, and the trees commonly are found still standing 8 years or longer after death (Orwig, 2002).

A similar pest, balsam woolly adelgid (BWA) devastated Balsam and Fraser Fir populations in the high altitudes of the Smoky Mountains since it was discovered in 1962 in the area despite clear cutting and insecticidal soap spraying (Johnson *et al.*, 2008). This pest did not result in increased mass wasting since their hosts are located along ridges with divergent water flow topography, contrary to hemlocks which grow in convergent topography. The case of BWA, does portray the magnitude that invasive pests can inflict in an area, and the slow decay of trees that die due to infestation (Figure 3.6). The additional sediment and roughness elements that would be entrained in the areas streams will alter channel morphology, potentially salmonid habitat. Appendix 2 documents a methodology in determining what areas are most at risk of HWA-induced landsliding, while this chapter examines

evidence of a single landslide to determine if it was induced by HWA. This chapter investigates a mass failure scar in the Smoky Mountains that exhibits characteristics of a debris flow induced by HWA infected trees by the use of root anatomical structure analysis.

Figure 3.6. Balsam woolly adelgid afflicted Fraser Fir as observed south of Clingmans Dome Road along the border of North Carolina and Tennessee.

An incised, dry channel exists in the headwaters of the Deep Creek watershed with dimensions approximately 120 by 4 by 2 meters containing imbricated cobbles along its banks, woody debris, and living trees at the pinnacle of its flanks (Figure 3.7). The age of this seemingly recent debris flow is unknown (Keith Langdon, National Park Service, personal communication). Trees including several large hemlocks that appear to have been infected with HWA are undercut by the headscarp of this feature. The timing of this feature will be approximated with analysis of root anatomical structure of trees adjacent to this debris flow. The timing of this debris flow is imperative since its occurrence after the discovery of HWA in

the area may warrant further examination into the impact that HWA will have upon slope instability and as an additional sediment source.

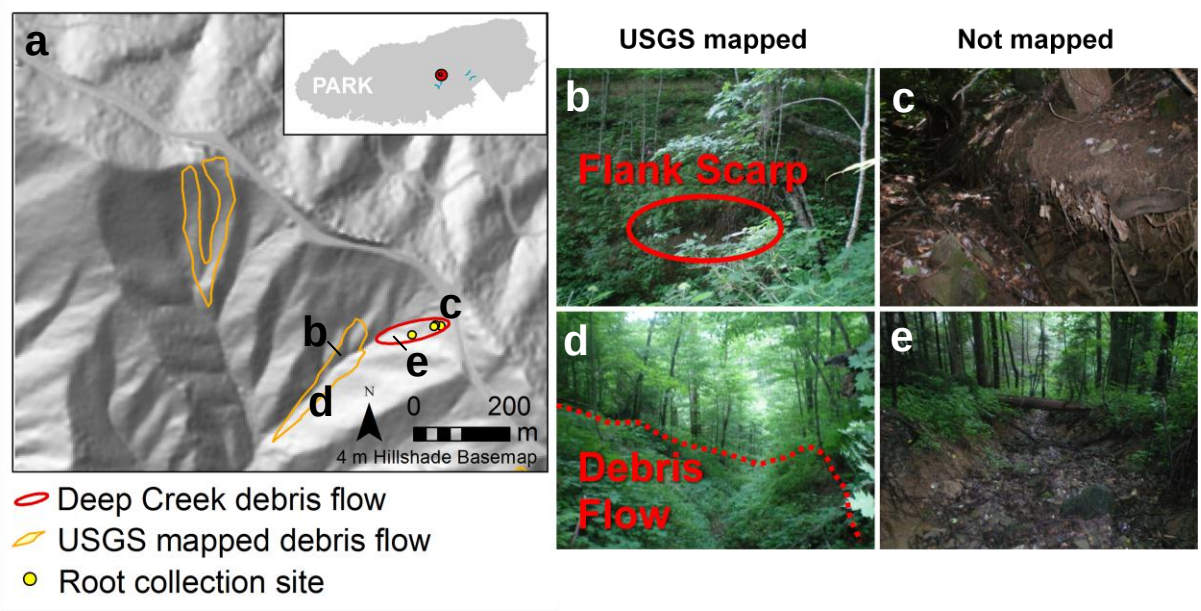

Figure 3.7. Deep Creek debris flow: (a) The Deep Creek debris flow is off of U.S. Highway 441 near the border of North Carolina and Tennessee. A USGS mapped debris flow is located directly downhill from the unmapped debris flow. Roots were collected along the flank scarps of the unmapped debris flow. These flows show separate initiation areas and flank scarps (b and c) as well as variation in revegetation (d and e).

The principles of dendrochronology most often applied to the above ground portion of trees also apply to their underground root systems. Anomalies in annual growth rings record stresses upon the tree especially when the stresses are introduced during the growing season (Gärtner *et al.*, 2001). Dendrochronologic data have the temporal resolution of a year, though a delay in recording of the exposure or erosional event may happen if the event occurs while tree growth is dormant until the following year (Malik, 2006). Alterations in the delivery of nutrients and moisture to the root cause variations in radial growth width of annual growth rings (George *et al.*, 1997). Exposed roots, such as those that could be caused by erosion or a debris flow, contain earlywood tracheids that are reduced by about 50%

in size and are increased in number compared to earlywood tracheids prior to exposure (Gärtner *et al.*, 2001). Researchers have exploited this phenomenon to calculate gully erosion rates (Malik, 2006), and determine the year of stem burial (Marin and Filion, 1992). The nature of root exposure, sudden or continuous denudation, must be determined to understand the conditions prior to exposure (Gartner, 2007). Orwig (2002) noted that hemlock growth ring width decreased concordant with HWA infestation synchronous with oak and maple growth ring increases. Anomalies in roots adjacent to the Deep Creek debris flow are examined for evidence of sudden exposure indicating rapid removal of soil due to mass wasting.

3.2. Methods

Channel geometry and sediment transport parameters were predicted in four streams with inputs from the 4 m bare earth DEM and parameterized with field data. Further, hydraulics were extrapolated to trunk streams of five watersheds to examine stream-wide grain size trends and the implications these trends may have upon salmonid habitat. A survey of observed salmonid species was used to evaluate predicted grain size across modeled streams.

3.2.1. Study Streams

Study streams were divided into two populations: surveyed streams where field data was collected and modeled streams. The surveyed streams include four second-order streams and were selected based upon similar bedrock, drainage area size, and anthropogenic disturbance history in the National Park (Table 3.1; Figure 3.8). The drainage area of these streams were subjected to diffuse or no logging, prevalent in the lower elevation areas of the mountain range in the late nineteenth and early twentieth century (Pyle, 1988). Due to this, the streams are minimally affected by variations of large woody debris entrainment caused by different canopy composition and structure vegetation succession stages (Hart, 2002). The streams

are perennial, confined in narrow valleys, the largest valley width measured between drainage divides is about 2.9 km, and contain bedrock and alluvial reaches. Bed material is comprised of gravel, boulders and bedrock of the Copperhill Formation that is principally composed of metagraywacke and metacongolerate interbedded with graphitic and sulfidic metasiltstone (Southworth *et al.*, 2005). The modeled streams include five third-order streams with varying bedrock and drainage area size of the transition from debris flow- to fluvial-dominated channels as determined in Chapter 2.

The surveyed streams also differ by recent debris flow activity. Deep Creek and Left Fork Deep Creek contain USGS mapped debris flows. There are not any mapped debris flows in Taywa and Chasteen Creek, indicating a lower probability of recent debris flows in the watersheds of these streams. These streams do have a higher average slope, though the average slope of adjacent hillslopes are much lower compared to the hillslopes of the debris flow population.

Table 3.1. Surveyed stream characteristics.

Study stream number	**1**	**2**	**3**	**4**
Channel name	Left Fork Deep Creek	Deep Creek	Taywa Creek	Chasteen Creek
Elevation (msl)	925 to 1128	988 to 1182	857 to 1169	783 to 1073
Drainage area (km^2)*	11.0 to 5.8	12.4 to 0.8	4.3 to 1.0	9.6 to 1.1
Channel Length (m)	3018	2975	2443	3027
Channel slope ($m \cdot m^{-1}$)†	0.067	0.064	0.128	0.096
Watershed slope (degrees)‡	29.0	27.9	28.4	28.6
Debris flow area (km^2)∞	0.28	0.06	0	0

* Calculated as the area that drains to the most downstream and upstream stations in the streams.
† Calculated as the slope of the study stream segment as the quotient of change of elevation and stream length.
‡ Calculated as the average slope of hillsides in the watershed. The slope values within a 10 m buffer of streams was not included in this calculation.
∞ USGS mapped debris flows from Southworth *et al.* (2005).

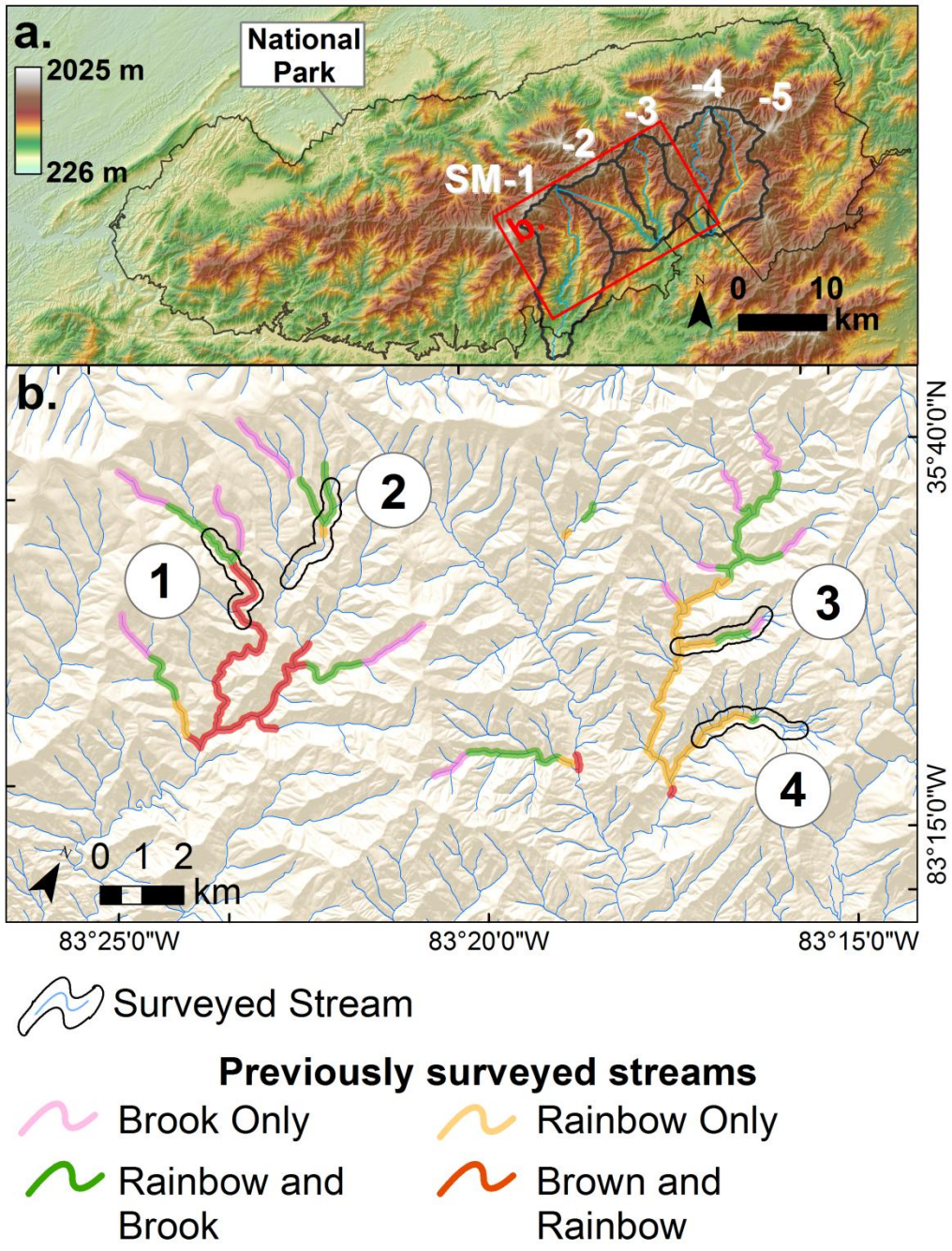

Figure 3.8. Study streams and salmonid surveys: (a) The modeled study streams (blue) and watersheds (black) are within the southern side of the range. (b) Four surveyed streams in the mid to upper elevations of the Smoky Mountains. Trout surveys were conducted by Kelly (1980).

Evaluation stations where stream metrics were surveyed, calculated, or predicted were spaced every 10 m up the streams. On each of the four surveyed streams, three reaches of 100 m in length where field surveys were conducted were spaced 400 to 500 m apart (Figure 3.9). These surveys provided inputs for calibration of stream metrics and were used for evaluation of modeled grain size.

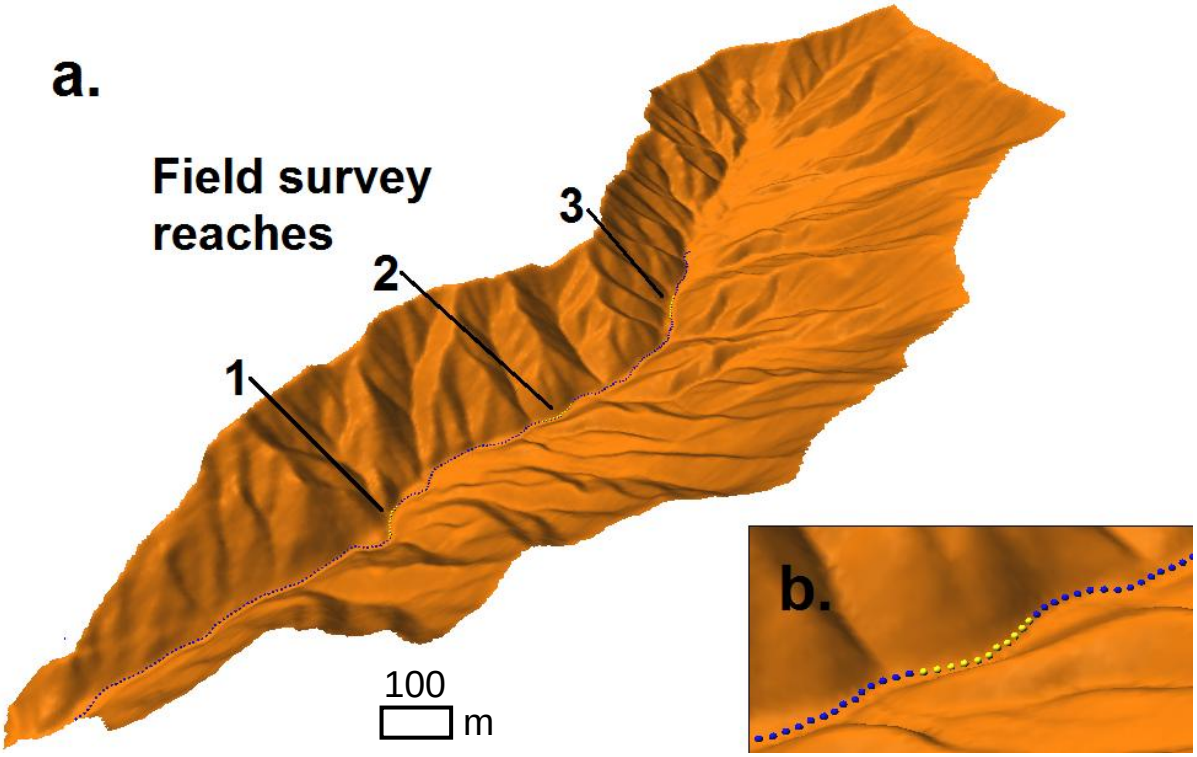

Figure 3.9. Study stream evaluation stations: (a) This oblique perspective model of the Taywa Creek watershed is a section of the DEM used for all streams and shows how evaluation stations were spaced along each of the surveyed streams. Each surveyed stream is comprised of three field surveyed reaches 100 m in length with evaluation stations every 10 m up the stream. (b) Evaluation stations in the field survey reaches coincide with the evaluation stations of the entire stream.

3.2.2. Field Surveys

Bankfull height and width, and channel slope were measured at each station in the field surveyed reaches in July of 2010. Additionally, the channel morphology type of the station was placed into one of the types following classification of

Montgomery and Buffington (1997): pool-riffle/plane-bed, wood forced pool-riffle, and step-pool/cascade (Figure 3.10). Three to four D_{50} measurements were conducted in each field surveyed reach with the Wolman (1954) methodology outlined as follows. The intermediate axis of 100 randomly selected grains was measured at the downstream station of each reach and every 20 to 30 m up the stream reach. The axis measurements was truncated to 2 to 256 mm. Bankfull height and width were collected with a meter tape (Figure 3.11). Slope was calculated along a channel as:

$$s = arctan\left(\frac{e}{d}\right) \quad \textbf{(3.1)}$$

where *e* is the eye height of the surveyor [m], and *d* is the distance between the surveyor and a point upstream that is level upstream [m]. The distance upstream from the surveyor, who was standing in the stream, where the stream intersected the height of the survey's eye level was determined (Figure 3.12). The point upstream level with the surveyor's eye height was located with a clinometer and the distance to that point was determined with a rangefinder with a 1 m resolution. Slope is slightly overestimated since the surveyor was standing in the water and the upstream point was above water, but this error is minimal since the objects selected were near the water level often at locations of shallow water.

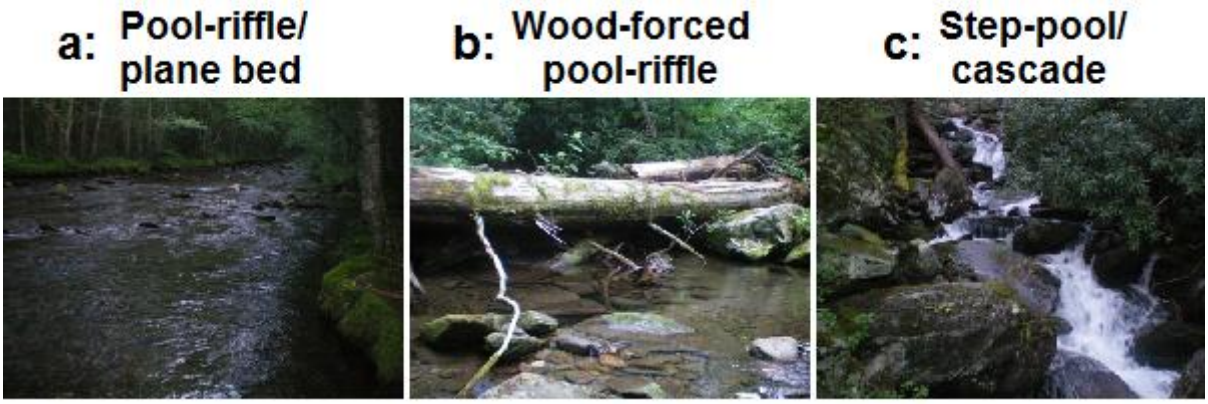

Figure 3.10. Photos of study site channel types were taken facing upstream July, 2010 at (a) Stream 2: Deep Creek; (b) Stream 1: Left Fork Deep Creek; (c) Stream 3: Taywa Creek.

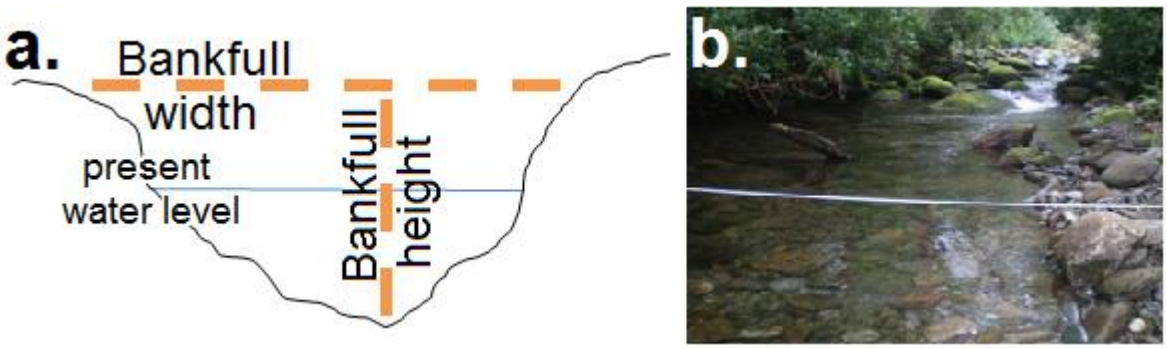

Figure 3.11. Representation of bankfull depth and width measured in the field: (a) Channel cross-section showing bankfull width measured at the streamside slope break where riparian vegetation ceased. Bankfull height is measured from the bankfull height elevation to the thalweg of the section. (b) Tape extended across Deep Creek to measure bankfull dimensions.

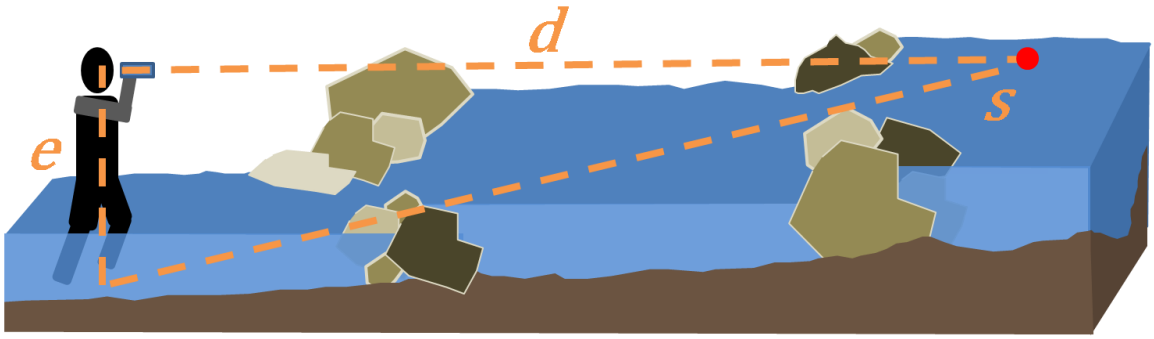

Figure 3.12. Method to calculate channel slope *in situ.* An object in the stream that was not highly displaced from the thalweg was used as the point from which *d*, distance, and *e*, eye height, was determined in order to calculate *s*, channel slope, using Equation 3.1.

3.2.3. Grain Size Modeling

Median grain size distribution throughout the length of the study streams was predicted at each of the evaluation stations with inputs from the bare earth DEM described in section 2.2.2.1. Channel geometry and hydraulics were also predicted since these values are required to predict median grain size.

Channel competence can be measured as streambed shear stress, τ_{bed}, as the force per unit area [pa = kg·m^{-1}·s^{-2}], and is often approximated with what is commonly referred to as the depth slope product:

$$\tau_{bed} = \rho g h S \quad \textbf{(3.2)}$$

where ρ is density of water [kg·m^{-3}], g is acceleration due to gravity [m·s^{-2}], h is bankfull height [m], and S is channel slope [m·m^{-1}]. Streambed grain entrainment begins at the moment of incipient motion, when streambed shear stress surpasses the critical stress, often defined as the dimensionless critical Shields parameter, τ_c^*, that overcomes gravitational and frictional forces acting to retain a grain of particular size, D [m], in the streambed:

$$\tau_c^* = \frac{\tau_{bed}}{(\rho_s - \rho) g D} \quad \textbf{(3.3)}$$

where ρ_s is density of sediment [kg·m^{-3}] (summarized by Shen and Julien, 1993). A τ_c^* of 0.06, often used for modeling applications in streams with homogenous grain sizes, cannot be applied to valleys subject to debris flows since debris flows often create streambeds with unsorted grain sizes (Benda, 1990; Buffington and Montgomery, 1997).

The critical shear stress required to initiate incipient motion of the median grain size, D_{50}, in turbulent flow has been used to predict grain size distribution (Buffington *et al.*, 2004). The prediction of D_{50} is possible by first determining the critical Shield value that mobilizes the local median grain size, $\tau_{c_{50}}^*$, and equating the Sheilds equation to D_{50} such that the size of the median grain size transported by the critical Sheilds value, D_{50}^*, is predicted:

$$D_{50}^* = \frac{\tau_{bed}}{(\rho_s - \rho) g \tau_{c_{50}}^*} \quad \textbf{(3.4)}$$

Equation 3.3 indicates that grains with a smaller diameter than D_{50}^* are not competent as streambed grains, thus grains smaller than this value will be mobilized during bankfull flow events.

Only $\tau_{c_{50}}^*$, channel slope, and bankfull height had to be determined since standard, constant values of gravity as 9.81 m·s^{-2}, and densities of water as 1000 kg·m^{-3} and sediment as quartz 2650 kg·m^{-3} were used. The median grain size and

bankfull depth of the field surveyed reaches were used to empirically determine $\tau^*_{c_{50}}$ at each of the evaluation stations. τ^*_c was approximated as the shear stress of the bankfull flow, τ_{bf}, such that $\tau^*_c \approx \tau^*_{bf}$ since a sediment transport threshold at or near bankfull stage has often been observed in gravel and cobble bedded channels, a typical channel type in the study area and the preferred type of salmonids (Andrews, 1984; Buffington *et al.*, 2004; Kondolf and Wolman, 1993). A power law model was constructed for the three channel morphologies identified in the field in order to extrapolate these metrics to the modeled reaches:

$$\tau^*_{bf} = k\tau^n_{bf} \quad \textbf{(3.5)}$$

where empirically determined *k* and *n* represent channel morphology and local catchment conditions (Buffington *et al.*, 2004). The channel morphology and the associated τ^*_{bf} power law applied to an evaluation station were determined by the station's channel slope due to the strong relationship between channel slope and hydraulic roughness (Buffington and Montgomery, 1999a). The channel types at each evaluation station in the field reaches, which more often existed as intermediate types as described by Montgomery (1997), were identified in the field. Channel slope central tendencies of mapped pool-riffle/plane-bed and wood forced-pool riffles do not overlap providing credence to using slope as proxy of channel type (Figure 3.13).

Channel slope was calculated from the bare earth DEM with Equations 2.2 and 2.3 and averaged over 100 m reaches in surveyed and modeled reaches. Bankfull height, h_{bf}, was predicted from watershed scale hydraulic relationships:

$$h_{bf} = \propto A^{\beta} \quad \textbf{(3.6)}$$

where empirical values α and β represent local physiography, sediment supply, and basin hydrology (Leopold, 1964). α and β were calculated separately in Equation 3.6 in each of the surveyed streams. Streambed grain size can be predicted with

DEM inputs and empirical values by inserting Equations 3.5 and 3.6 into Equation 3.3 (Buffington *et al.*, 2004):

$$D_{50} = \frac{(\rho \propto A^{\beta} S)^{1-n}}{(\rho_s - \rho) k g^n} \quad \textbf{(3.7)}$$

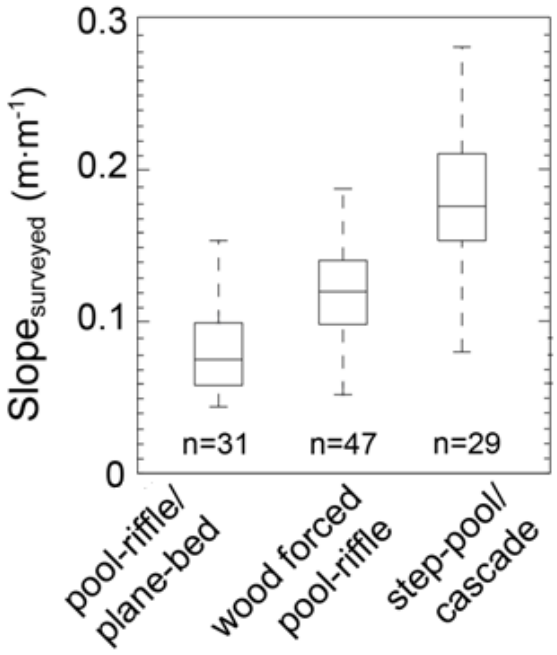

Figure 3.13. Channel morphology type slope. The non-overlapping central tendencies of field surveyed slope in channel types is shown in this box plot. The central horizontal line is the median. The bottom and top edges of the box are the 25th and 75th percentile, respectively. The whiskers extend to the minimum and maximum data points.

Prediction of D_{50} and other stream metrics at each evaluation stations along surveyed streams facilitates comparison between the predicted and field measured values. Prediction of D_{50} in modeled streams facilitates the investigation of grain size trends in the longer trunks streams in the study area. Comparison of predicted reach averaged grain size and trends can be conducted in both stream populations.

Field surveyed and DEM derived stream metrics are evaluated in the field surveyed reaches to evaluate the goodness of fit of these two populations to a 1:1 relationship and with root mean-square error (RMSE). Previous researchers have used the bounds of 1:2 and 2:1 ratios of surveyed to modeled values to determine the relative goodness of fit amongst metrics (Wilkins and Snyder, 2011). RMSE is calculated as the square root of the mean of squared differences between modeled (x_i) and surveyed values (t_i) for n surveyed reaches:

$$\mathrm{RMSE} = \sqrt{\frac{\sum_{i=1}^{n}(x_i - t_i)^2}{n-1}} \quad \textbf{(3.8)}$$

Equation 3.8 indicates that low RMSE values indicate similar surveyed and modeled values. However, large errors between surveyed and modeled values have a disproportionate effect on RMSE since values are squared (Warren *et al.*, 2004).

3.2.4. Root Dendrochronology

A potential, additional source of recently detached large woody material and sediment that can be entrained into streams is investigated. The potential source is HWA-induced landsliding and it is investigated with root dendrochronology. Roots of eastern hemlock *Tsuga canadensis* , flowering dogwood *Cornus florida*, and red oak *Quercus rubra* were collected adjacent to a debris flow located at the headwaters of Deep Creek (Table 3.2). Additional roots were collected but were not analyzed. The location of the root provides the geomorphologic context needed to consider the history of the tree (Gärtner *et al.*, 2001), thus the location of the roots were carefully noted and the root distance to tree was less than 1 m for all samples. Roots were dislodged from the tree with a handsaw. Roots were supported in soil containing cobbles and small boulders, providing additional support to the tree, though making it difficult to extract deeply buried roots.

Table 3.2. Root sample metadata.

Sample ID	Common Name	Location		DBH (m)
R01	Flowering Dogwood	35.60040°N	83.42350°W	0.75
R02	Red Spruce	35.60037°N	83.42353°W	0.47
R03	Eastern Hemlock	35.60039°N	83.42338°W	0.71
R04	Eastern Hemlock	35.60041°N	83.42332°W	0.75

Once in the laboratory, the roots were sectioned with a band saw and further cut into segments perpendicular from the cross-section. Cross-sections were then cut from the segments with a sledge microtome to a thickness of 15 to 30 µm, stained with safranin, and mounted on slides. A Nikon SMZ 800 microscope was used to analyze the slides. Cross-sections were reconstructed in slide images to correspond with the orientation of the roots' orientation when cut from the tree. The total count of growth ring thickness anomalies, where abnormally thin rings indicate a disturbance to the tree, is determined for each root. The number of annual growth rings since the disturbance, likely representing the year of hillslope failure, is compared with the discovery of HWA in the area in 2002 (Johnson *et al.*, 2008).

Cores were also extracted from the trunk of sampled trees with an increment borer in order to determine if growth ring thickness anomalies appear in the trunk as well. Cores were extracted approximately a meter up the trunk from the ground and perpendicular to the ground's slope direction in order to minimize the amount of reaction wood in the cores (Stoffel and Bollschweiler, 2008). In the laboratory, growth ring thickness was measured from the bark towards the pith with the use of a trinocular stereoscope on a 24" Velmex Unislide positioning stage with a 1µm Acu-Rite linear encoder.

3.3. Results

3.3.1. Comparison of Field and Modeled Metrics in Surveyed Streams

Field surveyed and DEM modeled stream metrics of the surveyed streams were evaluated in the locations of the field surveyed reaches. Modeled channel slope was under-predicted relative to field surveyed slope with a coefficient of determination, r^2, of 0.34 and a RMSE of 0.040 (Figure 3.14). Under-prediction increased as field surveyed slope increased. Other researchers have observed that sinuosity is not well represented in low slope streams, though synthetic streams often match the plan view dimensions well when the slope is high (Snyder, 2009). Removal of the outlying lowest reach of Stream 2 raises the r^2 to 0.55, though it is still apparent that slope measured from the DEM is under-predicted relative to field measurements. The seemingly systematic nature of slope under-prediction may be explained by the following two possibilities. The *d* values of Equation 3.1 used to determine channel slope in the field ranges between 2 and 32 m and the modeled slope was calculated in 4 m grid cells. The measurements in the field may have included large elevation increases, such that would occur in step pool sequences and log jams that may have not been recognized in the DEM. Secondly, channel width is typically smaller in areas with large slopes, so bare earth lidar returns are less likely to reach all of these areas, thus channel slope in the upper reaches may have included lower hillslopes in the reach average calculations.

Potential sources of error in channel slope calculations include resolution of the rangefinder used to calculate surveyed channel slope, incorrect reconciliation of survey and DEM station locations, incorrect removal or inclusion of lidar point during post processing filtering of point cloud prior to DEM creation, incorrect tension and smoothing parameters during DEM creation, and misalignment of the streams in between the field and DEM.

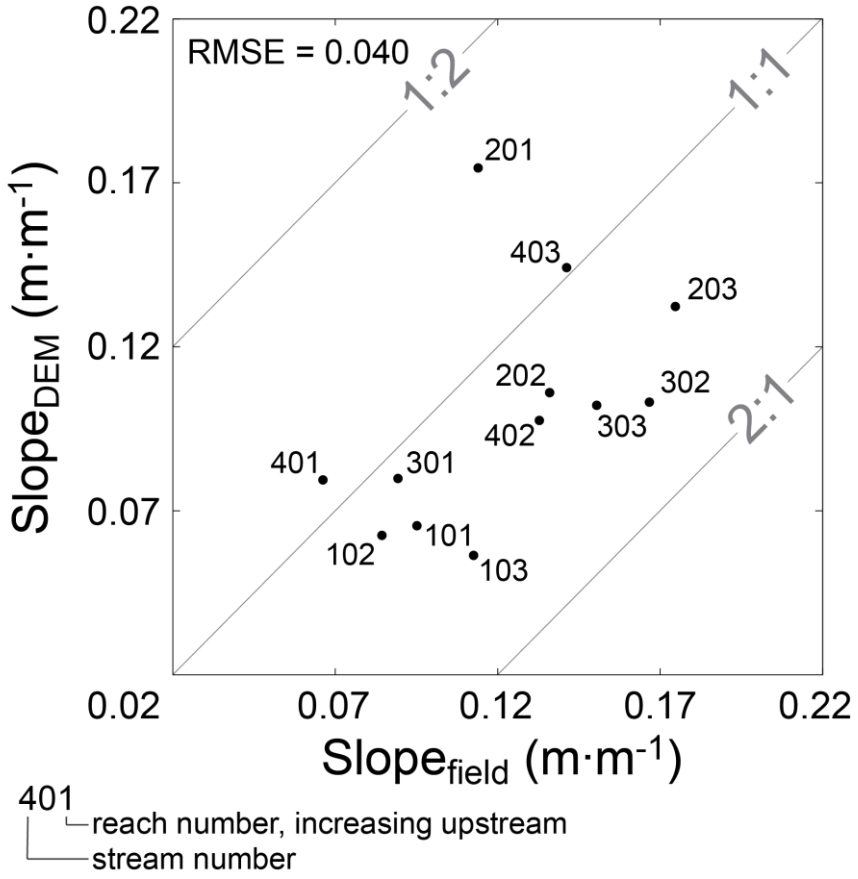

Figure 3.14. Comparison of field and modeled channel slope. Slope is reach averaged in the location of the field surveyed reaches.

Empirically derived bankfull height exhibits a near 1:1 ratio with field surveyed bankfull height and has a r^2 of 0.93 and RMSE of 0.0813 (Figure 3.15a). Prediction of bankfull height by calculating α and β values for each surveyed stream improved bank full prediction from a r^2 of 0.58 to 0.93. Streambed shear stress, τ_{bed}, was slightly under-predicted for the majority of the surveyed reaches, and has a r^2 of 0.38 and RMSE of 339 pa (Figure 3.15b). Channel slope and bankfull width under-prediction is transmitted to the shear stress calculations. Nevertheless, all field surveyed reaches were predicted within a factor of two with exception of the uppermost reach of Stream 1 where slope was highly under-predicted.

The surveyed and modeled critical Shields value, τ_c^*, has a r^2 of 0.41 and RMSE of 1.04 (Figure 3.16c). The low slope of these reaches classified many of the evaluation points as pool-riffles, thus τ_c^* was the result of the lowest coefficient and exponent determined for the three channel types. D_{50} calculated with the modified Shields equation was predicted within a factor of two for all reaches except the central reach of Stream 4 with a r^2 of 0.58 and RMSE of 14.1 mm.

Modeled channel metrics of the entirety of surveyed streams were calculated to compare these values with field measured values (Figure 3.16). Longitudinal profiles of streams appear smooth in reach scale since evaluation stations spaced 10 m apart reduced the influence of artifacts that exist within lidar data and that are created during DEM interpolation. However, the prominent knickzone in Stream 3 is apparent approximately 850 to 950 m up the stream in this stream's longitudinal profile. Reach-average channel slope slightly decreases downstream in Streams 1 and 2 with the exception of the large slopes in the two most downstream reaches of Stream 2. Slope in Streams 3 and 4 decreases more appreciably especially near the knickzone in Stream 3.

Bankfull height increases gradually, as a function of drainage area, in all streams except in Stream 3 where the opposite trend is observed. An inverse relationship between drainage area and bankfull height was observed during field surveys in only this stream. Bankfull height decreases upstream in all of the surveyed streams with exception of the uppermost reach of Stream 3 where the observed bankfull height is at its maximum in this stream (Figure 3.17). The bankfull width to height ratio of this reach is significantly lower in this reach compared to the other reaches of this stream. Further, the reach variance of the width to depth ratio of surveyed streams is notable higher in Stream 3 compared to the other streams indicating that this reach differs from all other surveyed reaches where variance is low and the standard deviations of channel metrics overlap. The influence of slope upon streambed shear stress, the critical Shields stress value, and D_{50} is apparent (Figure 3.16). However, bankfull height appears to be an important control upon the

trend of these metrics since the downstream decrease of bankfull height in Stream 3 causes downstream decreases in bed shear stress, the Shields parameter, and D_{50}. Field surveyed D_{50} in all streams follow the trend of downstream coarsening in the modeled grain size data, though again with exception of Stream 3 where modeled D_{50} fines downstream.

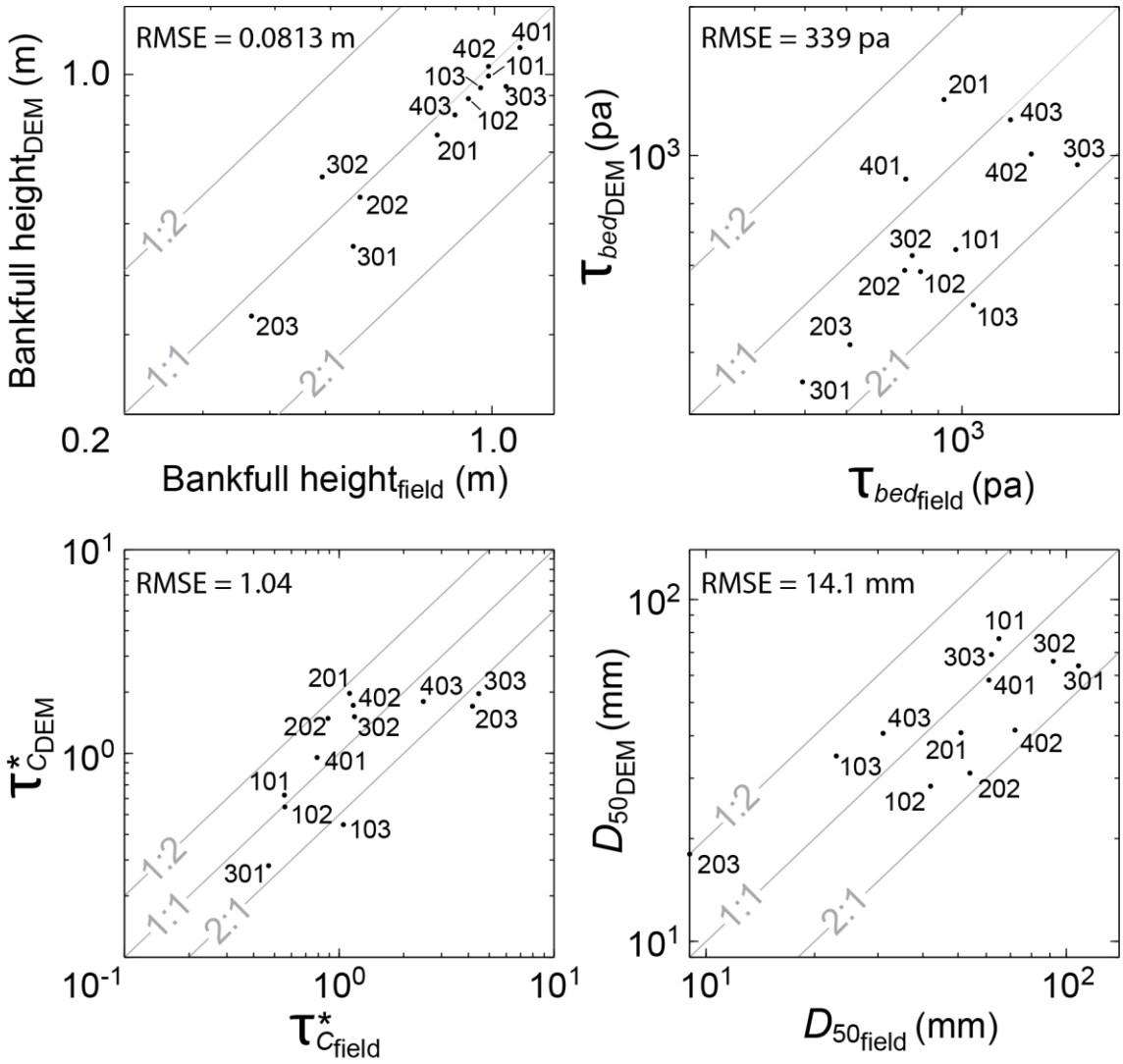

Figure 3.15. Comparison of surveyed and modeled stream metrics. Evaluation of reach averages in field surveyed reaches (black points) relative to a 1:2 and 2:1 relationship between field and surveyed data. Root mean square error is defined in Equation 3.8.

Figure 3.16. Modeled geometry and hydraulics of surveyed streams. Stream longitudinal profiles were created from extracting the elevation value from the DEM at each evaluation station. The other metrics were averaged in 100 m reaches.

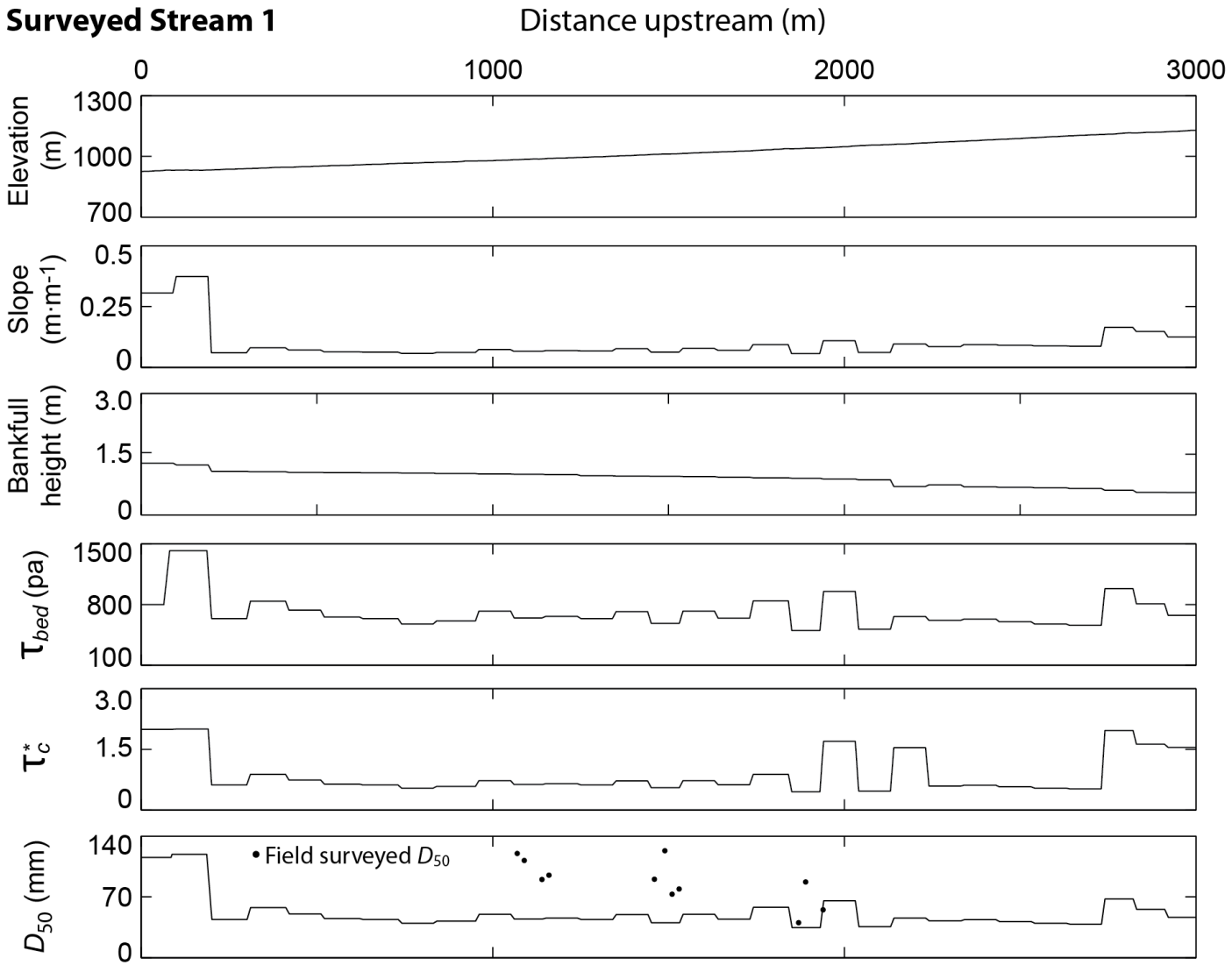
Surveyed Stream 1
Distance upstream (m)
0
1000
2000
3000
Elevation (m)
1300
1000
700
Slope (m·m-1)
0.5
0.25
0
Bankfull height (m)
3.0
1.5
0
τbed (pa)
1500
800
100
τ*c
3.0
1.5
0
D50 (mm)
140
70
0
• Field surveyed D50

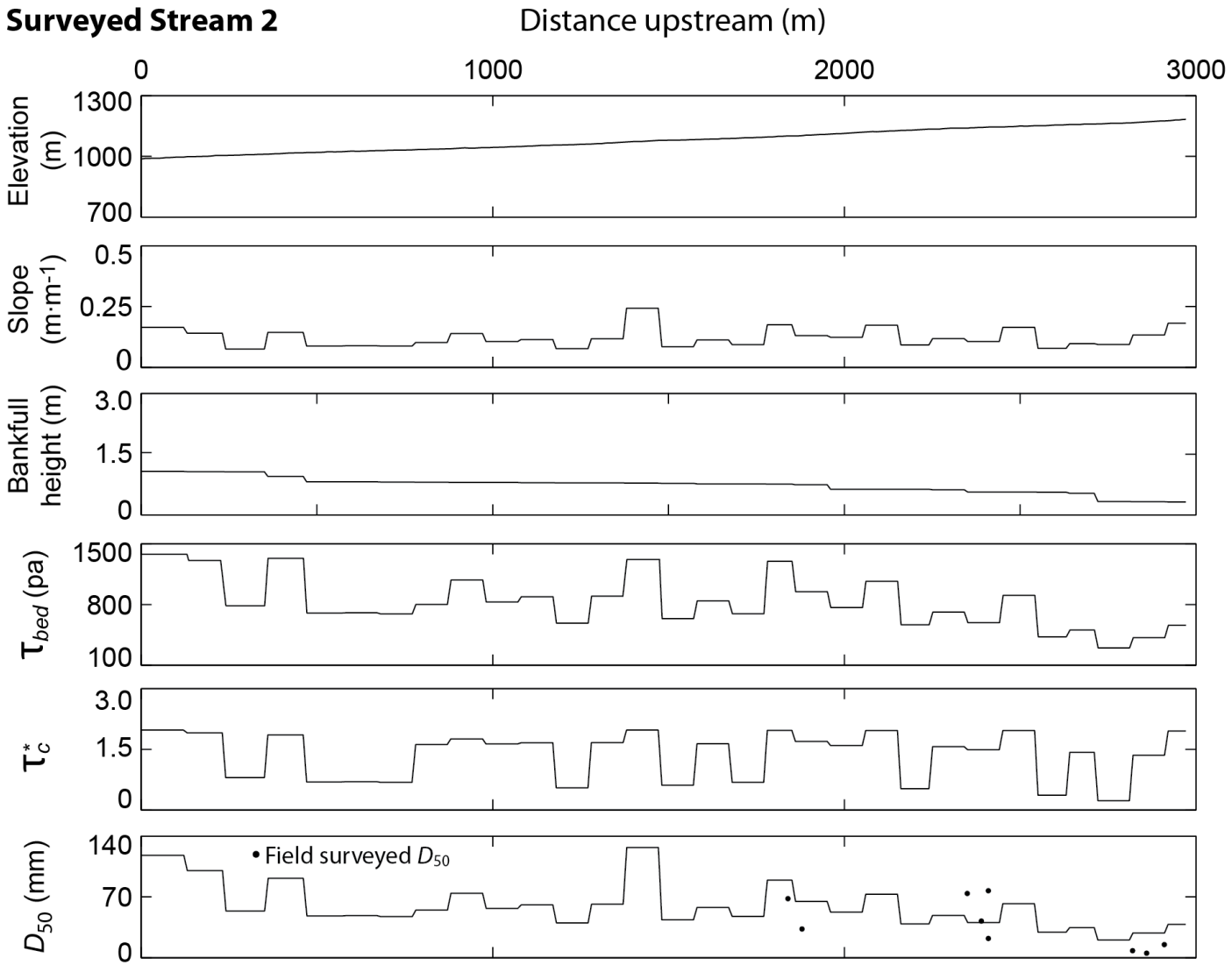
Surveyed Stream 2
Distance upstream (m)
0
1000
2000
3000
Elevation (m)
1300
1000
700
Slope (m·m-1)
0.5
0.25
0
Bankfull height (m)
3.0
1.5
0
τbed (pa)
1500
800
100
τ*c
3.0
1.5
0
D50 (mm)
140
70
0
• Field surveyed D50

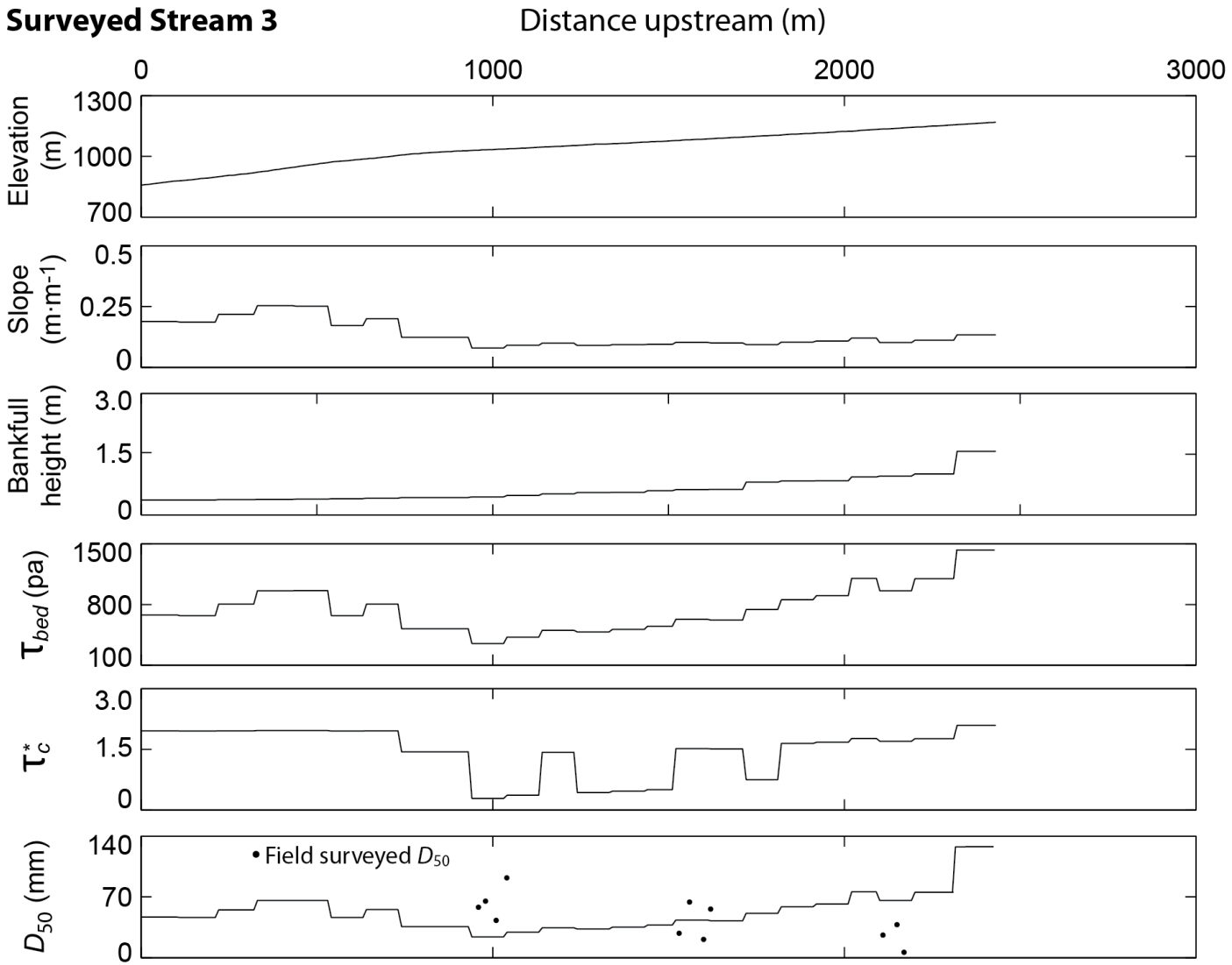
Surveyed Stream 3
Distance upstream (m)
0
1000
2000
3000
Elevation (m)
1300
1000
700
Slope (m·m-1)
0.5
0.25
0
Bankfull height (m)
3.0
1.5
0
τbed (pa)
1500
800
100
τ*c
3.0
1.5
0
D50 (mm)
140
70
0
• Field surveyed D50

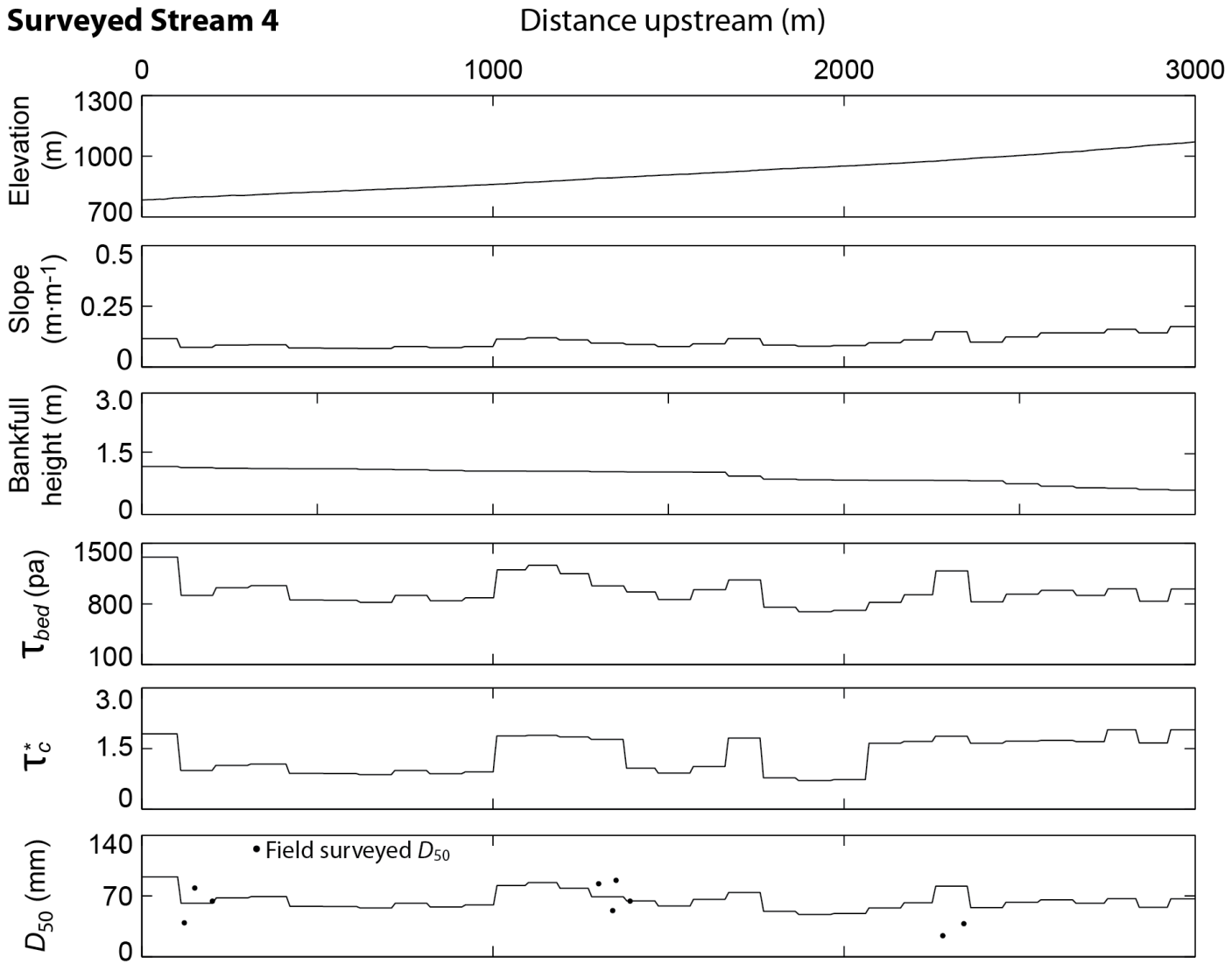
Surveyed Stream 4
Distance upstream (m)
0
1000
2000
3000
Elevation (m)
1300
1000
700
Slope (m·m-1)
0.5
0.25
0
Bankfull height (m)
3.0
1.5
0
τbed (pa)
1500
800
100
τ*c
3.0
1.5
0
D50 (mm)
140
70
0
• Field surveyed D50

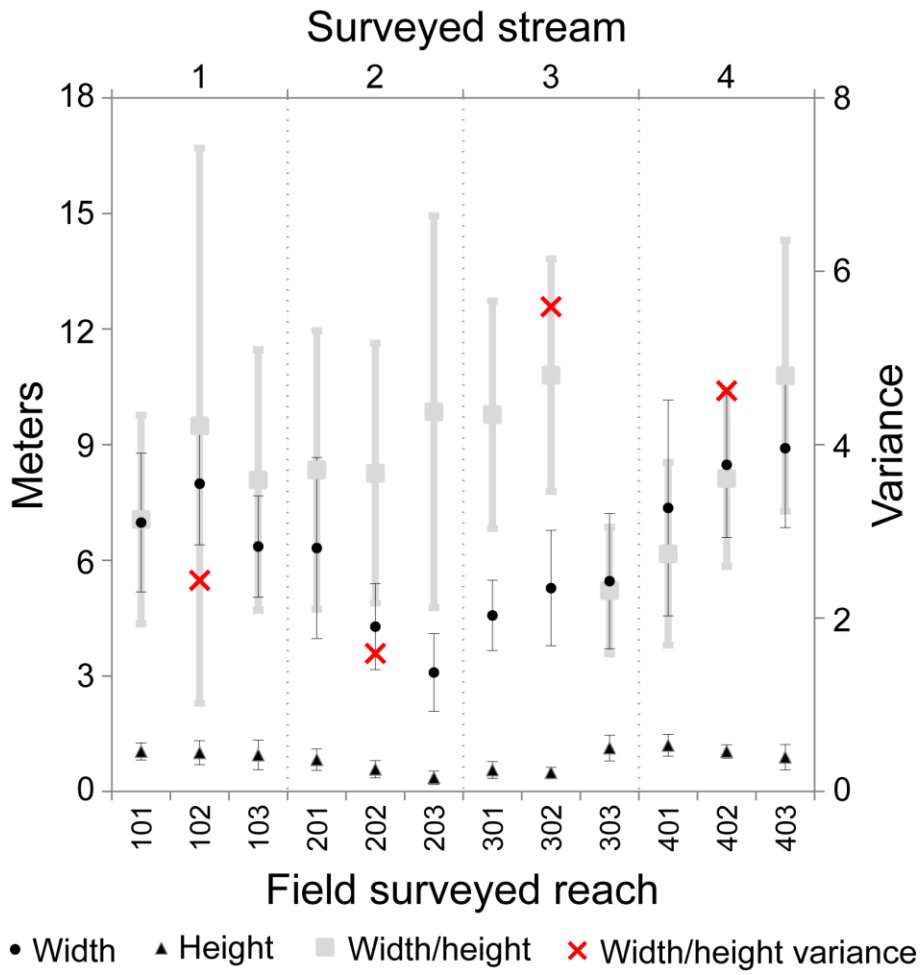

Figure 3.17. Averages of bankfull width, height and width/height were calculated by field survey reach. Width/height variance was calculated by stream. Bars are one standard deviation.

3.3.2. Modeled Grain Size in Modeled Streams

Modeled hydraulics and D_{50} were predicted at each of the evaluation stations along the study streams from reach averaged stream metrics to determine grain size trends in larger streams relative to the scaling break in DS Plots. Grain size trend in modeled streams follows the general trend of field surveyed reach averaged D_{50}, which coarsens downstream in all of the study streams (Figure 3.18). However, in the modeled streams, the modeled grain size reaches its maximum in drainage areas between 10 and 40 km^2, proximal to the scaling break in each of the modeled

stream watersheds. This drainage area size is equivalent to transition of downstream coarsening to fining at drainages of 10 km^2 observed by Brummer and Montgomery (2003). The maximum drainage area of the modeled streams is similar to this size, so the grain size trend downstream of the study watersheds is not fully apparent, though it does appear at least that this value is at or is approaching the maximum grain size in each of these streams.

The monotonically increasing median grain size in all modeled streams is contrary to the often observed downstream fining trend. Median grain size in surveyed streams also coarsens downstream. The entirety of surveyed streams are above the channel process type scaling break, and only a small portion of the modeled streams are downstream of the scaling break. In the modeled streams, median grain size reaches a maximum at approximately the location of each streams' scaling break. In SM-1 and 2, it appears that median grain size begins to decrease, though stream length is minimal beyond the scaling break making trends beyond it difficult to ascertain.

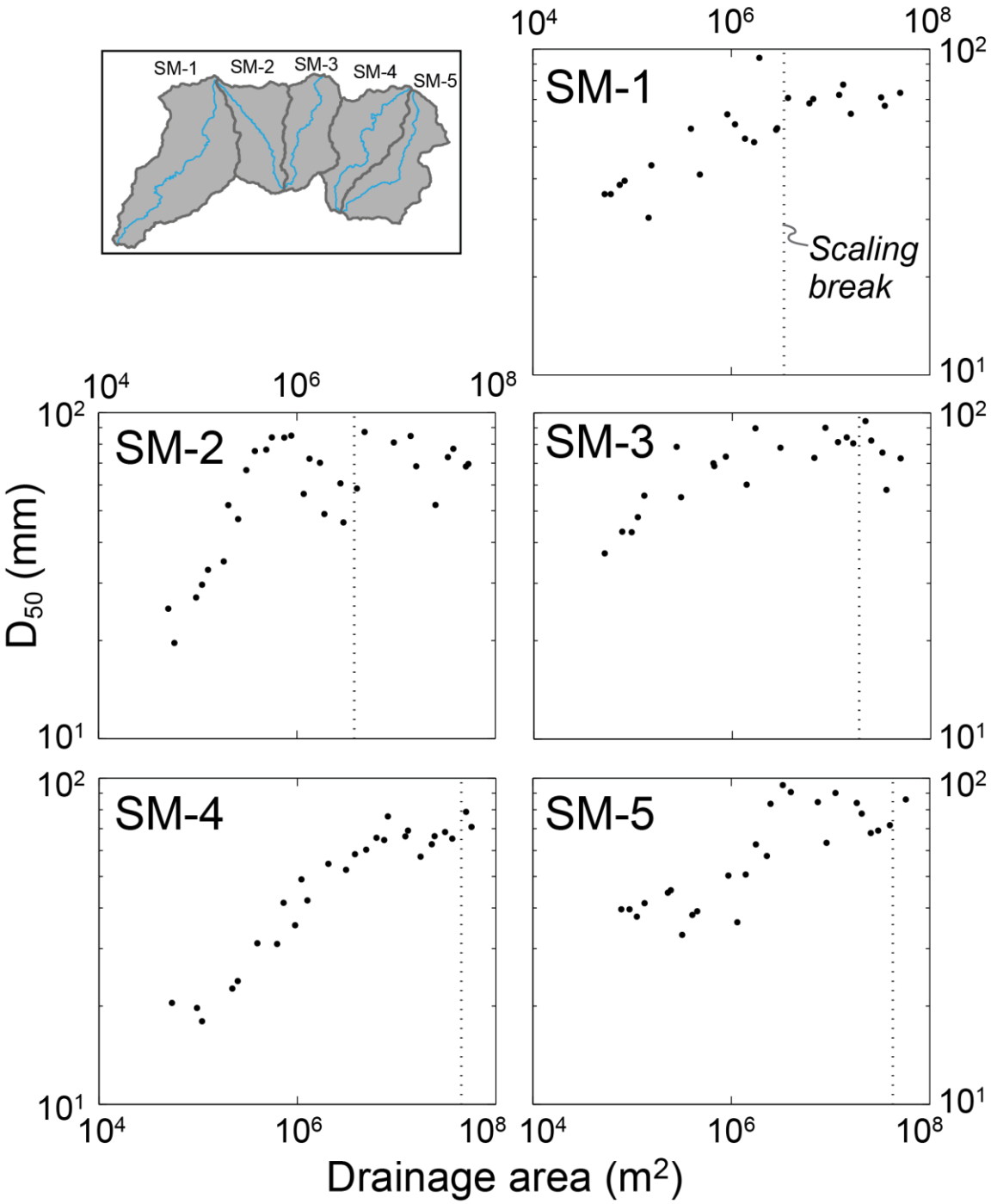

Figure 3.18. Logarithmically bin-averaged drainage area versus grain size. Median grain size of modeled streams is averaged in bins that logarithmically increase in size downstream to be in accords with the scale of the DS plots.

3.3.3. Modeled Grain Size in Comparison to Surveyed Salmonid Location

If salmonid distribution is in part controlled by median grain size trends, then a downstream coarsening trend would be observed in the Smoky Mountains since the trout species that uses a smaller grain size occupies headwater streams. Median grain size distribution of surveyed streams compared with salmonid surveys conducted by Kelly (1980) show a seemingly unsystematic trend from reach to reach (Figure 3.19). However, reaches with the smallest median grain size quantile, 19 to 41 mm, in each stream are relegated to the upper 60% of the streams with exception of the reach directly upstream of the knickpoint in Stream 3 and three reaches in the lower half of Stream 1 where channel slope is unusually low. The values of the reach-averaged D_{50} in Stream 4 falls only within the upper two quantile classes where allopatric zones of brook trout were not observed by Kelly (1980). All of the grain sizes classes are observed in Stream 2, but similar to Stream 4, Figure 3.19 shows that an allopatric brook zone does not exist in this stream. However, unlike Stream 4, an allopatric brook zone does exist upstream Surveyed Stream 2, but not visible in the figure.

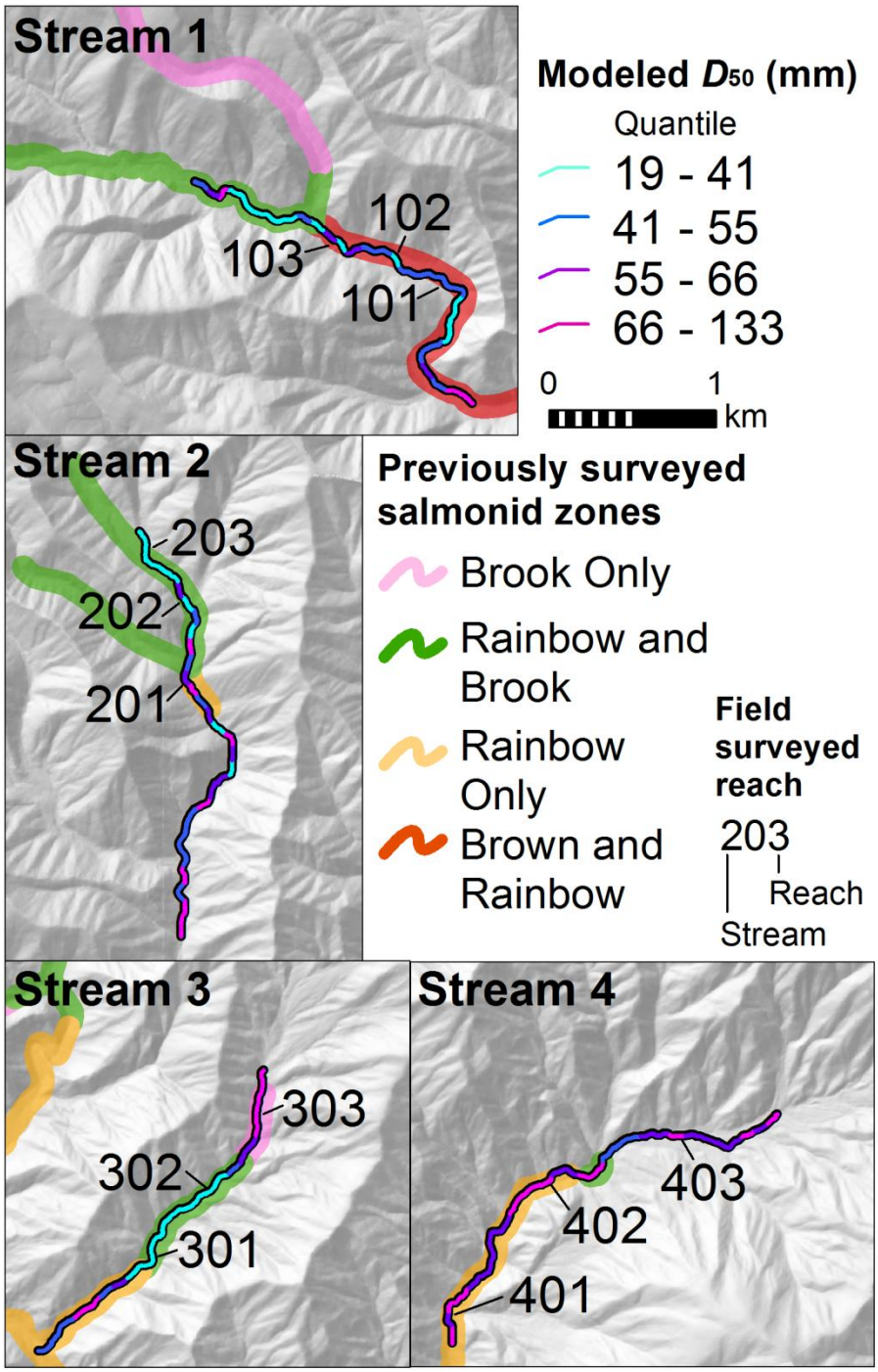

Figure 3.19. Modeled median grain size relative and observed salmonid distribution. Trout surveys were conducted by Kelly (1980).

3.3.4. Root Thin-Sections and Trunk Cores

The roots of trees adjacent to the Deep Creek debris flow were examined for evidence of exposure near the time of HWA infestation in the Smoky Mountains in 2002. All four of the root cross-sections, which are representative cross-sections of these roots where they were exposed, exhibit a notable reduction in growth ring size in the most recent years of growth. The range of abnormally thin growth rings for all samples is 6 to 19 rings.

Root samples 1 and 2, located along the flanks of the Deep Creek debris flow, were cut from trees that are not hemlocks, but similar to all samples, were sampled to confine the age of the debris flow. Root Sample 1, collected from a flowering dogwood, contains 9 to 15 abnormally thin growth rings. Root Sample 2, collected from a red oak, contains 7 to 11 abnormally thin growth rings (Figure 3.20). A marginally buried segment of this root also contains this many thin growth rings.

Roots sample 3, collected from an eastern hemlock approximately 2.4 m from the debris flow's headscarp, contains the most abnormally thin growth rings of the samples collected (Figure 3.21). This tree leans more towards the debris flow scar than the trees where the other root samples were cut. The affect of the high degree of this tree's leaning can be seen in the root's cross-section where the pith is greatly off-centered. This tree is also the only sample that was fully exposed on all sides of the root, thus was only supported by other roots.

Root sample 4, also collected from an eastern hemlock, is less than 2 m from head scarp and contains 5 to 9 abnormally thin growth rings (Figure 3.22). The thin growth rings are comprised of 3 to 5 earlywood cells and appear to make up a higher proportion of the annual growth compared to the growth rings more towards the pith of Root Sample 4 (Figure 3.23).

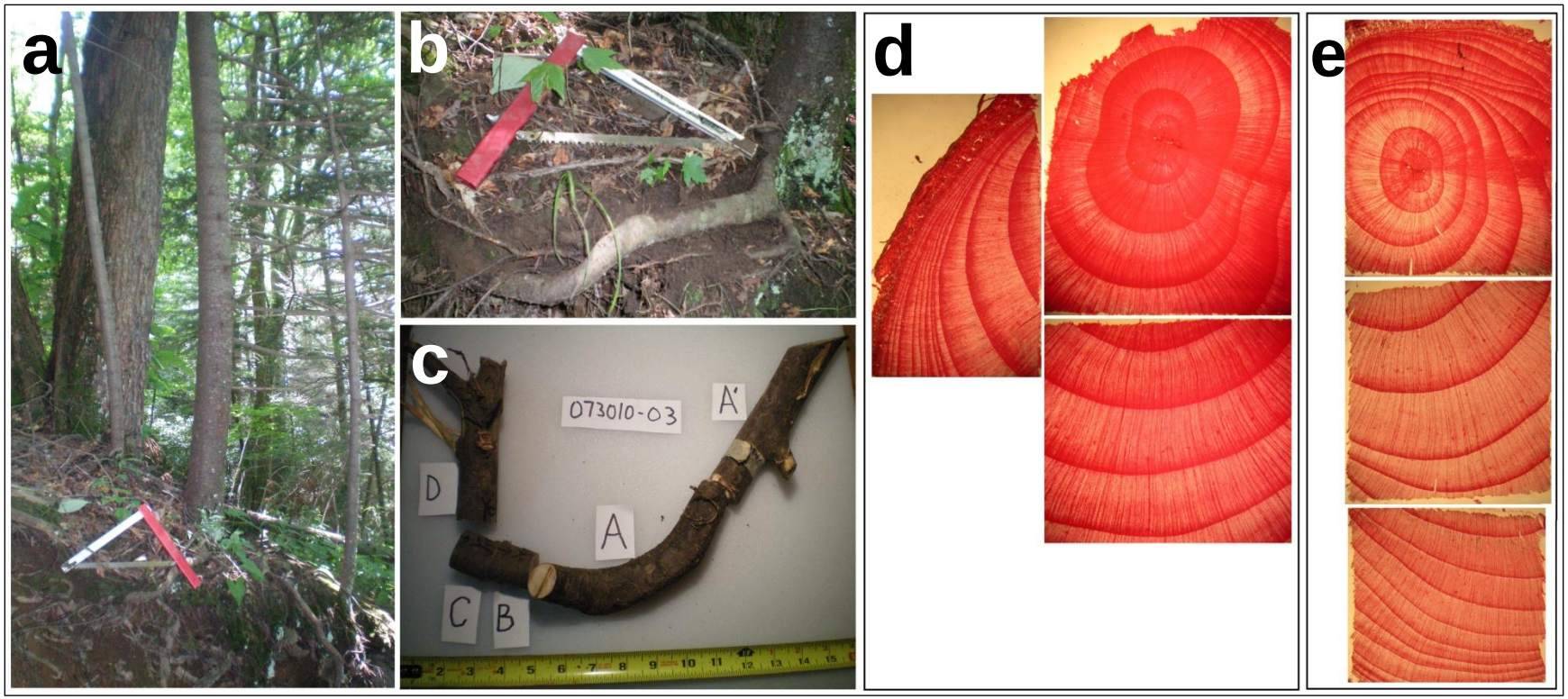

Figure 3.20. Root Sample 2 images: (a) Root sample 2 was cut from the red spruce to the right of the handsaw. This tree had no needles on its lower limbs and few on its higher limbs. Other red spruces in the area not adjacent to the Deep Creek feature, however, where much more fully covered with needles. The root cut is directly beneath the saw and the flank scarp of the Deep Creek feature is shown in the foreground. (b) The majority of the root was exposed with the exception of approximately 15 cm of the root section furthest from the trunk. (c) This root was cut into five sections. Section D was buried. (d) Segment A and (e) Segment D show 9 to 11 abnormally thin growth rings during the most recent years of growth.

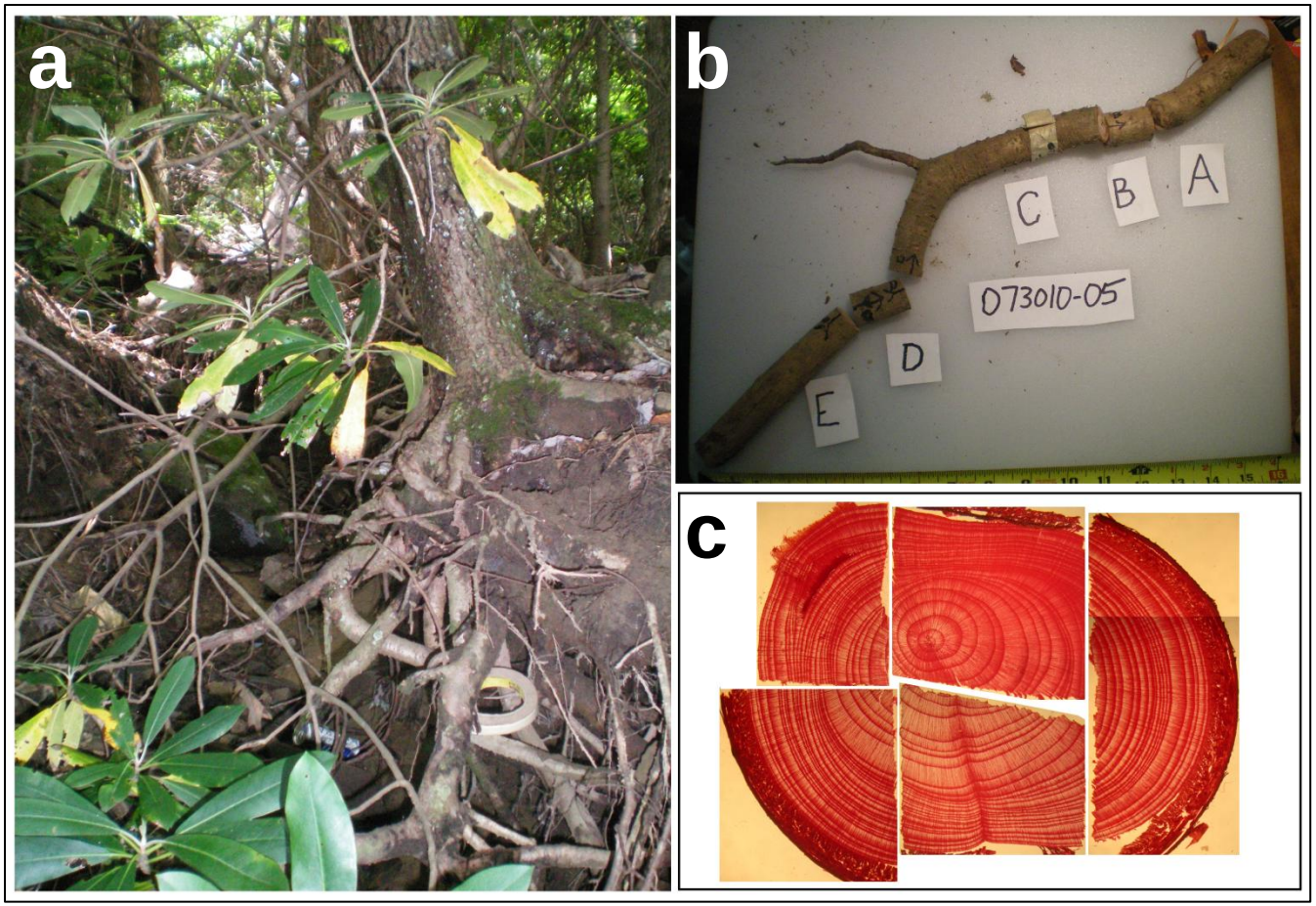

Figure 3.21. Root Sample 3 images: (a) The root collected from this eastern hemlock is partially shown below the masking tape. (b) Five segments were cut and were mostly exposed. (c) Segment D shows 19 abnormally thin growth rings.

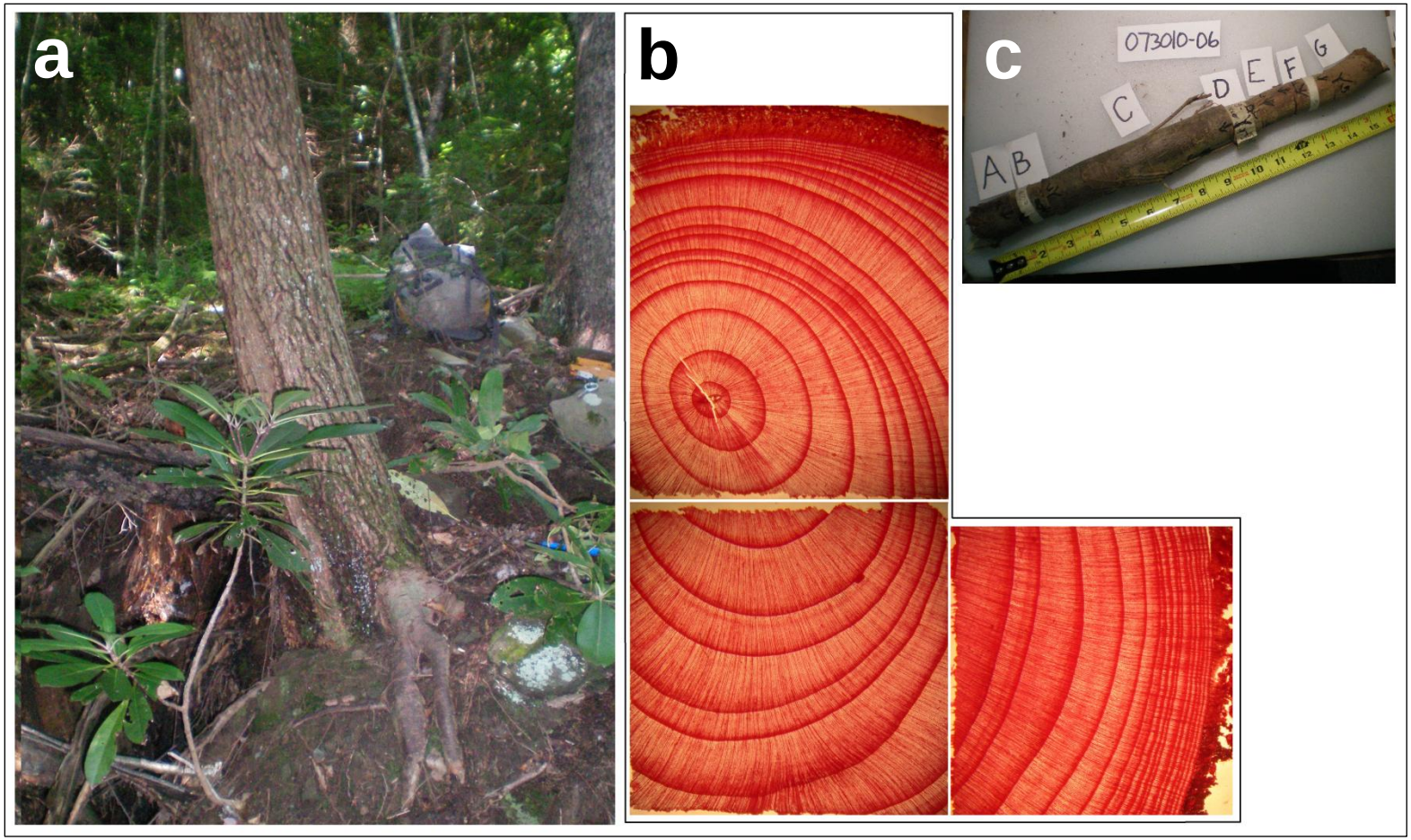

Figure 3.22. Root Sample 4 images: (a) The root collected from this eastern hemlock is partially shown below the masking tape. (b) Segment D shows 6 to 11 abnormally thin growth rings. (c) Seven segments were cut: A thru C were exposed, D was slightly covered, and E thru G were fully covered.

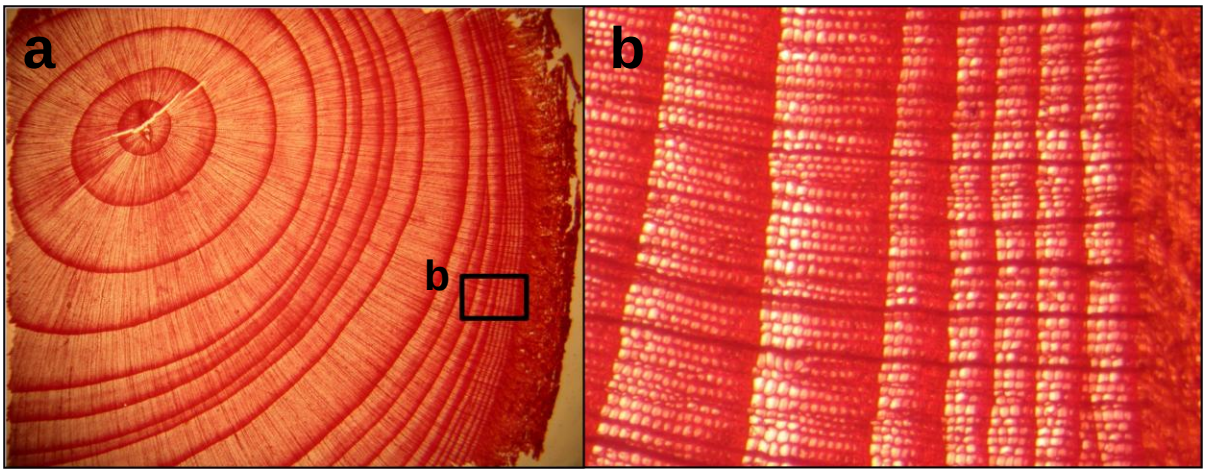

Figure 3.23. Roots Section 4 segment close-up.

The range of years when the geomorphic disturbance occurred as recorded in the sampled roots is indicated in Table 3.3 assuming that one growth ring was added per year to the roots prior to 2010, when the roots were cut from the trees. The years since disturbance overlap in R01, R02, R04, though the numerous abnormally thin rings of R03 indicate a longer time has passed since the disturbance.

Table 3.3. Root sample results.

Sample ID	Common Name	Approximate year(s) of disturbance
R01	Flowering Dogwood	1995 to 2001
R02	Red Spruce	1999 to 2003
R03	Eastern Hemlock	1991
R04	Eastern Hemlock	1999 to 2006

The growth ring thickness of trunk cores do show similarities between samples, such as the thicker rings that exist in most cores approximately 15 to 20 and 40 to 50 rings from the bark (Figure 3.24). The cores correspond to the most recent growth of the trunk near the bark. The roots contain an approximate

maximum of 30 rings, so the growth of the tree prior to these rings is not represented in the cores. The cores do not contain abnormally thin rings when ring thickness is considered in the times span represented in the root samples. The ring thickness in the cores of R01 and R03 decrease by nearly half their value in the past ten years, though the opposite trend is observed in the cores of R02 and R04.

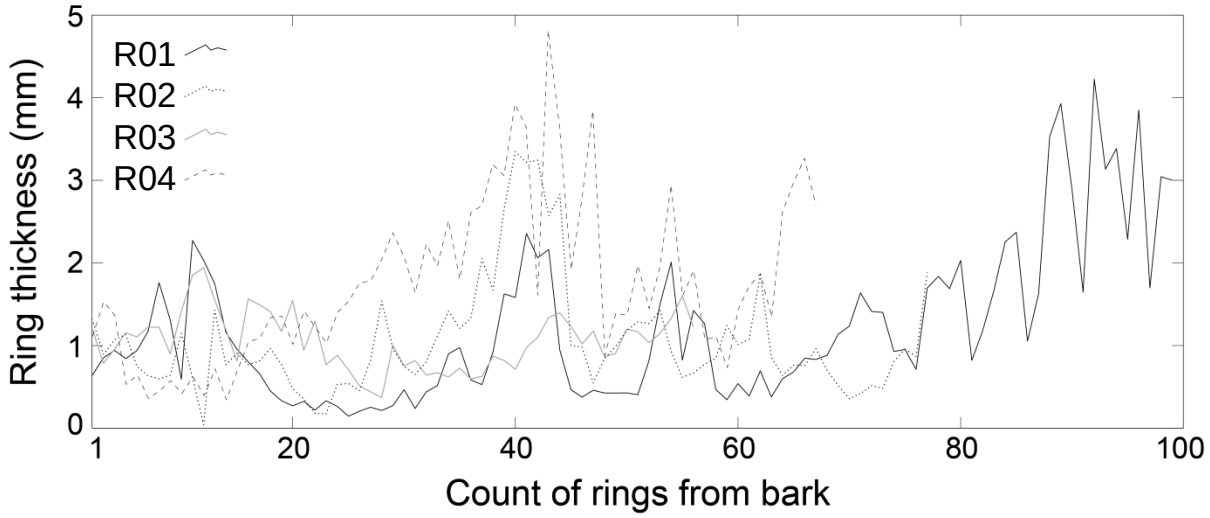

Figure 3.24. Growth ring thickness of trunk cores. Trunk core ID corresponds with the root sample ID, for example the R01 trunk core in this plot was extracted from the same tree that the R01 root sample was collected.

3.4. Discussion

3.4.1. Reconciling Field Surveyed and DEM Modeled Channel Metrics

Moderate correlation of field surveyed and DEM modeled stream metrics is used to predict grain size trends (Wilkins and Snyder, 2011), though deviations between surveyed and modeled metrics are investigated first here. The abnormality of the high surveyed bankfull height in Surveyed Stream 3 raises the possibility that high magnitudes of variation in this metric may exist in areas not surveyed. In all other streams, except Surveyed Stream 3, bankfull height decreases downstream. This is an important anomaly to consider since the opposite trend in bankfull height relative to drainage area results in the opposite grain size trend downstream. To

consider this in the context of this study area, three potential explanations for the abnormally high surveyed bankfull height of Stream 3 follow. Southworth *et al.* (2005) mapped a large colluvial fan at the headwaters of this stream, visible in the uncharacteristically smooth topography of the higher elevations in Figure 3.9. While the fan does extend down the length of this stream, I observed in the field during stream surveys a decrease in width and thickness of colluvium downstream. To explain the high bankfull depth of the uppermost reach of this stream, incision through this thicker mantle of colluvium could be causing the abnormality. Stream 4 also contains a colluvial fan in its headwaters, though not as significant as in Stream 3 relative to its drainage area, which is consistent with the slight under-prediction of the uppermost reach of Stream 4 as well.

The second possible explanation is variation in stream incision rates due to differences in rock mass strength, also proposed in Matmon *et al.* (2003a) to explain spatial variation in stream incision rates over million year timescales in the Smoky Mountains. Rock mass strength variations can be caused by different lithologies, such that would be associated with the interbedded, alternating layers of metagraywacke and metasiltstone in the undifferentiated bedrock map unit that underlies all of this study's streams. This phenomenon is expressed in large scales on streams by knickpoints (Frankel *et al.*, 2007), which this stream is the only surveyed stream that contains a prominent knickzone. Knickpoints are characterized by high slopes downstream and low slopes upstream of the knickpoint that interrupt a stream longitudinal profile that is typically, in this area, a concave up profile with monotonically increasing slopes upstream. The observation that Survey Stream 3 has a concave up profile upstream from the knickzone poses the possibility that channel adjustment upstream from the knickzone is driving accelerating stream incision at points higher in elevation. This proposal is not supported by surveyed channel slope (Figure 3.14) since the middle reach has the steepest slope, though modeled slope indicates a gradual increase in its magnitude up the stream, potentially driving increased incision.

The final proposal is motivated by the presence of a gravel service road that parallels much of this stream and crosses it directly above and below the lowest surveyed reach and transitions to a stony, slightly vegetated equestrian/hiking trail between the middle and uppermost survey reach. Moore *et al.* (1983) suggested that the finer streambed sediment size observed in this stream compared to other streams they surveyed in the Smoky Mountains was due to this gravel road. Increased stream aggradation may result from the road and its associated low hydraulic roughness, and the minimal buffer between the two that ranges between approximately 10 to 30 m.

The regression of bankfull height and drainage area following Equation 3.6 causes the opposite trend of modeled bankfull depth relative to drainage area observed in the other surveyed streams. The effect of this calculation is transmitted to the prediction of bed shear stress, as are all reach metrics, via the depth-slope product. A high τ_{bed} results from the high bankfull depth of the uppermost reach of Stream 3 from the depth-slope product, which represents an increase in the wetted perimeter of the channel, effectively reducing drag forces on the stream bed resulting in a high $\tau^*_{c_{50}}$. The model correctly shows that a high median grain size results as more intense precipitation events are required to transport larger grains. This series of relationships amongst channel hydraulics follows this trend downstream in Stream 3 due to the abnormally high bankfull width in the uppermost field surveyed reach.

Despite the cause of the opposite trend in bankfull height in Stream 3, this trend is assumed to be erroneous. The lowest and middle field surveyed reaches do not follow this trend and additional field surveyed reaches in this stream may change the result. The highly steep portion of the stream downstream of the knickpoint is likely to have a high bankfull height, which could led to an overall increase of bankfull height with drainage area. If this was the case, modeled D_{50} would then be in accordance with the downstream coarsening trend surveyed in the field and as modeled in other streams. This case highlights the value of modeling in this

application is in locating areas where modeled results grossly deviate from what is expected with established hydraulic and geomorphic relationships, and not that the modeling technique precisely predicts metrics in all channel areas. In the case of the bankfull height uppermost reach of Stream 3, it is not possible to determine which of the proposed possibilities is the case without further field observations, though it is clear that this reach deviates from the others, potential causes for this deviation exist, and that unexpected results can be traced backed by the relationships amongst channel geometry and hydraulics. Errors propagate through subsequent calculations of bankfull shear stress and critical shear stress, though importantly, field surveyed and modeled D_{50} do reside within a 2:1 and 1:2 relationship, portraying the model's robustness in this application.

Moderate correlations of empirically determined parameters are likely a primary source of error as well as the inherit complexity and the stochastic nature of stream systems. Nevertheless, this model implies a strong control of slope, when bankfull height is accurately predicted, that is highly variable in the Smoky Mountains and further efforts that incorporate additional parameters and models additional streams may yield more precise results in small scales.

3.4.2. Grain Size Coarsening in Debris-Flow Dominated Channels

The often observed downstream fining trend of streambed grains is not present in any of the modeled streams, or the majority of the surveyed streams, raising an inquiry into the mechanisms that cause downstream coarsening. The metric that causes downstream fining in grain size modeling in one of the surveyed streams is believed to be caused by a biased sampling population. Mechanisms affiliated with debris flow-dominated channels are indicted here given the coincidence of maximum modeled grain size and the DS Plot scaling breaks.

The parameters used in locating DS Plot scaling breaks in Chapter 2 provide insight into the mechanisms of downstream coarsening in this study area. Decreases in channel slope, signifying the scaling break in DS Plots, are areas

upstream of channel knickpoints or knickzones. These areas contain grains that require a larger critical shear stress for incipient motion due to the lower slopes. Increases in stream power in the downstream direction allow coarse sediment provided by debris flows and other mass wasting events to accumulate progressively in these areas. However, given the low recurrence interval of debris flows in small watersheds in the Smoky Mountains, wood loading and the high residence time of logjams (Hart, 2002), large woody debris and log jams appear to be an important contributor in maintaining the downstream coarsening trend. Shear stress empirical values, *k* and *n* are assumed to have inherited roughness variation in calculations of modeled shear stress. This was transmitted to the model by defining channel morphology type by channel slope and equating the critical Shields value to surveyed D_{50}.

A higher prevalence of roughness elements in step-pool sequences and cascades forces slackwater areas in adjacent pool-riffle areas. This is supported by the consistent observation of an upstream fining trend in the study streams and observations by Hart (2002) of large stores of fine grained sediment behind log jams, especially in non-debris flow valleys. A constantly available source of fine sediment to fill wood forced pools in upper reaches is available from the thick mantle of saprolite on hillslopes and coves transported by the high amount of precipitation in the area. Fine sediment channel entrainment is made possible by the high degree of hillslope-channel connectivity typically high in headwater reaches (Brummer and Montgomery, 2003).

The application of this grain size model in this area reveals a dissimilar balance of sediment supply and transport between debris flow and fluvial-dominated channels. The channel network of the Smoky Mountains is a sediment detachment-limited system, and without debris flows, grain size may resemble trends observed in fluvial systems with lower channel slope. In a landscape scenario without debris flows, infrequent, yet intense storms would rapidly transport sediment out of the system, and bedrock channels would be even more common. In the consideration

of frequent discharge events, small drainage areas provide little discharge that can actively incise channels causing little erosion that is possibly counteracted by isostactically-driven uplift in long time spans. Stream power still can increase systemically downstream as observed by Brummer and Montgomery (2003), but a mechanism that locally lowers slopes necessary for fine sediment deposition does not exist in this scenario. Infrequent debris flows, though providing large amounts of geomorphic work, detach fine and coarse sediment, incise channels at high rates, and temporally store the sediment detached from the mass failure, as well as other sediment being transported after the flow, behind logjams. Given systematic increases in stream power downstream observed in mountainous settings (Brummer and Montgomery, 2003), and increases in wood loading upstream in the Smoky Mountains (Hart, 2002), grain size here coarsens downstream until the influence of high discharge from a large drainage area surpasses the influence of channel slope in stream power in the scale of reaches. Other mechanisms deliver wood to channels, but the higher frequency of logjams in debris flow valleys observed by Hart (2002) indicates the important of this geomorphic agent. At the point where discharge surpasses the influence of channel slope, proximal to the transition from debris flow to fluvial dominated channels, the often observed downstream fining trend begins. As a mechanism that controls not only grain size, but reach morphology and watershed hypsometry, widespread effects of debris flow-dominated channels likely impact numerous geomorphic and biologic realms.

3.4.3. Implications of Grain Size Trends upon Salmonid Distribution

The importance of median grain size distribution throughout a stream network to provide salmonid substrate has been realized in other regions (Buffington *et al.*, 2004; Kondolf and M.G., 1993). High fine grain substrate availability may be an additional advantage for native brook trout in headwater streams of the Smoky Mountains, though the often observed trend of downstream grain fining refutes this possibility. Debris flow-dominated channels and high frequencies of logjams and

other roughness increasing elements create environments that would otherwise not contain salmonid spawning gravels, especially the small sizes used by brook trout. This study did not attempt to isolate the control of grain size upon salmonid habitat from other known factors advantageous for brook trout that exist in headwaters streams. However, the occurrence of debris flows in Appalachians, downstream coarsening in debris flow-dominated streams shown in this study, and precedence of a grain size control upon salmonid fecundity make this topic an area of needed research.

The hypothesis proposed by Fausch (2008) that salmonid species thrive in environments where the flow regime affects the species annual life history is supported by grain size trends and salmonid species in the Smoky Mountains. Fausch (2008) states that brook trout are at a disadvantage in the Smoky Mountains since their incubation coincides with annual high flows. Larson *et al.* (1995) found that the ebb and flow of the two salmonid species' extent is due to water flow variations and rainbow trout's preference for warmer waters and brook trout's increased ability to survive high flows. These factors likely overshadow the importance of grain size availability in salmonid distribution, though grain size may act as a second-order control. Brook trout spawning and incubation coincides with the timing of low annual precipitation averages, which implies higher finer bedload grain size availability during this time. Conversely, rainbow trout spawning and incubation coincides with the timing of high annual precipitation averages, implying coarser grain size availability.

The short length of sympatric zones, stream reaches containing both brook and rainbow trout, of 1300 m exists at an average elevation of 1100 m (Larson and Moore, 1985). The elevations of the scaling break at the trunk channels of the five extrapolated streams are 1138, 1149, 989, 1083, 927 m for Streams 1 through 5, respectively. This indicates an important control of salmonid species distribution as a function of the dominant-channel process, though the influence of other controls, such as water temperature and pH, in turned controlled by elevation, likely have a

stronger influence than grain size availability upon salmonid species distribution (Larson *et al.*, 1995). However, a clear explanation of why pH and water temperature control the position of sympatric zones at 1100 m is not known. Water flow and possibly grain size trends, factors controlled largely by slope and thus affiliated with the dominant channel process, act in addition to pH and water temperature as likely controls upon salmonid distribution. The trout survey by Kelly *et al.* (1980) is not sufficient to determine reach-scale trout extent.

3.4.4. HWA-induced Debris Flows in the Smoky Mountains

The potential of debris flows to be initiated by hemlock woolly adelgid was not supported in the case of the Deep Creek debris flow given the apparent disparate timing of the debris flow and HWA discovery in the Smoky Mountains. One of the samples, Root Sample 3, contained 19 abnormally small growth rings, far exceeding the discovery of HWA in the Smoky Mountains in 2002 assuming approximately one growth ring per year. Other root samples indicate that the hillslope failure occurred within 2 to 3 years of HWA discovery in the area. Hemlocks in the area typically do not decline so rapidly after infestation. Further, many of the other debris flows in the area are outside of hemlock community extent mapped by Madden *et al.* (2004) and none of them remain as sparsely vegetated as this debris flow.

The proximity of the debris flow scar to a prominent ridge and major highway suggests that a spring may be directing high volumes or frequent flows of water to this area, though a culvert or other engineering devices is not located at this site. The seemingly recent occurrence of this flow, assumed by the lack of vegetation, may be related to the potential of recurrent high and cobbles along the bottom of the flow impeding vegetation reestablishment.

3.5. Conclusions

A model of channel geometry and hydraulics applied to the Smoky Mountains was created with the goal to predict grain size trends across the transition from

debris flow to fluvial dominated channels. A downstream grain size coarsening trend was observed in field and modeled data of five mountainous streams in the Smoky Mountains. The maximum grain size approaches the scaling break that represents the transition from debris flow to fluvial- dominated channels indicating that downstream coarsening is a characteristic of debris flow-dominated channels. Wood entrainment and log jams become necessary mechanisms of fine sediment in supply limited channels. Pools in high elevation step-pool sequences become important environments where fine substrate can accumulate and low flow velocity exists for native brook trout. Regional controls upon watershed hypsometry thus control in large part the total stream length of habitat available to salmonid species.

Given the high complexity and stochastic nature of stream systems, empirically-based probabilistic rather than deterministic modeling is often a more realistic approach, which may be a necessary step toward improving geospatial modeling efforts (Mitasova *et al.*, 2011a). Further, it is assumed here that simplistic modeling methods suffice in this application given that stream-wide grain size trends, and not meter or reach scale results, is the objective. Future efforts to improve this model and apply it to other geomorphic and biologic questions will benefit from more representative surveyed populations, significant effort to reconcile field and surveyed data, and a high degree of integrative investigations amongst the numerous geomorphic mechanism that control grain size.

Evidence of debris flows initiated by deteriorating eastern hemlocks infected with hemlock woolly adelgid was not found. However, precedence of slope instability cause by other insects, the widespread distribution of HWA, and the slow yet deteriorating response of hemlocks should be monitored for indicators of HWA-induced mass wasting.

REFERENCES

Andrews, E.D., 1984, Bed-material entrainment and hydraulic geometry of gravel-bed rivers in Colorado: Geological Society of America Bulletin, v. 95, p. 371-378.

Annand, P.N., 1924, A new species of Adelges (Hemiptera, Phylloxeridae): Pan-Pacific Entomologist, v. 1, p. 79-82.

Barlow, J., Franklin, S., and Martin, Y., 2006, High spatial resolution satellite imagery, DEM derivatives, and image segmentation for the detection of mass wasting processes: Photogrammetric Engineering and Remote Sensing, v. 72, p. 687-692.

Benda, L., 1990, The influence of debris flows on channels and valley floors in the Oregon Coast Range, U.S.A: Earth Surface Processes and Landforms, v. 15, p. 457-466.

Bogucki, D.J., 1976, Debris Slides in Mt Le Conte Area, Great Smoky Mountains National-Park, Usa: Geografiska Annaler Series A-Physical Geography, v. 58, p. 179-191.

Borghuis, A.M., Chang, K., and Lee, H.Y., 2007, Comparison between automated and manual mapping of typhoon-triggered landslides from SPOT-5 imagery: International Journal of Remote Sensing, v. 28, p. 1843-1856.

Bouman, C.A., and Shapiro, M., 1994, A multiscale random field model for Bayesian image segmentation: Image Processing, IEEE Transactions on, v. 3, p. 162-177.

Brardinoni, F., Slaymakerl, O., and Hassan, M.A., 2003, Landslide inventory in a rugged forested watershed: a comparison between air-photo and field survey data: Geomorphology, v. 54, p. 179-196.

Brummer, C.J., and Montgomery, D.R., 2003, Downstream coarsening in headwater channels: Water Resources Research, v. 39.

Buffington, J.M., and Montgomery, D.R., 1997, A systematic analysis of eight decades of incipient motion studies, with special reference to gravel-bedded rivers: Water Resources Research, v. 33, p. 1993-2029.

—, 1999a, Effects of hydraulic roughness on surface textures of gravel-bed rivers: Water Resources Research, v. 35, p. 3507-3521.

—, 1999b, Effects of sediment supply on surface textures of gravel-bed rivers: Water Resources Research, v. 35, p. 3523-3530.

Buffington, J.M., Montgomery, D.R., and Greenberg, H.M., 2004, Basin-scale availability of salmonid spawning gravel as influenced by channel type and hydraulic roughness in mountain catchments: Canadian Journal of Fisheries and Aquatic Sciences, v. 61, p. 2085-2096.

Busing, R.T., Stephens, L.A., and Clebsch, E.E.C., 2005, Climate data by elevation in the Great Smoky Mountains: a database and graphical comparison to long-term data, U.S. Geological Survey Data Series Report, Volume DS-115.

Carrara, A., and Pike, R.J., 2008, GIS technology and models for assessing landslide hazard and risk: Geomorphology, v. 94, p. 257-260.

Crosby, B.T., and Whipple, K.X., 2006, Knickpoint initiation and distribution within fluvial networks: 236 waterfalls in the Waipaoa River, North Island, New Zealand: Geomorphology, v. 82, p. 16-38.

Cruden, D.M., and Varnes, D.J., 1996, Landslide Types and Processes, *in* Turner, A.K., and Schuster, R.J., eds., Landslides: Investigation and Mitigation: Washington D.C., Transportation Research Board, National Research Council, p. 36-75.

Davis, W.M., 1899, The Geographic Cycle: The Geographical Journal, v. 14, p. 481-504.

Definiens, 2007, Definiens Developer 7 Reference Manual: München, Germany.

Desta, F., Colbert, J.J., Rentch, J.S., and Gottschalk, K.W., 2004, Aspect induced differences in vegetation, soil, and microclimatic characteristics of an Appalachian watershed: Castanea, v. 69, p. 92-108.

Dietrich, W.E., de Asua, R.R., Coyle, J., Orr, B., and Trso, M., 1998, A validation of the shallow slope stability model, SHALSTAB, in forested lands of Northern California: Berkeley, CA, 59 pp p.

Dietrich, W.E., and Dunne, T., 1978, Sediment budget for a small catchment in mountainous terrain: Geomorphologie Supplementenband, v. 29, p. 191-206.

Dietrich, W.E., Reiss, R., Hsu, M.L., and Montgomery, D.R., 1995, A Process-Based Model for Colluvial Soil Depth and Shallow Landsliding Using Digital Elevation Data: Hydrological Processes, v. 9, p. 383-400.

Dunham, J.B., Adams, S.B., Schroeter, R.E., and Novinger, D.C., 2002, Alien invasions in aquatic ecosystems: Toward an understanding of brook trout invasions and potential impacts on inland cutthroat trout in western North America: Reviews in Fish Biology and Fisheries, v. 12, p. 373-391.

Dyke, A.S., Andrews, J.T., Clark, P.U., England, J.H., Miller, G.H., Shaw, J., and Veillette, J.J., 2002, The Laurentide and Innuitian ice sheets during the Last Glacial Maximum: Quaternary Science Reviews, v. 21, p. 9-31.

Eaton, L.S., Morgan, B.A., Kochel, R.C., and Howard, A.D., 2003, Role of debris flows in long-term landscape denudation in the central Appalachians of Virginia: Geology, v. 31, p. 339-342.

Fausch, K., 2008, A paradox of trout invasions in North America: Biological Invasions, v. 10, p. 685-701-701.

Fausch, K.D., 1989, Do gradient and temperature affect distributions of, and interactions between, brook charr (Salvelinus foniintilis) and other resident salmonids in streams?: Physiology and Ecology Japan, Special Edition, v. 1, p. 303-322.

Fenneman, N.M., 1928, Physical division of the United States: Annals of the Association of Geographers, v. 18, p. 261-353.

Frankel, K.L., Pazzaglia, F.J., and Vaughn, J.D., 2007, Knickpoint evolution in a vertically bedded substrate, upstream-dipping terraces, and Atlantic slope bedrock channels: Geological Society of America Bulletin, v. 119, p. 476-486.

Gabet, E.J., Reichman, O.J., and Seabloom, E.W., 2003, THE EFFECTS OF BIOTURBATION ON SOIL PROCESSES AND SEDIMENT TRANSPORT: Annual Review of Earth and Planetary Sciences, v. 31, p. 249-273.

Gaffin, D.M., Holtz, D.G., and Getz, T.I., 2009, An Evaluation of Temperature Variations around the Great Smoky Mountains National Park and their Associated Synoptic Weather Patterns, Volume 2009, National Oceanic and Atmospheric Administration.

Gallen, S.F., Wegmann, K.W., Frankel, K.L., Hughes, S., Lewis, R.Q., Lyons, N., Paris, P., Ross, K., Bauer, J.B., and Witt, A.C., 2011, Hillslope response to knickpoint migration: An investigation of channel-hillslope coupling and slope stability in the Cullasaja River Basin, North Carolina, USA: Earth Surface Processes and Landforms.

Gartner, H., 2007, Tree roots - Methodological review and new development in dating and quantifying erosive processes: Geomorphology, v. 86, p. 243-251.

Gärtner, H., Schweingruber, F.H., and Dikau, R., 2001, Determination of erosion rates by analyzing structural changes in the growth pattern of exposed roots: Dendrochronologia, v. 19, p. 81-91.

George, E., Seith, B., Schaeffer, C., and Marschner, H., 1997, Responses of Picea, Pinus and Pseudotsuga roots to heterogeneous nutrient distribution in soil: Tree Physiology, v. 17, p. 39-45.

Glenn, N.F., Streutker, D.R., Chadwick, D.J., Thackray, G.D., and Dorsch, S.J., 2006, Analysis of LiDAR-derived topographic information for characterizing and differentiating landslide morphology and activity: Geomorphology, v. 73, p. 131-148.

Hack, J.T., 1960, Interpretation of erosional topography in humid temperate regions: American Journal of Science, v. 258-A, p. 80-97.

Hales, T.C., Ford, C.R., Hwang, T., Vose, J.M., and Band, L.E., 2009, Topographic and ecologic controls on root reinforcement: J. Geophys. Res., v. 114, p. F03013.

Haralick, R.M., Shanmugam, K., and Dinstein, I., 1973, Textural features for image classification: IEEE Transactions on Systems, Man, and Cybernetics, v. SMC-3.

Harden, C.P., 2006, Human impacts on headwater fluvial systems in the northern and central Andes: Geomorphology, v. 79, p. 249-263.

Harmon, M.E., 1983, Disturbance and vegetation response in relation to environmental gradients in the Great Smoky Mountains: Vegetation, v. 55, p. 129-139.

Hart, E.A., 2002, Effects of woody debris on channel morphology and sediment storage in headwater streams in the Great Smoky Mountains, Tennessee-North Carolina: Physical Geography, v. 23, p. 492-510.

Hatcher, R.D., and Goldberg, S.A., 1991, The Blue Ridge Geologic Province, *in* Horton, J.W., and Zullo, V.A., eds., The Geology of the Carolinas: Knoxville, TN, University of Tennessee Press.

Hayes, J.P., Guffey, S.Z., Kriegler, F.J., McCracken, G.F., and Parker, C.R., 1996, The Genetic Diversity of Native, Stocked, and Hybrid Populations of Brook Trout in the Southern Appalachians: Conservation Biology, v. 10, p. 1403-1412.

Hershfield, D.M., 1961, Rainfall frequency atlas of the United States for durations from 30 minutes ti 24 hours and return periods from 1 to 100 years, Volume Technical Paper 40, Weather Bureau, U.S. Department of Commerence.

Horton, R.E., 1945, Erosional development of streams and their drainage basins; Hydrophysical approach to quantitative morphology: Geological Society of America Bulletin, v. 56, p. 275-370.

Hovius, N., Stark, C., Tutton, M.A., and Abbott, L.D., 1998, Landslide-driven drainage network evolution in a pre-steady-state mountain belt: Finisterre Mountains, Papua New Guinea: Geology, v. 26, p. 1071-1074.

Howard, A.D., 1994, A Detachment-Limited Model of Drainage-Basin Evolution: Water Resources Research, v. 30, p. 2261-2285.

Iverson, R.M., Reid, M.E., Iverson, N.R., LaHusen, R.G., Logan, M., Mann, J.E., and Brien, D.L., 2000, Acute Sensitivity of Landslide Rates to Initial Soil Porosity: Science, v. 290, p. 513-516.

Johnson, K., Taylor, G., and Remaley, T., 2008, Managing hemlock wooly adelgid and balsam wooly adelgid at Great Smoky Mountains National Park., *in* Rearden, R., and Onken, B., eds., Third Symposium on Hemlock Wooly Adelgid in the Eastern United States: Asheville, NC, USDA Forest Service, p. 232-233.

Keller, H.W., Skrabal, M., Eliasson, U.H., and Gaither, T.W., 2004, Tree Canopy Biodiversity in the Great Smoky Mountains National Park: Ecological and Developmental Observations of a New Myxomycete Species of Diachea: Mycologia, v. 96, p. 537-547.

Kelly, G.A., Griffith, J.S., and Jones, R.D., 1980, Changes in distribution of trout in Great Smoky Mountains National Park, 1900-1977.: U.S. Fish and Wildlife Service Technical Paper, v. 102.

King, P.B., Neuman, R.B., and Hadley, J.B., 1968, Geology of the Great Smoky Mountains National Park, Tennessee and North Carolina, U.S. Geological Survey Professional Paper and Geological Map (1:125,000), Volume 587.

Kochel, R.C., 1990, Humid fans of the Appalachian Mountains, *in* Rachocki, A.H., and Church, M., eds., Alluvial Fans: A Field Approach: New York, Wiley, p. 109-129.

Kondolf, G.M., and M.G., W., 1993, The sizes of salmonid spawning gravels: Water Resources Research, v. 29, p. 2275-2285.

Kondolf, G.M., and Wolman, M.G., 1993, The sizes of salmonid spawning gravels: Water Resources Research, v. 29, p. 2275-2285.

Korup, O., Densmore, A.L., and Schlunegger, F., 2010, The role of landslides in mountain range evolution: Geomorphology, v. 120, p. 77-90.

Kulp, M.A., and Moore, S.E., 2005, A Case History in Fishing Regulations in Great Smoky Mountains National Park: 1934–2004: North American Journal of Fisheries Management, v. 25, p. 510-524.

Larson, G.L., and Moore, S.E., 1985, Encroachment of Exotic Rainbow Trout into Stream Populations of Native Brook Trout in the Southern Appalachian Mountains: Transactions of the American Fisheries Society, v. 114, p. 195-203.

Larson, G.L., Moore, S.E., and Carter, B., 1995, Ebb and Flow of Encroachment by Nonnative Rainbow Trout in a Small Stream in the Southern Appalachian Mountains: Transactions of the American Fisheries Society, v. 124, p. 613-622.

Leigh, D.S., and Webb, P.A., 2006, Holocene erosion, sedimentation, and stratigraphy at Raven Fork, Southern Blue Ridge Mountains, USA: Geomorphology, v. 78, p. 161-177.

Leopold, L.B., 1964, Fluvial Processes in Geomorphology: San Francisco, Ca, W.H. Freeman and Company.

Lyons, N.J., Mitasova, H., Peszlen, I., and Wegmann, K.W., 2010, Geospatial determination of potential hillslope response to an invasive species in the southern Appalachians, Binghampton Geomorphology Symposium: Columbia, SC, October 15-17, 2010.

Madden, M., Welch, R., Jordan, T., Jackson, P., Seavey, R., and Seavey, J., 2004, Digital Vegetation Maps for the Great Smoky Mountains National Park, Center for Remote Sensing and Mapping Science (CRMS), Department of Geography, The University of Georgia.

Maidment, D.R., 2002, Arc hydro: GIS for water resources: Redlands, CA.

Malamud, B.D., Turcotte, D.L., Guzzetti, F., and Reichenbach, P., 2004, Landslide inventories and their statistical properties: Earth Surface Processes and Landforms, v. 29, p. 687-711.

Malik, I., 2006, Gully erosion dating by means of anatomical changes in exposed roots (Proboszczowicka Plateau, Southern Poland): Geochronometri, v. 25, p. 57-66.

Marin, P., and Filion, L., 1992, Recent dynamics of subarctic dunes as determined by tree-ring analysis of white spruce, Hudson Bay, Québec. : Quarternary Research, v. 38, p. 316-330.

Marston, R.A., 2010, Geomorphology and vegetation on hillslopes: Interactions, dependencies, and feedback loops: Geomorphology, v. 116, p. 206-217.

Martha, T.R., Kerle, N., Jetten, V., van Westen, C.J., and Kumar, K.V., 2010, Characterising spectral, spatial and morphometric properties of landslides for semi-automatic detection using object-oriented methods: Geomorphology, v. 116, p. 24-36.

Matmon, A., Bierman, P.R., Larsen, J., Southworth, S., Pavich, M., and Caffee, M., 2003a, Temporally and spatially uniform rates of erosion in the southern Appalachian Great Smoky Mountains: Geology, v. 31, p. 155-158.

Matmon, A., Bierman, P.R., Larsen, J., Southworth, S., Pavich, M., Finkel, R., and Caffee, M., 2003b, Erosion of an Ancient Mountain Range, The Great Smoky Mountains, North Carolina and Tennessee: American Journal of Science, v. 303, p. 817-855.

May, C.L., and Gresswell, R.E., 2004, Spatial and temporal patterns of debris-flow deposition in the Oregon Coast Range, USA: Geomorphology, v. 57, p. 135-149.

McCauley, J.D., and Engel, B.A., 1995, Comparison of scene segmentations: SMAP, ECHO, and maximum likelihood: IEEE Transactions on Geoscience and Remote Sensing, v. 33, p. 1313-1316.

Merritt, W.S., Letcher, R.A., and Jakeman, A.J., 2003, A review of erosion and sediment transport models: Environmental Modeling and Software, v. 18, p. 761-799.

Metternicht, G., Hurni, L., and Gogu, R., 2005, Remote sensing of landslides: An analysis of the potential contribution to geo-spatial systems for hazard assessment in mountainous environments: Remote Sensing of the Environment, v. 98, p. 284-303.

Mitasova, H., Barton, M., Ulah, I., Hofierka, J., and Harmon, R.S., 2011a, Geospatial erosion modeling: Treatise in Geomorphology: Remote Sensing and GI Science, v. 3.

Mitasova, H., Harmon, R.S., Weaver, K.J., Lyons, N.J., and Overton, M.F., 2011b, Scientific visualization of landscapes and landforms: Geomorphology, v. Special issue on Geospatial Technologies and Geomophological Mapping.

Mitasova, H., and Hofierka, J., 1993, Interpolation by regularized spline with tension: II. Application to terrain modeling and surface geometry analysis: Mathematical Geology, v. 25, p. 657-669.

Mitasova, H., and Mitas, L., 1993, Interpolation by regularized spline with tension: I Theory and Implementation: Mathematical Geology, v. 25, p. 641-655.

Mitasova, H., Mitas, L., and Harmon, R.S., 2005, Simultaneous spline approximation and topographic analysis for lidar elevation data:Methods for open source GIS: IEEE Geoscience and Remote Sensing Letters, v. 2, p. 375-379.

Moine, M., Puissant, A., and Malet, J.-P., 2009, Detection of landslides from aerial and satellite images with a semi-automatic method. Application to the Barcelonnette basin (Alpes-de-Haute-Provence, France), *in* Matel, J.-P., Remaitre, A., and Bogaard, T., eds., Landslide Processes: From Geomorphological Mapping to Dynamic Modelling: Strasbourg, France, Cerg, p. 63-68.

Montgomery, D.R., Abbe, T.B., Buffington, J.M., Peterson, N.P., Schmidt, K.M., and Stock, J.D., 1996, Distribution of bedrock and alluvial channels in forested mountain drainage basins: Nature, v. 381, p. 587-589.

Montgomery, D.R., and Buffington, J.M., 1997, Channel-reach morphology in mountain drainage basins: Geological Society of America Bulletin, v. 109, p. 596-611.

Moore, S.E., Ridley, B., and Larson, G.L., 1983, Standing Crops of Brook Trout Concurrent with Removal of Rainbow Trout from Selected Streams in Great Smoky Mountains National Park: North American Journal of Fisheries Management, v. 3, p. 72-80.

Nakamura, F., and Swanson, F.J., 1993, Effects of coarse woody debris on morphology and sediment storage of a mountain stream system in western Oregon: Earth Surface Processes and Landforms, v. 18, p. 43-61.

NCDC, 2011, National Cliamte Data Center, National Oceanic and Atmospheric Administration Satellite and Information Service.

NCFMP, 2006, LIDAR Accuracy Assessment Report - Swain County, North Carolina Technical Cooperating State Flood Mapping Program.

—, 2011, Floodplain Mapping Information System Lidar Data Volume 2011, North Carolina Flood Mapping Project

Nichol, J., and Wong, M.S., 2005, Satellite remote sensing for detailed landslide inventories using change detection and image fusion: International Journal of Remote Sensing, v. 26, p. 1913-1926.

Orwig, D.A., 2002, Stand dynamics associated with chronic hemlock woolly adelgid infestations in southern New England, *in* Reardon, R.C., Onken, B.P., and Lashomb, J., eds., Symposium on the Hemlock Woolly Adelgid in Eastern North America: New Brunswick, NJ, New Jersey Agricultural Experiment Publication, p. 36-47.

Orwig, D.A., Foster, D.R., and Mausel, D.L., 2002, Landscape patterns of hemlock decline in New England due to the introduced hemlock woolly adelgid: Oxford, ROYAUME-UNI, Blackwell, 13 p.

Pazzaglia, F.J., 2003, Landscape evolution models: Developments in Quaternary Sciences, v. 1, p. 247-274.

Pearce, A.J., and Watson, A., 1983, Medium-term effects of two landsliding episodes on channel storage of sediment: Earth Surface Processes and Landforms, v. 8, p. 29-39.

Pittillo, J.D., Hatcher, R.D., and Buol, S.W., 1998, Introduction to the Environment and Vegetation of the Southern Blue Ridge Province: Castanea, v. 63, p. 202-216.

Pyle, C., 1988, The Type and Extent of Anthropogenic Vegetation Disturbance in the Great Smoky Mountains before National-Park-Service Acquisition: Castanea, v. 53, p. 183-196.

Renschler, C.S., Doyle, M.W., and Thoms, M., 2007, Geomorphology and ecosystems: Challenges and keys for success in bridging disciplines: Geomorphology, v. 89, p. 1-8.

Rivenbark, B.L., and Jackson, C.R., 2004, Average discharge, periennal flow initiation, and channel initiation: Small southern Appalachian basins: JAWRA Journal of the American Water Resources Association, v. 40, p. 639-646.

Roering, J.J., Schmidt, K.M., Stock, J.D., Dietrich, W.R., and Montgomery, D.R., 2003, Shallow landsliding, root reinforcement, and the spatial distribution of trees in the Oregon Coast Range: Canadian Geotechnical Journal, v. 40, p. 237-253.

Sear, D.A., 1996, Sediment transport processes in pool-riffle sequences: Earth Surface Processes and Landforms, v. 31, p. 241-262.

Seidl, M.A., and Dietrich, W.E., 1992, The problem of channel erosion into bedrock, *in* Schmidt, K., and DePloey, J., eds., Functional geomorphology: Catena Supplement, Volume 23, p. 101-124.

Shen, H.W., and Julien, P., 1993, Erosion sediment and transport, *in* Maidment, D.R., ed., Handbook of Hydrology, McGraw-Hill.

Snyder, N.P., 2009, Studying Stream Morphology With Airborne Laser Elevation Data: EOS, Transactions, American Geophysical Union, v. 90, p. 45-52.

Snyder, N.P., Castele, M.R., and Wright, J.R., 2008, Bedload entrainment in low-gradient paraglacial coastal rivers of Maine, USA: Implications for habitat restoration: Geomorphology, v. 103, p. 430-446.

Southworth, S., Schultz, A., and Denenny, D., 2005, Geologic map of the Great Smoky Mountains National Park Region, Tennessee and North Carolina, Volume 2005-1225, U.S. Geological Survey Professional Report and Geological Map (1:100,000 scale).

Souto, D., Luther, T., and Chianese, B., 1996, Past and current status of HWA in eastern and Carolina hemlock stands, *in* Salom, S.M., Tignor, T.C., and Rearden, R.C., eds., Proceedings of the First Hemlock Woolly Adelgid Review: Morgantown, WV, USDA Forest Service, p. 9-15.

SRCC, 2009, Southeast Regional Climate Center: Historical Climate Summaries website.

Stock, J., and Dietrich, W.E., 2003, Valley incision by debris flows: Evidence of a topographic signature: Water Resources Research, v. 39.

Stock, J.D., and Dietrich, W.E., 2006, Erosion of steepland valleys by debris flows: Geological Society of America Bulletin, v. 118, p. 1125-1148.

Stock, J.D., Montgomery, D.R., Collins, B.D., Dietrich, W.E., and Sklar, L., 2005, Field measurements of incision rates following bedrock exposure: Implications for process controls on the long profiles of valleys cut by rivers and debris flows: Geological Society of America Bulletin, v. 117, p. 174-194.

Stoffel, M., and Bollschweiler, M., 2008, Tree-ring analysis in natural hazards research - an overview: Natural Hazards and Earth System Sciences, v. 8, p. 187-202.

Thornthwaite, C.W., 1948, An Approach toward a Rational Classification of Climate: Geographical Review, v. 38, p. 55-94.

Tucker, G.E., and Slingerland, R., 1997, Drainage basin responses to climate change: Water Resources Research, v. 33, p. 2031-2047.

USGS, 2011, Center for LIDAR Information, Coordination, and Knowledge, Volume 2011, United States Geological Survey.

Van Den Eeckhaut, M., Poesen, J., Verstraeten, G., Vanacker, V., Nyssen, J., Moeyersons, J., van Beek, L.P.H., and Vandekerckhove, L., 2007, Use of LIDAR-derived images for mapping old landslides under forest: Earth Surface Processes and Landforms, v. 32, p. 754-769.

Varnes, D.J., 1978, Slope movement types and processes., *in* R.J., K., ed., Landslides, analysis and control, Volume Special Report 176, Transportation Research Board, National Academy of Sciences, p. 11-33.

Warren, S.D., Hohmann, M.G., Auerswald, K., and Mitasova, H., 2004, An evaluation of methods to determine slope using digital elevation data: Catena, v. 58, p. 215-233.

Whipple, K., Wobus, C., Crosby, B., Kirby, E., and Sheehan, D., 2007, New Tools for Quantitative Geomorphology: Extraction and Interpretation of Stream Profiles from Digital Topographic Data, GSA Annual Meeting: Boulder, CO.

Whipple, K.X., and Tucker, G.E., 1999, Dynamics of the stream-power river incision model: Implications for height limits of mountain ranges, landscape response timescales, and research needs: Journal of Geophysical Research-Solid Earth, v. 104, p. 17661-17674.

White, P., and Moore, J., 2000, The Science Plan for the all taxa biodiversity inventory in Great Smoky Mountains National Park, North Carolina and Tennessee. Discover Life in America, Gatlinburg, Tennessee.

Whittaker, R.H., 1956, Vegetation of the Great Smoky Mountains: Ecological Monographs, v. 26, p. 2-80.

Wieczorek, G.F., Morgan, B.A., and Campbell, R.H., 2000, Debris-flow hazards in the Blue Ridge of central Virginia: Environmental and Engineering Geoscience, v. 6, p. 3-23.

Wilkins, B.C., and Snyder, N.P., 2011, Geomorphic comparison of two atlantic coastal rivers- toward an understanding of physical controls on atlantic salmon habitat: River Research and Applications, v. 27, p. 135-156.

Witt, A.C., 2005, A Brief History of Debris Flow Occurrence in the French Broad River Watershed,Western North Carolina: The North Carolina Geographer, v. 13, p. 59-82.

Woods, F.W., and Shanks, R.E., 1959, Natural replacement of chestnut by other species in the Great Smoky Mountains National Park: Ecology, v. 40, p. 349-361.

Wooten, R.M., Gillon, K.A., Witt, A.C., Latham, R.S., Douglas, T.J., Bauer, J.B., Fuemmeler, S.J., and Lee, L.G., 2008, Geologic, geomorphic, and meteorological aspects of debris flows triggered by Hurricanes Frances and Ivan during September 2004 in the Southern Appalachian Mountains of Macon County, North Carolina (southeastern USA): Landslides, v. 5, p. 31-44.

Wooten, R.M., Latham, R.S., Witt, A.C., Fuemmeler, S.J., Gillon, K.A., Douglas, T.J., and Bauer, J.B., 2006, Downslope hazard map of Macon County, North Carolina: For shallow translational slope movements, Slope Movement Hazards if Macon County, North Carolina, North Carolina Geological Survey.

Young, R.F., Shields, K.S., and Berlyn, G.P., 1995, Hemlock woolly adelgid (Homopetera: Adelgidae): Stylet bundle insertion and feeding sites: Annals of the Entomologial Society of America, v. 88, p. 827-835.

APPENDICES

A.1. Geospatial Analysis Processing Scripts

GRASS GIS 6.4, Python 2.6, ArcMap 10.0, and MATLAB R2009a were used in geospatial processing. The program(s) used in the below scripts can be distinguished as follows:

- GRASS GIS commands inputted into this program's command line are indicated as such in headers
- Python used with GRASS GIS is designated by a ".py" extension in the header name and the importation of the module, grass.script
- Python used with ArcMap is designated by a ".py" extension in the header name and the importation of the module, arcpy
- MATLAB m-files: distinguished by a ".m" extension in the header name

Some of the variables were manually changed during iterations, while some were dynamically programmed to iterate through all variables.

A.1.1. Stream Buffer DEM Resolution Increase

A DEM was created with a 1 m resolution, though was not used to fulfill any objectives in this thesis. Unfiltered points obtained from the USGS (http://lidar.cr.usgs.gov/) that appeared to be erroneously removed from the bare earth dataset were reintroduced into the 100 m stream buffer. Points were deemed to be erroneously removed if the elevation of the unfiltered point differed from the 4 m DEM constructed from filtered points by less than 0.3 m.

```
% ****************************************************************
%   Name: resImprove.m
%   Created by: Nathan Lyons (12/30/10)
%   Purpose:Creates point cloud that represents bare ground by
%           finding all return points that are less than 0.3 m
%           from a bare earth DEM
% ****************************************************************

%% create vector with points that may be ground surface
RawPts=load('st1MrBe.txt');%columns:x,y,Zmr,Zbe; in utm
canopy=RawPts(:,3) - RawPts(:,4);%canopy height
indexRawPts=find(canopy<=0.3);%points that may be ground surface
PtsReduced=RawPts(indexRawPts,:);
PtsGround=[PtsReduced(:,1) PtsReduced(:,2) PtsReduced(:,3)];
```

```
%% find points in be vector that arent in above vector
bePts=load('st1BufBePts.txt');
PtsGroundAll=vertcat(bePts,PtsGround);
[UniqueCords UniqueIndex] = unique(PtsGroundAll(:,1:2),'rows');
PtsGroundUni=PtsGroundAll(UniqueIndex,:);

%duplicates removed
indexMax=1:max(UniqueIndex);
missingindices = setdiff(indexMax,UniqueIndex);
duplicates=PtsGroundAll(missingindices,:);

%% save
save St1PtsGround.txt PtsGroundUni /ascii

# ************************************************************************
#   GRASS GIS Commands
#   Purpose:Creation of scaled maps for classification
# ************************************************************************

g.region vect=st1Buffer100@PERMANENT res=1
r.mask -r input=st1Buffer100rast@PERMANENT maskcats=.1
r.rescale input=St2GroundSlo_1m output=St2GroundSlo_255 to=0,255

r.mapcals input=St2GroundSlo_1mNull
r.texture -k input=St2GroundSlo_1mNull prefix=st2sloTex size=3

r.out.arc input=st2sloTex_Corr_0
output=C:\Users\Admin\Documents\NCSU_thesis\data\ARC_data\created\aReaches
\bankWorkingDir\st2sloCorr_0.txt

v.surf.rst -t input=st1GroundPts layer=1 elev=st1GroDem1m
slope=st1GroSlo1m aspect=st1GroAsp1m pcurv=st1GroPc1m zcolumn=z
tension=300 smooth=2.5 segmax=40 npmin=120 dmin=.5 dmax=3 zmult=1.0

g.region vect=TAC_ws@PERMANENT res=1
r.mask -o input=TAC_ws_rast@PERMANENT

v.surf.rst -t input=hwaBE layer=1 elev=st1WSDem1m zcolumn=Z_m tension=300
smooth=2.5 segmax=40 npmin=120 dmin=.5 dmax=3 zmult=1.0
```

A.1.2. sedDEM: Sediment Transport Testbed

```
'''
Title:  sedDEMexec.py
Author: Nathan Lyons (3/15/11, last modified 10/13/11):
Purpose:Runs sedDEM bedload grain size modeling initiatied by ArcGIS 10
       sedDEM toolbox or with the following inputs.
Input:  [projectName, sourceDirectory, destinationDirectory, streamCount,
        reachCount, pointDistance, sedimentDensity, roughMap,
        waterDepthBoolean, createPlotsBoolean, plotOutputFormat]
'''

import arcpy
from arcpy.sa import *
arcpy.CheckOutExtension('spatial')
import numpy
import sedDEMmod as sedDEM
import sys
import itertools


## INITIALIZE-----------------------------------------------------------------

arcpy.SetProgressorLabel('Initializing...')

# assign input parameters to project object
proj = sedDEM.project(sys.argv)

# set arcpy environmental variables
arcpy.env.workspace = proj.arcDir
arcpy.env.overwriteOutput = 1

arcpy.AddMessage('-Output directories created or present.')


## FIELD DATA PROCESSING------------------------------------------------------

arcpy.SetProgressorLabel('Processing field data...')

# COMPILE FIELD DATA INTO OBJECT DICTIONARIES
stObjects = [] # list of stream class objects
alphaDict = {}
betaDict = {}
fdBankDepAll = []
fdDrainAreaAll = []
for st in proj.sts:
    alphaDict[st] = []
    betaDict[st] = []
    # create temporary stream variable for current iteration
```

```
    stX = sedDEM.stream(st, proj.res)

    # create reach instances populating data dictionaries from txt files
    fdBankDep = []
    fdDrainArea = []
    for re in stX.res:
        # compile reach data to its associated stream
        curRe = sedDEM.reach(st, re, proj.name, proj.inDir, proj.reCount)
        stX.dataDict[re] = curRe.dataDict

        # creat list of field values for regression in study stream
        da = stX.dataDict[re]['drainArea']
        bw = stX.dataDict[re]['FdBankDep']
        minIndex = min(len(da), len(bw))
        daNoNulls = []
        bwNoNulls = []
        for i in range(0, minIndex):
            if da[i] != -9999 and bw[i] != -9999:
                daNoNulls.append(da[i])
                bwNoNulls.append(bw[i])
        fdDrainArea.append(daNoNulls)
        fdBankDep.append(bwNoNulls)

        # creat list of field values for regression for all study streams
        fdDrainAreaAll.append(daNoNulls)
        fdBankDepAll.append(bwNoNulls)

    # Get empirically derived bankfull height values for D50 calculations
    fdDrainArea = list(itertools.chain(*fdDrainArea))
    fdBankDep = list(itertools.chain(*fdBankDep))
    (alpha, beta) = proj.powLaw(fdDrainArea, fdBankDep,
                        'drainVbankDep', 'Drainage Area (m$^2$)',
                        'Bankfull Depth (m)')

    alphaDict[stX.stNum] = alpha
    betaDict[stX.stNum] = beta

    # assign temporary to global variables
    exec 's%d = stX' % st
    exec 'stObjects.append(s%d)' % st

del stX

# Get empirically derived bankfull height values for D50 calculations
fdDrainAreaAll = list(itertools.chain(*fdDrainAreaAll))
fdBankDepAll = list(itertools.chain(*fdBankDepAll))
(alphaAll, betaAll) = proj.powLaw(fdDrainArea, fdBankDep,
                    'drainVbankDep', 'Drainage Area (m$^2$)',
                    'Bankfull Depth (m)')
```

```
arcpy.AddMessage('-Field data processed.')
arcpy.AddMessage('----------')
arcpy.AddMessage('alphaDict')
arcpy.AddMessage(alphaDict)
arcpy.AddMessage('betaDict')
arcpy.AddMessage(betaDict)
arcpy.AddMessage('----------')

## ADD DATA TO SHAPEFILES-------------------------------------------------

fdGradComp = []
mdGradComp = []
fields = ['FdGrad', 'MdGrad']

for st in stObjects:
    arcpy.AddMessage('st' + str(st.stNum))
    arcpy.SetProgressorLabel('Adding Stream %s field data to ' % st.stNum +
                             'shapefiles in destination directory...')
    # Parameters are added from data dictionaries and directly from input
    # shapefiles. Grain size is calculated as data is added to the shapefile.
    st.modelGeometry(alphaDict, betaDict, proj)
    # get grad data
    temp1 = []
    for field in fields:
        temp2 = sedDEM.field2List(st.shapefile, field, 'reachPtId > 100')
        for i in temp2:
            temp1.append(i)
    exec '%sComp = temp1' % field
    # Calculate hydraulic parameters
    st.fieldHydraulics(proj)

kDict, nDict = sedDEM.createKNdicts(proj)

for st in stObjects:
    st.modelHydraulics(alphaDict, betaDict, kDict, nDict, proj)

# Model stream parameters
sedDEM.modelStreams(kDict, nDict, alphaAll, betaAll, proj)

arcpy.AddMessage('-New shapefile(s) created with field data and modeled
D50.')


## MODEL REACH VALUES-----------------------------------------------------

vars = ['MdGrad', 'MdD50', 'dem']
modelDict = {}
```

```
modRchGrad = []
modRchD50 = []

# GET MODEL REACH DATA FROM SHAPEFILE TABLES AND ADD TO modelDict
for st in stObjects:
    stModRches = sedDEM.unique(sedDEM.field2List(st.shapefile,
                                'reachPtId',
                                'reachPtId < 100'))
    modelDict[st.stNum] = {}
    for rch in stModRches:
        modelDict[st.stNum][rch] = {}
        # get lists of var data from shapefile
        for var in vars:
            modelDict[st.stNum][rch][var] = []
            modelDict[st.stNum][rch][var] = sedDEM.field2List(st.shapefile,
                                            var,
                                            'reachPtId = %d'
                                            % rch)

        # gradient mean
        rchMean = numpy.mean(modelDict[st.stNum][rch]['MdGrad'])
        modelDict[st.stNum][rch]['MdGrad'] = rchMean
        modRchGrad.append(rchMean)
        # D50 mean
        rchMean = numpy.mean(modelDict[st.stNum][rch]['MdD50'])
        modelDict[st.stNum][rch]['MdD50'] = rchMean
        modRchD50.append(rchMean)


## WATER DEPTH-----------------------------------------------------------

# Optional functionality that compares modeled water depths to bankfull height.
if proj.watDepBool == 'true':
    arcpy.SetProgressorLabel('Water depth processing...')

    for st in stObjects:
        shp = 'St%sSurveyPts.shp' % st.stNum
        rast = '%s/St%swaterdep' % (proj.inDir, st.stNum)

        if arcpy.Exists(rast) == 'False':
            sys.exit('%s does not exists or is not named correctly ' % rast +
                  'in source directory')

        ExtractMultiValuesToPoints(shp, '%s watDep' % rast)

        for re in st.res:
            st.dataDict['watDep'] = sedDEM.field2List(shp, 'watDep',
                                    'reachPtId = %d' % re)
```

```
        proj.addDatasetToMxd('%s/St%dwaterdep' % (proj.inDir, st.stNum))

    arcpy.AddMessage('Water depth procesed')


## CREATING PLOTS-------------------------------------------------------------

# CREATES PLOT IF THIS OPTION IS SELECTED BY THE USER,

if proj.figBool == 'true':
    arcpy.SetProgressorLabel('Creating plots...')

    # GET INPUTS
    fields = ['reachPtId','chanType',
           'FdBankDepR','MdBankDepR','FdGradR','FdD50R',
           'FdBankWidR','MdGradR','MdGradCa',
           'fiTauBeta','fiTauStar','fiFdD50',
           'MdTauBeta','MdTauStar','MdD50R',
           'FdGrad', 'FdBankDepR','sloDemR']
    if proj.watDepBool == 'true':
        fields.append('watDep')
    for field in fields:
        temp1 = []
        for st in stObjects:
            temp2 = sedDEM.field2List(st.shapefile, field, 'reachPtId > 100')
            for i in temp2:
                if field == 'chanType':
                    temp1.append(str(i))
                else:
                    temp1.append(i)
        exec '%sComp = temp1' % field

    del temp1, temp2
    FdWD = numpy.divide(FdBankWidRComp, FdBankDepRComp)
    FdWD = FdWD.tolist()
    # assign values to channel types
    chanTypeDict = {'pr':1,'wpr':2,'sp':3}
    chanTypeVals = [chanTypeDict[chanTypeComp[i]]
                    for i, item in enumerate(chanTypeComp)]
    # write to file
    f = open('%s/reachData.txt' % proj.tabDir, 'w')
    for i,item in enumerate(FdGradRComp):
        f.write('%s,%s,%s,%s,%s,%s,%s,%s,%s,%s,%s,%s,%s,%s,%s,%s\n'
                %(reachPtIdComp[i],chanTypeVals[i],
                  FdBankDepRComp[i], FdGradRComp[i], FdD50RComp[i],
                  MdBankDepRComp[i], MdGradRComp[i], MdGradCaComp[i],
                  fiTauBetaComp[i], fiTauStarComp[i], fiFdD50Comp[i],
                  MdTauBetaComp[i], MdTauStarComp[i], MdD50RComp[i],
```

```
            FdGradComp[i]))
    f.close

    # PLOT: STREAM LONGITUDINAL PROFILES, GRADIENT, AND MODELED GRAIN SIZE
    proj.profilePlots()

    # PLOT: GRADIENT VS. BANKFULL WIDTH/DEPTH
    chanMarkers = {'pr': '^', 'wpr':'o', 'sp': 'd'}
    kwargs = {'c' : 'black'}

    proj.genericPlot(MdGradRComp, FdWD, 'gradVbfWD',
                'Stream Gradient', 'Bankfull width / depth',
                kwargs, chanMarkers, chanTypeComp)

    # PLOT: GRADIENT COMPARISON
    kwargs = {'color' : 'black', 'marker' : '.', 'linestyle': 'None'}
    proj.genericPlot(FdGradRComp, MdGradRComp, 'fdGradVmdGrad',
                'Gradient (field)', 'Gradient (modeled)', kwargs)

    # PLOT: BANKFULL DEPTH COMPARISON
    kwargs = {'color' : 'black', 'marker' : '.', 'linestyle': 'None'}
    proj.genericPlot(FdBankDepRComp, MdBankDepRComp, 'fdBankDepVmdBankDep',
                'Gradient (field)', 'Gradient (modeled)', kwargs)

    # PLOT: WATER DEPTH (ADDITIONAL OPTION)
    if proj.watDepBool == 'true':
       kwargs = {'color' : 'black', 'marker' : '.', 'linestyle': 'None'}
       proj.genericPlot(FdBankDepRComp, watDepComp,
                   'bankVwatDepth', 'Bankfull Depth (m)',
                   'Modeled water depth (m)', kwargs)

    arcpy.AddMessage('-Plots created.')
else:
    arcpy.AddMessage('-Create plots was not selected, so plots were not \
      created.')


'''
Title:  sedDEMmod.py
Author: Nathan Lyons (3/15/11, last modified 10/13/11):
Purpose:Contains procedures for sedDEM bedload grain size modeling.
'''

import arcpy
from arcpy.sa import *
arcpy.CheckOutExtension('spatial')
import math
import numpy
```

```
import os
import sys

# attempt to import matlabplot if Create Plots parameter is selected
if sys.argv[10] == 'true':
    try:
        import matplotlib.pyplot as plt
    except:
        arcpy.AddMessage('**matlabplot could not be imported**\n' +
                         'Download from:\nmatplotlib.sourceforge.net or ' +
                         'deselect Plot profiles.\nExiting sedDEM...')

class project:
    '''Contains procedures implemented for all of the project's streams.'''

    def __init__(self, userInput):

        # user inputs
        self.sedDEMDir =  userInput[0].replace('\\', '/')
        self.name = userInput[1]
        self.inDir = userInput[2].replace('\\', '/')
        self.outDir = userInput[3].replace('\\', '/')
        self.stCount = userInput[4]
        self.reCount = int(userInput[5])
        self.ptDist = int(userInput[6])
        self.sedDen = int(userInput[7])
        self.roughMap = userInput[8]
        self.watDepBool = userInput[9]
        self.figBool = userInput[10]
        self.figForm = userInput[11]

        # derived inputs
        self.sts = range(1, int(self.stCount) + 1)
        self.res = range(1, int(self.reCount) + 1)
        dirList = {'arcDir': 'arcData',
                   'figDir': 'figures',
                   'tabDir': 'tabData'}
        for dirName in dirList.keys():
            dir = '%s/%s' % (self.outDir, dirList[dirName])
            exec 'self.%s = "%s"' % (dirName, dir)

            # create output sub-directories
            if not os.path.exists(dir):
                os.makedirs(dir)

        # model constants
        self.p = 1000 # water density in kg/m^3
        self.g = 9.81 # acceleration due to gravity in m/s^2
```

```
def powLaw(self, x, y, saveName, xLabel, yLabel):
    '''Fits a power law to x and y. Plots if indicated by the user.'''
    # regression
    (p1, p2) = numpy.polyfit(numpy.log10(x), numpy.log10(y), 1)
    Y = (10**(p2)) * (x**p1)
    # create figure
    if self.figBool == 'true':
        plt.loglog(x, y, '.k', x, Y, '-k')
        plt.xlabel(xLabel, fontsize=20)
        plt.ylabel(yLabel, fontsize=20)
        plt.text(max(x)*.02, max(y)*2.5, 'y = %.3fx$^{%.3f}$' % (p2, p1),
                 fontsize=16)
        plt.savefig('%s/%s.%s' % (self.figDir, saveName, self.figForm),
                    dpi=300, format=self.figForm)
        plt.close()

    return 10**p2, p1

def addDatasetToMxd(self, dataset):
    '''Adds a dataset to current mxd.'''

    mxd = arcpy.mapping.MapDocument('CURRENT')
    df = arcpy.mapping.ListDataFrames(mxd)[0]

    addLayer = arcpy.mapping.Layer(dataset)
    arcpy.mapping.AddLayer(df, addLayer, 'BOTTOM')

def profilePlots(self):
    '''Plot stream longitudinal profiles, stream gradient, and modeled D50
    plots.'''

    vars = ['dem', 'mdGrad', 'MdD50']

    # get data
    for st in self.sts:
        for var in vars:
            exec '%s = []' % var
        f = open('%s/profileStream%s.txt' % (self.tabDir, st), 'r')
        for line in f:
            line = line.rstrip('\n').split(',')
            for i, var in enumerate(vars):
                eval('%s.append(float(line[i]))' % var)
        for var in vars:
            exec '%sSt%s = %s' % (var, st, var)

    # find range of vars for plots to standard axes range across all plots
    stMax = -9999
```

```
for var in vars:
    exec '%sMin = 9999' % var
    exec '%sMax = -9999' % var
for st in self.sts:
    curTest = len(eval('demSt%s' % st)) * 10
    if curTest > stMax:
        stMax = curTest
    for var in vars:
        curMinTest = min(eval('%sSt%s' % (var, st)))
        curMaxTest = max(eval('%sSt%s' % (var, st)))
        curMin = eval('%sMin' % var)
        curMax = eval('%sMax' % var)
        if curMinTest <= curMin:
            curMin = curMinTest
        if curMaxTest >= curMax:
            curMax = curMaxTest
        else:
            curMax = curMax
        exec '%sMin = curMin' % var
        exec '%sMax = curMax' % var

# plot data
plotDict = {'dem':{'order':1,'ytitle':'Elevation (m)', 'step':100},
        'mdGrad':{'order':2,'ytitle':'Gradient (m/m)', 'step':.1},
        'MdD50':{'order':3,'ytitle':'D50 (mm)', 'step':1}}

# get plot input variables
for st in self.sts:
    x = len(eval('demSt%s' % st))
    x = range(0, x * self.ptDist, self.ptDist)
    dem = eval('demSt%s' % st)
    mdGrad = eval('mdGradSt%s' % st)
    MdD50 = eval('MdD50St%s' % st)

    # create subplots
    for var in vars:
        plt.subplot(3, 1, plotDict[var]['order'])
        plt.plot(x, eval(var), "k")
        plt.ylabel(plotDict[var]['ytitle'])
        project.plotAxis(self, 0, stMax, 'x', 100)
        project.plotAxis(self, eval('%sMin' % var),
                         eval('%sMax' % var), "y",
                         plotDict[var]['step'])
    plt.xlabel('Distance upstream (m)')

    # save figure to figure directory
    plt.savefig('%s/profileStream%s.%s' %
            (self.figDir, str(st), self.figForm),
```

```
                dpi=300, format=self.figForm)
        plt.close()

    def plotAxis(self, min, max, axis='x', base=10, increments=5):
        '''Scales plot axes and ticks by data min and max rounded to base.'''

        min = base * math.floor(min / base)
        max = base * math.ceil(max / base)
        interval = (max - min) / increments
        interval = base * math.ceil(float(interval) / base)
        max = interval * increments + min
        # set axis range
        exec 'plt.%slim(min, max)' % axis
        # set axis ticks
        exec 'plt.%sticks(numpy.arange(min, max, interval))' % axis

    def genericPlot(self, x, y, saveName, xLabel, yLabel, kwargs,
                markerDict=None, markerList=None):
        '''Creates loglog plot with plot formatting arguments (kwargs).
        Optionally, input lists x and y can be dividing into subsets and plots
        as additioonaly series. Subsets are divided by the indices of
        markerList, defined by the keys of markerDict, and symbolized by the
        values of markerDict.'''

        plt.hold(True)
        if markerDict != None:
            array = numpy.array(markerList)
            for key in markerDict.keys():
                ind = numpy.where(array == key)
                ind = ind[0].tolist()
                x2 = []
                y2 = []
                for i in ind:
                    x2.append(x[i])
                    y2.append(y[i])
                    m = markerDict[markerList[i]]
                plt.loglog(x2, y2, m, **kwargs)
        else:
            plt.loglog(x, y, **kwargs)

        plt.xlabel(xLabel)
        plt.ylabel(yLabel)

        plt.savefig('%s/%s.%s' % (self.figDir, saveName, self.figForm),
                dpi=300, format=self.figForm)
        plt.close()

    def calibrateGrad(self, fieldComp, modelComp, sts):
        '''Calibrates gradient.'''
```

```
        m = 0.4803
        b = 0.0306
        for st in sts:
            uc = arcpy.UpdateCursor(st.shapefile)
            for i, row in enumerate(uc):
                x = (row.MdGradR - b) / m
                row.MdGradCa = x
                row.MdGradCa = row.MdGradR
                uc.updateRow(row)
            del uc
            st.metricAve('MdGradCa')

class stream:
    '''Contains procedures for individual streams.'''
    def __init__(self, st, res):
        self.stNum = st
        self.res = [int('%d0%d' % (st, re)) for re in res]
        self.dataDict = {}
        for re in self.res:
            self.dataDict[re]={}
        self.shapefile = 'st%sSurveyPts.shp' % st

    def modelGeometry(self, alphaDict, betaDict, proj):
        '''Adds fields to stream shapefile in sts for project, proj, contained
        in inDir. A copy of this shapefile will be made in outDir with new
        fields with names of variables in vars corresponding to reach data of
        each study reach, reCount.'''

        arcpy.Copy_management('%s/st%sSurveyPts.shp' % (proj.inDir,
                                        self.stNum),
                    '%s/st%sSurveyPts.shp' % (proj.arcDir,
                                        self.stNum))

        # add fields in table
        vars = ['FdGrad','FdBankWid','FdBankDep','FdD50',
              'MdBankDep','MdGrad','MdGradCa',
              'fiTauBeta','fiTauStar','fiFdD50',
              'MdTauBeta','MdTauStar','MdD50']
        for var in vars:
            arcpy.AddField_management(self.shapefile, var, 'DOUBLE')

        # add field data from dataDict into table
        tempDict = self.dataDict

        uc = arcpy.UpdateCursor(self.shapefile)
        for i, row in enumerate(uc):
            rowReach = row.reachPtId
            for var in vars:
                try:
```

```
                exec ('row.%s = tempDict[%s]["%s"][0]'
                    % (var, rowReach, var))
                exec ('tempDict[%s]["%s"].pop(0)' % (rowReach, var))
            except:
                exec ('row.%s = 0' % var)

        # get gradient for survey points without field data
        if i == 0:
            row.MdGrad = .05 # insert low gradient value into first point
        elif row.MdGrad == 0 or row.MdGrad == -9999:
            sloDemRad = row.sloDem * (math.pi / 180)
            sloDemGrad = math.tan(sloDemRad)
            row.MdGrad = sloDemGrad

        # model bankfull height
        row.MdBankDep = (alphaDict[self.stNum] *
                         (row.fac**betaDict[self.stNum]))
        uc.updateRow(row)
    del uc

    # Add reach average field data to table
    self.metricAve('FdD50')
    self.metricAve('FdGrad')
    self.metricAve('FdBankDep')
    self.metricAve('FdBankWid')
    # Add reach average model data to table
    self.metricAve('MdGrad')
    self.metricAve('MdBankDep')
    self.metricAve('sloDem')

def fieldHydraulics(self, proj):

    # CALCULATE tauStar, tauBeta, AND D50; ADD TO TABLES
    # calculate for field survey points from field data

    # Compute and add field calculated D50 to table
    uc = arcpy.UpdateCursor(self.shapefile, 'reachPtId > 100')
    for row in uc:
        tauBed = proj.p * proj.g * row.FdBankDepR * row.FdGradR #depth slope product
        d50Meters = row.FdD50R * 0.001 # convert to m
        tauStar = tauBed / ((proj.sedDen - proj.p) * proj.g * d50Meters)
        d50 = tauBed / ((proj.sedDen - proj.p) * proj.g * tauStar)
        d50 = d50 * 1000 # convert to mm
        row.fiTauBeta = tauBed
        row.fiTauStar = tauStar
        row.fiFdD50 = d50
        uc.updateRow(row)
    del uc
```

```
def modelHydraulics(self, alphaDict, betaDict, kDict, nDict, proj):

    # find k and n for each channel type
    arcpy.AddMessage('kDict')
    arcpy.AddMessage(kDict)
    arcpy.AddMessage('nDict')
    arcpy.AddMessage(nDict)
    uc = arcpy.UpdateCursor(self.shapefile)
    for row in uc:
        if row.MdGradR <= 0.095 and row.MdGradR > 0:
            k = kDict['low']
            n = nDict['low']
        elif row.MdGradR <= .15 and row.MdGradR > 0.095:
            k = kDict['mid']
            n = nDict['mid']
        elif row.MdGradR > .15:
            k = kDict['high']
            n = nDict['high']
        # Compute and add modeled D50 to table
        tauBed = proj.p * proj.g * row.MdBankDepR * row.MdGradR
        MdTauStar = k * (tauBed**n)
        d50 =(((proj.p * alphaDict[self.stNum] * (da**betaDict[self.stNum])*
              (row.MdGradR))**(1-n)) /
             ((proj.sedDen - proj.p) * k * proj.g**n))
        d50 = d50 * 1000 # convert to mm
        row.MdTauStar = MdTauStar
        row.MdTauBeta = tauBed
        row.MdD50 = d50
        # update row, write row to tabular file
        uc.updateRow(row)
    del uc
    self.metricAve('MdD50')
    self.writeTxt(proj.tabDir)
    proj.addDatasetToMxd('st%sSurveyPts.shp' % self.stNum)

def metricAve(self, metric):
    sc = arcpy.SearchCursor(self.shapefile)
    curRch = 1
    curRchList = []
    rchAveDict = {}
    for row in sc:
        exec 'val = row.%s' % metric
        if row.reachPtId == curRch and val != -9999:
            curRchList.append(val)
        elif val != -9999:
            rchAveDict[curRch] = numpy.mean(curRchList)
            curRchList = []
```

```
            curRchList.append(val)
            curRch = row.reachPtId
        del sc
        rchAveDict[curRch] = numpy.mean(curRchList)

        exec 'arcpy.AddField_management(self.shapefile, "%sR", "DOUBLE")' %
metric

        uc = arcpy.UpdateCursor(self.shapefile)

        for row in uc:
            exec 'row.%sR = rchAveDict[row.reachPtId]' % metric
            uc.updateRow(row)
        del uc

    def writeTxt(self, tabDir):
        '''Create file for stream profile plots'''
        f = open('%s/profileStream%s.txt' % (tabDir, self.stNum), 'w')
        sc = arcpy.SearchCursor(self.shapefile)
        for row in sc:
            f.write('%s,%s,%s,%s,%s,%s,%s,%s,%s,%s,%s,%s,%s\n'
                    % (row.dem, row.FdGrad, row.FdGradR,
                       row.MdGrad, row.MdGradR,
                       row.FdD50, row.FdD50R, row.MdD50, row.MdD50R,
                       row.MdTauBeta, row.MdTauStar,
                       row.FdBankDep, row.MdBankDepR))
        del sc

class reach:
    '''Contains procedures for individual reaches.'''

    def __init__(self, st, re, proj, inDir, reCount):
        re = re - (st * 100)
        self.reInd = st * reCount - reCount + re - 1 #index of project reaches
        self.dataDict = {'FdGrad':[],'FdBankWid':[],'FdBankDep':[],'FdD50':[],
                         'drainArea':[]}
        self.rchAve = {}
        self.shapefile = 'st%sSurveyPts.shp' % st

        # add field data from txt files to self.dataDict
        for var in self.dataDict.keys():
            if var == 'drainArea':
                facList = field2List('%s/%s' % (inDir, self.shapefile),
                                     'fac', 'reachPtId = %d%d%d' % (st,0,re))
                self.dataDict['drainArea'] = facList
            else:
                varList = []
                f = open('%s/%s%s.txt' % (inDir, proj, var ), 'r')
                for line in f:
```

```
                line = line.rstrip('\n').split(',')
                value = line[self.reInd]
                # convert to float or arc null value(-9999) if no data
                try:
                    varList.append(round(float(value),3))
                except:
                    varList.append(-9999)
            self.dataDict[var] = varList


# SUPPORT PROCEDURES

def field2List(table, field, scCon):
    'Gets a field data from a table from rows with conditions in scCon.'

    data = []
    sc = arcpy.SearchCursor(table, scCon)
    for row in sc:
        data.append(eval('row.%s' % field))
    del sc

    return data

def unique(input):
    'Returns list of unique values in input list.'

    output = []
    for x in input:
        if x not in output:
            output.append(x)
    return output

def createKNdicts(proj):
    fiTauStarDict = {'low':[], 'mid':[], 'high':[]}
    tauBfDict = {'low':[], 'mid':[], 'high':[]}

    for st in proj.sts:
        shp = 'st%sSurveyPts.shp' % st
        sc = arcpy.UpdateCursor(shp, 'reachPtId > 100')
        for row in sc:
            # get tau values for different channel types based on slope
            if row.FdGrad <= 0.095:
                fiTauStarDict['low'].append(row.fiTauStar)
                tauBfDict['low'].append(row.fiTauBeta)
            elif row.FdGrad <= 0.15 and row.FdGradR > 0.095:
                fiTauStarDict['mid'].append(row.fiTauStar)
                tauBfDict['mid'].append(row.fiTauBeta)
            elif row.FdGrad > 0.15:
                fiTauStarDict['high'].append(row.fiTauStar)
```

```
            tauBfDict['high'].append(row.fiTauBeta)

    kDict = {'low':[], 'mid':[], 'high':[]}
    nDict = {'low':[], 'mid':[], 'high':[]}

    for key in kDict.keys():
        (kDict[key], nDict[key]) = proj.powLaw(tauBfDict[key],
                                   fiTauStarDict[key],
                                   'tauBfVfiTauStar_' + key,
                                   'tauBf', 'fiTauStar')
        arcpy.AddMessage('tauBfDict')
        arcpy.AddMessage(tauBfDict[key])
        arcpy.AddMessage('fiTauStarDict')
        arcpy.AddMessage(fiTauStarDict[key])
    return kDict, nDict

def modelStreams(kDict, nDict, alpha, beta, proj):
    # MODEL TRUNK STREAMS
    for st in range(1,6,1):
        dictD50 = {}
        curRchListD50 = []
        dictSlo = {}
        curRchListSlo = []
        curFid = 9
        shp = 'ws%sPts.shp' % st
        uc = arcpy.UpdateCursor(shp)
        arcpy.AddField_management(shp, 'MdBankDep', 'DOUBLE')
        f = open('%s/profileStreamWs%s.txt' % (proj.tabDir, st), 'w')
        for row in uc:
            # model bankfull height
            da = row.fac * 16 # convert fac [cells] to to area (res=4m)
            row.MdBankDep = (alpha *(da**beta))
            if row.sloDem <= 0.095 and row.sloDem > 0:
                k = kDict['low']
                n = nDict['low']
            elif row.sloDem <= .15 and row.sloDem > 0.095:
                k = kDict['mid']
                n = nDict['mid']
            elif row.sloDem > .15:
                k = kDict['high']
                n = nDict['high']
            # Compute and add modeled D50 to table
            d50 =(((proj.p * alphaDict[1] * (row.fac**betaDict[1]) *
(row.sloDem))**(1-n)) /
                  ((proj.sedDen - proj.p) * k * (proj.g**n)))
            d50 = d50 * 1000 # convert to mm
            tauBed = proj.p * proj.g * row.MdBankDep * row.sloDem
            MdTauStar = k * (tauBed**n)
```

```
            row.MdD50 = d50
            uc.updateRow(row)
            if row.FID > curFid:
                dictD50[curFid] = numpy.mean(curRchListD50)
                dictSlo[curFid] = numpy.mean(curRchListSlo)
                curFid = curFid + 10
                curRchListD50 = []
                curRchListSlo = []
            curRchListD50.append(row.MdD50)
            curRchListSlo.append(row.sloDem)
        dictD50[curFid] = numpy.mean(curRchListD50)
        dictSlo[curFid] = numpy.mean(curRchListSlo)
        del uc
        curFid = 9
        uc = arcpy.UpdateCursor('ws%sPts.shp' % st)
        for row in uc:
            if row.Fid > curFid:
                curFid = curFid + 10
            row.MdD50R = dictD50[curFid]
            row.sloDemR = dictSlo[curFid]
            uc.updateRow(row)
            f.write('%s,%s,%s,%s,%s,%s\n'
                    % (row.dem, row.fac, row.sloDem, row.sloDemR,
                       row.MdD50, row.MdD50R))
        del uc
arcpy.Merge_management("ws1Pts;ws2pts;ws3pts;ws4pts;ws5pts",
                       "wsPtsMerge")
```

A.1.3. Debris Flow Inventory

```
#!/usr/bin/env python
# ********************************************************************
#       Name: r.qdfClass.py
#       Created by: Nathan Lyons (2/19/11)
#       Purpose:Classifies areas and outputs statistics with
#               verification map
# ********************************************************************
import grass.script as grass

## VARIABLES-----------------------------------------------------------
trainingMap='chpTrainingMap'     # training map
slo='hwa1100slo255agg20'         # slope
sLength='hwaSlopeLength255agg20' # slope length
asp='hwa1100asp255agg20'         # aspect
pc='hwa1100pc255agg20'           # profile curvature
ndvi='hwaNdvi1998255agg20'       # ndvi
bs = 36                          # block size
inputs=[ndvi,slo,pc]

## CLASSIFICATION------------------------------------------------------
#VAR NAMES
signatures = 'hwaClassSigs'
outputName = 'hwaClassTrain'
#GRASS CLASSIFICATION
grass.run_command('i.group',group='hwaClassGroup',subgroup=\
                  'hwaClassSubGroup',input=inputs)
grass.run_command('i.gensigset',trainingmap=trainingMap,\
                  group='hwaClassGroup',subgroup=\
                  'hwaClassSubGroup',signaturefile=signatures)
grass.run_command('i.smap',group='hwaClassGroup',subgroup=\
                   'hwaClassSubGroup',signaturefile=signatures,\
                  output=outputName,blocksize=bs)
grass.run_command('g.remove',group='hwaClassGroup')

## STATS---------------------------------------------------------------
#FIND AREAS
grass.mapcalc("hwaTruePos = if($qdfClassed==1 & $mappedFlows==1,1,\
              null())",qdfClassed=outputName,mappedFlows=\
              hwaMappedFlows')
grass.mapcalc("hwaTrueNeg = if($qdfClassed==2 & $mappedFlows==0,1,\
              null())",qdfClassed=outputName,mappedFlows=\
              'hwaMappedFlows')
grass.mapcalc("hwaFalsPos = if($qdfClassed==1 & $mappedFlows==0,1,\
              null())",qdfClassed=outputName,mappedFlows=\
              'hwaMappedFlows')
grass.mapcalc("hwaFalsNeg = if($qdfClassed==2 & $mappedFlows==1,1,\
              null())",qdfClassed=outputName,mappedFlows=\
              'hwaMappedFlows')
#CREATE IDENTIFICATION STAT MAP
grass.mapcalc("hwaQdfClassAreas = if(isnull(hwaTruePos),\
```

```
            if(isnull(hwaTrueNeg),if(isnull(hwaFalsPos),\
            if(isnull(hwaFalsNeg),null(),4),3),2),1)")
#OUTPUT STAT TEXT FILE
outputTxt='C:/Users/Admin/Documents/NCSU_thesis/data/GRASS_data/'+\
        'hwaQdfClassAreas/hwaQdfClassAreas'+str(trialNum+i)+'.txt'
grass.run_command('r.stats',input='hwaQdfClassAreas',output=\
                outputTxt,flags='a')
#RECORD STATS
totalArea=226475973 #in m^2
#COMPILE STATS
f=open(outputTxt,'r')
cat=[]
for line in f:
    num=line.split(' ')  #seperate fields for indexing
    percent=float(num[1])/totalArea #calculate percent area
    percent=round(percent,4)
    cat.append(str(percent))
f.close()
#WRITE STATS TO SUMMARY FILE
f=open('C:/Users/Admin/Documents/NCSU_thesis/data/GRASS_data/'+\
      'hwaQdfClassAreas/hwaSummary.txt','a')
trues=float(cat[0])+float(cat[1])
falses=float(cat[2])+float(cat[3])
f.write(str(trialNum+i)+','+str(trues)+','+str(falses)+','+\
       str(cat[0])+','+str(cat[1])+','+str(cat[2])+','+str(cat[3])+\
       ','+str(bs)+','+str(trials[i])+'\n')
f.close
print 'done'
```

A.2. Geospatial Determination of Potential Hillslope Response to Hemlock Woolly Adegid

This appendix is adapted from Lyons *et al*. (2010).

A.2.1. Introduction

The old growth forests of the Smoky Mountains are highly valued for their ecological diversity and are juxtaposed with landslide prone surfaces since these high elevation areas did not succumb to heavy logging in the early twentieth century (Johnson *et al.*, 2008). Here and elsewhere in the tree's range, hemlocks provide important contributions to ecologies and economies (Orwig, 2002). Determining the areas that contain not only HWA invasions, but also confounding disturbances to trees such as landslides, can assist land managers in prioritizing their efforts to mitigate the impacts of this invasion.

A methodology to determine the areas susceptible to HWA-induced hillslope response in the form of debris flows or other types of mass failure in the Smoky Mountains of North Carolina is presented. Hillslope areas at risk were determined by intersecting vegetation maps with topographic derivatives derived from lidar DEM. Elevation and its derivatives (slope, curvature, and aspect) along with bedrock and hydrologic geospatial data are used to limit at risk areas to slopes that contain topographic characteristics similar to previously mapped debris flows. Predicting the spatial extent of potential hillslope failures due in part to HWA infestations will assist in the management of the geomorphic response to this invasive insect.

A.2.2. Methods

The study area was iteratively reduced to confine areas that may be at risk to HWA-induced hillslope failures. Numerous datasets obtained from other workers were examined to determine the topographic and geologic characteristics of debris flows. The resultant reduced area was intersected with hemlock forested areas once the characteristics of debris flows were determined, further reducing the area

that is deemed to be susceptible of HWA-induced landsliding. The DEM and derivities described in section 2.2.2.1. were used. Aspect was extracted for analysis at the geographic location of lidar data. Sample points of aspect were divided into two populations: inside and outside of USGS mapped debris flows. All points in the debris flow areas were included in analysis. However, the non-debris flow population was comprised of randomly selected points equal in quantity to the points in the debris flow population. Additionally, debris flow and bedrock type polygons, bedrock orientation point data, and bedrock structure vectors, produced by means of aerial photo interpretation, compilation of smaller extent maps, and field traverses, were obtained from (Southworth *et al.*, 2005). A vegetation dataset containing overstory and understory vegetation classes contained within polygons, produced from color infrared aerial photos within 10 m of their ground position, was obtained from Madden, *et al*. (2004).

All of the USGS mapped debris flows within the study area are located at or above an elevation of 1100 m. The Copperhill and Anakeesta Formation underlie these elevations and are prone to hillslope failures (Southworth, *et al.* 2005). These formations also underlie areas below this elevation, though with exception to the two easternmost watersheds where the bedrock is composed of an assemblage of gneiss and quartzite. The 1100 m contour line and the spatial distribution of debris flows are lowest in latitude in these two watersheds. This suggests that the bedrock of these watersheds, composed of highly resistant rocks, has resisted erosion to a high degree (see sections 1.7 for more detail). This hypothesis provides cause to limit the study area to elevations above 1100 m, which roughly approximates the drainage area-slope scaling break of the study area. Lastly, ground surfaces with aspects that that fell between 124 and 238° were deemed susceptible to debris flows, as explained in section 2.2.3, since surfaces that contain these aspects values are where USGS mapped debris flows exist.

A.2.3. Results and Discussion

A reduction of the study area to include elevations above 1100 m, and aspect within one standard deviation in debris flow areas (Figure 2.17) was intersected with hemlock forests (Figure A.1). The resultant extent of potential hillslope response due to HWA encompasses 19 km^2. Elevation, as surrogate for areas that drain to debris flow dominated channels, and aspect, important when this derivative is roughly parallel to bedrock orientation, contribute to landslide spatial distribution in this area and can be used to confine the area of potential hillslope response. At risk areas were reduced by 39% by considering these surrogates, where the original extent compared is the area of hemlock forests. Contributions from other topographic derivatives, slope and curvature, were not found that were exclusive to only one of the study's populations. It is important to stress here that a case of HWA-induced hillslope failure in the region is yet to be documented, though landslides initiated by a reduction in root strength raises a threat this potential phenomenon.

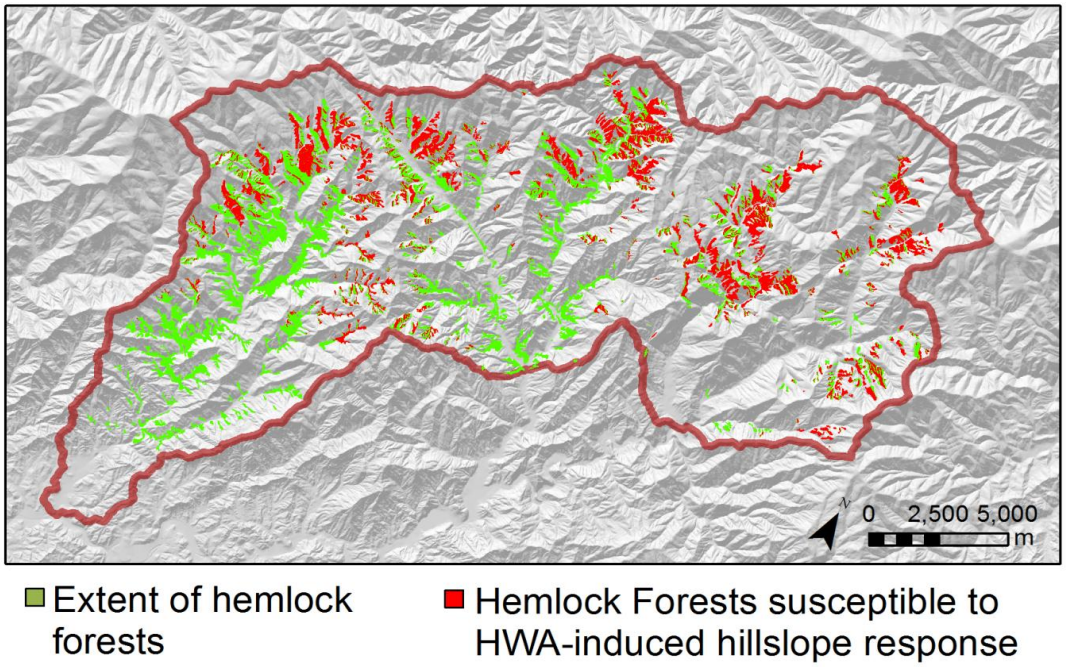

Figure A.1. Areas susceptible to HWA-induced hillslope response.